A STUDY OF BOVINE BETA LACTOGLOBULIN: ITS CATALYTIC ACTIVITY AND ROLE IN THE BIOSYNTHESIS OF CYCLORETINAL, A KEY LIPOFUSCIN

A Dissertation

by

VISHRUTH GOWDA

Submitted to the Office of Graduate and Professional Studies of
Texas A&M University
in partial fulfillment of the requirements for the degree of

DOCTOR OF PHILOSOPHY

Chair of Committee,	Coran M.H. Watanabe
Committee Members,	David P. Barondeau
	Tadhg P. Begley
	Deborah A. Siegele
Head of Department,	Simon W. North

May 2018

Major Subject: Chemistry

ABSTRACT

The accumulation of lipofuscins such as all-trans retinal dimer/cycloretinal in the retina may contribute to the progression of age-related macular degeneration (AMD). While the biosynthesis of cycloretinal is not fully understood, it has been shown that the milk protein β-lactoglobulin (BLG) can promote the cyclodimerization of *all-trans* retinal to cycloretinal both *in vitro* and *in vivo*. To further our understanding of this cyclodimerization, we have used site-directed mutagenesis of BLG as well as mass spectrometric analysis with substrate analogs to demonstrate that lysine residues play a key role in catalysis. It is shown that catalytic activity necessitates the presence of a physical binding site and cannot be mediated by a peptide chain. We also report that BLG is a promiscuous enzyme (a feature common to enzymes with a hydrophobic binding site and an active site lysine) that can catalyze the retroaldol cleavage of α, β unsaturated aldehydes. Retroaldolase activity was seen to be most effective on substrates with phenyl or napththyl side-chains. While the fluorescence images reported in this dissertation suggest that BLG may not be crossing into the retina to be the major protein responsible for cycloretinal biosynthesis, it might be possible that the blood-retina barrier becomes less coherent with age. These studies provide insight into the mechanism of the cyclodimerization process and provide a model system for biocatalysis and biosynthesis of cycloretinal *in vivo*. In the long term, these studies may pave the way for drug development and inhibitor design as an early treatment regimen for AMD.

.

DEDICATION

This dissertation is dedicated to all my teachers (from family to school to university) who have inspired me, believed in me and kept me on the path to success despite my continuous efforts to veer off.

ACKNOWLEDGEMENTS

I thank Dr. Watanabe for the opportunity to work in her lab, for her guidance in everything, from research skills to scientific writing and for her constant support during all these years of working on this dissertation. I am extremely grateful to my committee members Dr. Barondeau, Dr. Begley and Dr. Siegele for their advice, time and scientific insight that helped me overcome some of the toughest obstacles in my research

During the course of my time here, I have had the opportunity to be mentored by wonderful people including Dr. Hillary Agbo, Dr. Jennifer Foulke-Abel, Dr. Dinesh Simkhada and Dr. Huitu Zhang. I have since spent a lot of time in the laboratory getting to know Rachel Lee, Dr. Shogo Mori, Dr. Keshav Nepal, Irum Perveen, Brendan Foley, Lauren Washburn, Brett Johnson and Jean Kim. Some days, when research was not working out, it was just these people who kept me going and I am thankful to them for putting up with me all these years and wish them well in their future endeavors.

I have had the opportunity to mentor some amazing undergraduate students, among whom I would like to specially thank Alyssa Olivas, Megan Esteb, Jooyeon Chae, Jasmine Du, Timothy Fan for all their contribution and cheerful attitudes that always helped brighten the mood in our lab.

I am thankful to the staff of the Chemistry department here, especially Sandy, Janet, Carrie, Julie and Amy whose assistance ensured that I could give my complete attention to research. Lastly, I am grateful to each and every one that I have not named here but helped me directly or indirectly throughout my time here at Texas A&M University.

CONTRIBUTORS AND FUNDING SOURCES

This work was supervised by a dissertation committee consisting of Professor Coran Watanabe [advisor] and Professors Begley and Barondeau of the Department of Chemistry and Professor Siegele of Department of Biology.

The trypsin digestion and mass spectrometric analysis reported in all chapters was obtained by Dr.Yohannes Rezenom and Dr. William Russell from the Laboratroy for Biological Mass Spectrometry. Dr. B.J. Bench performed the citral trapping experiment reported in Chapter III. Brendan Foley synthesized the α, β unsaturated aldehydes used in Chapter IV. Taylor Hinsdale from Dr. Maitland's lab in the Department of Biomedical Engineering helped obtain the confocal microscopy images reported in Chapter V. Jinny Johnson from the Protein Chemistry Laboratory performed the amino acid analysis reported in Chapter V.

All other work conducted for the dissertation was completed by the student independently.

This work was made possible in part by National Science Foundation under grant number CHE-1608580 and the Welch Foundation under grant number A-1828.

Its contents are solely the responsibility of the authors and do not necessarily represent the official views of the National Science Foundation or the Welch Foundation.

NOMENCLATURE

AMD	Age-related macular degeneration
BLG	β-lactoglobulin
ATR	All-trans retinal
RPE	Retinal pigment epithelium
MBP	Maltose binding protein
DTT	Dithiothreitol
SDS	Sodium dodecyl sulfate

TABLE OF CONTENTS

Page

ABSTRACT ii

DEDICATION iii

ACKNOWLEDGEMENTS iv

CONTRIBUTORS AND FUNDING SOURCES v

NOMENCLATURE vi

TABLE OF CONTENTS vii

LIST OF FIGURES ix

LIST OF TABLES xii

CHAPTER I INTRODUCTION AND LITERATURE REVIEW 1

1.1 Epidemiology of AMD 2
1.2 Structure of the eye 3
1.3 Etiology of AMD 6
1.4 Drusen and lipofuscin, a biochemical analysis 8
1.5 Treatment of AMD 10
1.6 Beta-lactoglobulin and AMD 12
1.7 Structure of BLG 13
1.8 Ligand binding of BLG 16
1.9 BLG functional analysis 17
1.10 Statement of purpose 24

CHAPTER II EXPRESSION AND PURIFICATION OF BLG 25

2.1 Introduction 25
2.2 Results and discussion 27
2.3 Significance 32
2.4 Experimental procedures 33

CHAPTER III LIPOFUSCIN FORMATION CATALYZED BY THE MILK PROTEIN BETA-LACTOGLOBULIN: LYSINE RESIDUES IN CYCLORETINAL SYNTHESIS 43

3.1 Introduction 43
3.2 Results and discussion 45

3.3 Significance 58
3.4 Experimental procedures 59

CHAPTER IV BIOCATALYSIS WITH THE MILK PROTEIN BETA-LACTOGLOBULIN: PROMOTING RETROALDOL CLEAVAGE OF CONJUGATED ALDEHYDES 66

4.1 Introduction 66
4.2 Results and discussion 68
4.3 Significance 76
4.4 Experimental procedures 76

CHAPTER V APPLICATION OF CONFOCAL FLUORESCENCE MICROSCOPY TO TRACK THE PASSAGE OF BLOOD-BORNE BLG IN MOUSE EYE 82

5.1 Introduction 82
5.2 Results and discussion 83
5.3 Significance 90
5.4 Experimental procedures 90

CHAPTER VI CONCLUSIONS 99

REFERENCES 102

APPENDIX 123

LIST OF FIGURES

Page

Figure 1 Prevalence of AMD in the USA by age and race 2

Figure 2 Structure of the human eye 3

Figure 3 Histopathological structure of the retina 5

Figure 4 The human vision cycle 6

Figure 5 Progression of AMD 7

Figure 6 Proposed biosynthesis of retinoid-derived compounds found to accumulate in lipofuscins of the RPE.R groups in phosphatidylethanolamine designate the long alkyl chains. 9

Figure 7 Proposed mechanism for cycloretinal formation mediated by A] phosphatidylethanoloamine B] proteinaceous lysine residues. 11

Figure 8 phylogenetic tree generated by comparing bovine BLG to BLG of other species 13

Figure 9 Central hydrophobic cavity of BLG with retinoic acid bound 14

Figure 10 Cartoon of 3-dimensional structure of BLG 15

Figure 11 Cartoon of 3-dimensional structure of RBP 18

Figure 12 His_6 TeV protease cleavage of MBP-BLG fusion protein 28

Figure 13 Screening of conditions for MBP-TeV protease catalyzed cleavage of fusion protein 28

Figure 14 Schematic diagram illustrating the BLG cleavage and purification process 30

Figure 15 Characterization of purified BLG by mass spectrometry and western blot analysis 31

Figure 16 SDS-PAGE gels of purified KA-BLG; A6069K-BLG; A7791K-BLG and A77K-BLG 32

Figure 17 BLG catalyzed cyclodimerization of retinal to cycloretinal 44

Figure 18 Proposed mechanism for BLG catalyzed cyclodimerization 44

Figure 19 BLG lysine residue pairs postulated to be involved in cycloterpenal catalysis: [A] Residues K60 and K69 on the β-barrel wall interior, [B] Residues K77 on the flexible loop and K91 on the β-barrel exterior, (1GX9), Lysine side chains are highlighted in red (1B8E), [C] Native dimer structure of BLG (1B8E)..... 46

Figure 20 Mass spectrometric results obtained after trypsin digestion of BLG showing cyclocitral (homodimer product) bound to K91 48

Figure 21 CD analysis of BLG catalyzed cyclodimerization of all-trans retinal 49

Figure 22 HPLC analysis of cyclodimerization activity of BLG and mutants: A] wtBLG, KA-BLG B] A77K/A91K-BLG, A60K/A69K-BLG, A77K-BLG 49

Figure 23 SDS-PAGE analysis [A] and HPLC analysis of cyclodimerization activity [B] of tDERA 51

Figure 24 1H-NMR analysis showing that SDS treated BLG does not catalyze cyclodimerization 52

Figure 25 Evaluation of the mechanism with substrates analogs: condensation reaction with compounds 5 and 6 53

Figure 26 Control reaction with compound 3.5 54

Figure 27 Mass spectrometric results obtained before trypsin digestion of BLG showing product bound to BLG 56

Figure 28 Mass spectrometric results obtained after trypsin digestion of product-bound BLG 57

Figure 29 Proposed mechanism for covalent labelling of BLG by 3.6..... 58

Figure 30 BLG catalyzed cyclodimerization of all-trans retinal to cycloretinal..... 67

Figure 31Oxidative cleavage as mediated by BLG: A] Synthesis of β-methyl naphthene aldehyde 4.5: i NaH, DCM; ii DIBAL-H, -60 °C; iii H2O; B] BLG catalyzed oxidative cleavage of β-methyl naphthene aldehyde 4.5..... 68

Figure 32 Evaluation of BLG reaction by HPLC analysis: A] BLG reaction with compound 4.5, B] BLG reaction with compound 4.13, C] acetonaphthone 4.3 synthetic standard 69

Figure 33 Control reaction showing that in the absence of protein, compound 3 does not non-enzymatically break down into acetonaphthone 70

Figure 34 Proposed mechanism for BLG catalyzed retroaldol cleavage 70

Figure 35 Effect of substrate analog 4.13 on retroaldol cleavage: [A] BLG catalyzed retroaldol cleavage of β-methyl naphthene aldehyde 3 in the presence of inhibitor 8; [B] Synthesis of substrate analog 4.13 73

Figure 36 Brominated analog of compound 4.5 75

Figure 37 When treated with NEM, the peak for N-Cys-BLG (mass=19404 a.m.u.) disappeared and a new peak corresponding to BLG+ 2 moles of NEM (mass= 19686 a.m.u.) was seen 84

Figure 38 Cysteine-4 containing peptide labeled with NEM analyzed by trypsin digestion and mass spectrometry 85

Figure 39 Trypsin digestion and peptide analysis showing cysteine-164 containing peptide labeled with NEM 85

Figure 40 Characterization of BLG-ATTO532 conjugate by SDS-PAGE analysis 87

Figure 41 Confocal images of retina of mouse A] saline injection B] ATTO532 injection 89

Figure 42 Confocal fluorescence image of mouse retina after A] 15 minutes B] 1 hour C] 48 hours 89

Figure 43 Various factors could potentially contribute to the progression of AMD 100

LIST OF TABLES

Page

Table 1 Prevalence of AMD in the USA..... 1

Table 2 Selected ligand binding constants for bovine BLG..... 16

Table 3 Primers used in this study 36

Table 4 Evaluation of scope of the retroaldol reaction using a series of substrates..... 72

Table 5 Labelling of BLG with brominated substrate analogs 75

CHAPTER I

INTRODUCTION AND LITERATURE REVIEW

Of the three most commonly diagnosed eye conditions (Table 1), Age-related macular degeneration is the most difficult to treat or detect.[(1)] Ever since surgical treatment of cataracts became a routine procedure[(2)], AMD has become the leading cause of blindness in people above the age of 50 in the United States of America.[(1, 3)]

Table 1 Prevalence of AMD in the USA

Eye disease	Prevalence
AMD	1.6 million people above the age of 50
Diabetic retinopathy	5.3 million people above the age of 18
Cataract	20.5 million people above the age of 40

1.1 Epidemiology of AMD

Studies into the prevalence of AMD in the United States of America by age and race have regularly found that Caucasians above the age of 80 are the highest at risk for AMD (Figure 1).[3-5] This drastic increase in the prevalence of AMD in Caucasians vs other races could be due to dietary or lifestyle dissimilarities. Moreover, compared to Caucasians in the USA, AMD appears to be less common in Japanese people above the age of 50.[5, 6] The authors have hypothesized that this could be related to the higher consumption of an antioxidant by

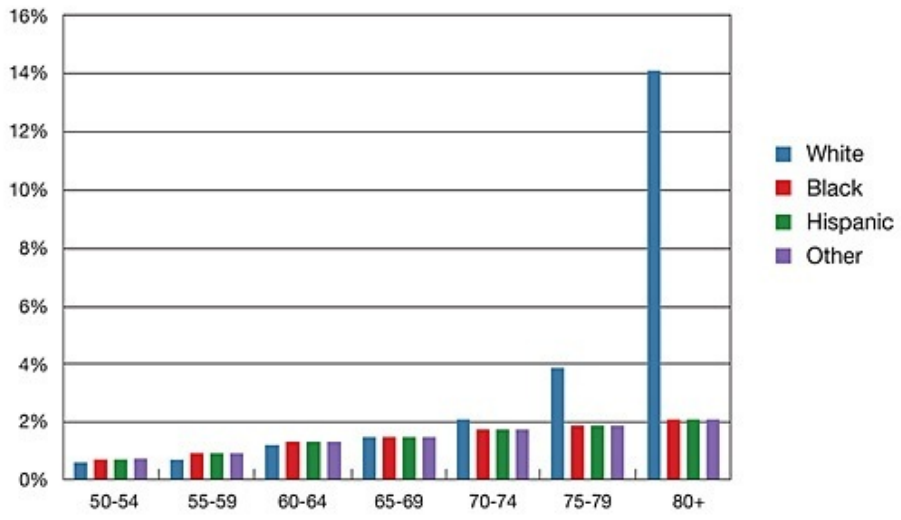

Figure 1 Prevalence of AMD in the USA by age and race

Japanese people. However, in the context of this dissertation, we should keep in mind that per capita milk consumption amongst Japanese is half the daily per capita milk consumption in the USA. [7]

1.2 Structure of the eye

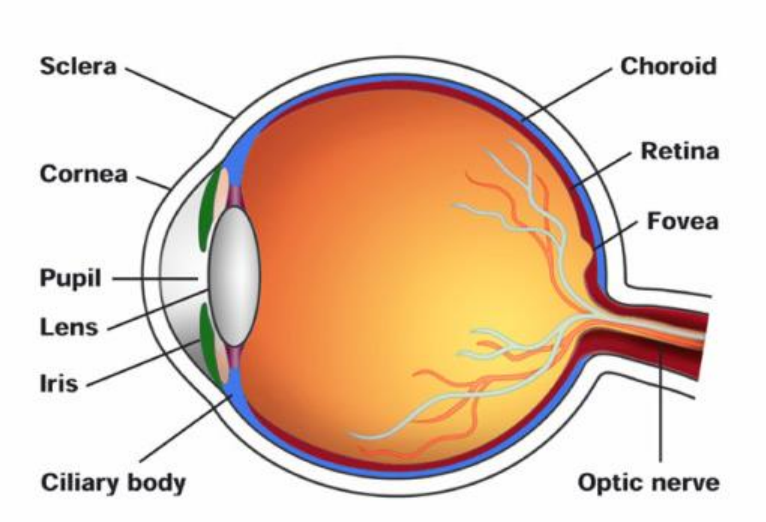

Figure 2 Structure of the human eye

To better understand the types, cause and treatment of AMD, a basic understanding of the histopathology of the cells responsible for vision is required.

The sclera is the outer layer of the eyeball (Figure 2). It is a protective layer and has little blood vessels.[8]

The choroid is the middle layer of the eyeball (Figure 2). The choroid has nearly all the blood vessels responsible for maintaining the retina

The retina is the innermost layer of the eye that is responsible for vision. Histological analysis of the retina (Figure 3) has shown that the retina can be divided into the following layers:

- Just in front of the choroid is the retinal pigment epithelium (RPE)
- Attached to the RPE are the photoreceptor cells (rods and cones). The area where the photoreceptor cells are present is called the outer nuclear layer
- Other layers including outer plexiform layer, inner plexiform layer, ganglion layer, nerve fiber layer and inner limiting membrane that are transparent to light are found above the outer nuclear layer.[(8)]

The macula is a collection of cells and specialized structures found in a disk under 250μm thick and less than 4mm in diameter near the center of the retina and is responsible for 20/20 vision.[(1)]

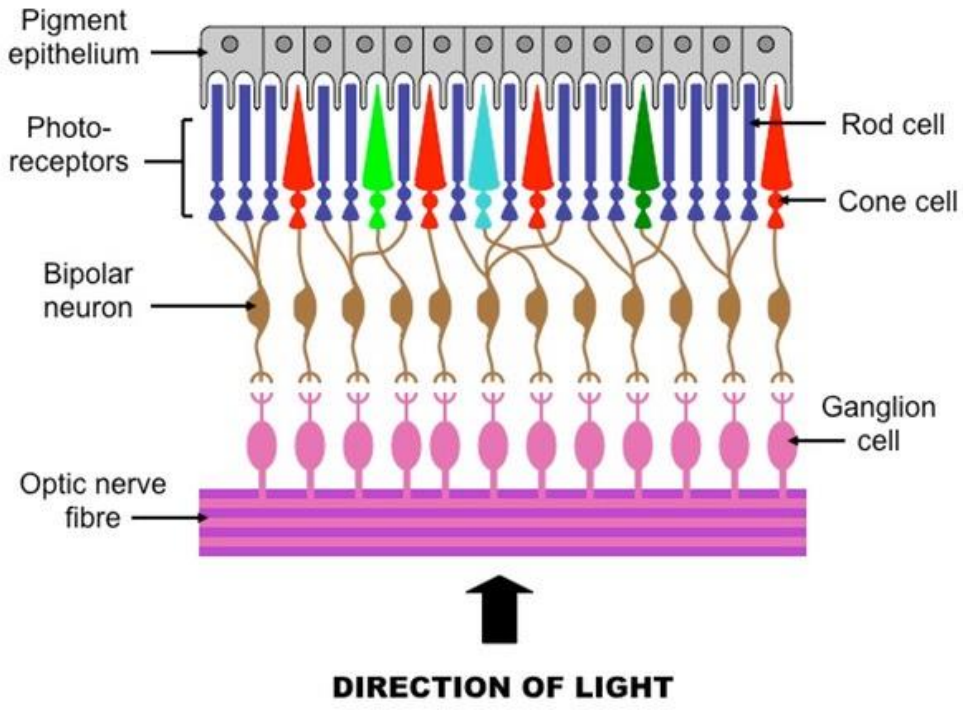

Figure 3 Histopathological structure of the retina

The photoreceptor cells (rods and cones) contain the enzymes and structures necessary for phototransduction (the process by which light is converted into electrical signals that can be transmitted to the brain). Light dependent isomerization of rhodopsin activated 11-cis-retinal to all-transretinal (ATR), a critical step in phototransduction occurs in the photoreceptor cells.[(9)] Subsequently, the all-trans retinol produced at the end of phototransduction is converted back into 11-cis retinal by enzymes found in the RPE (Figure 4). [(9)]

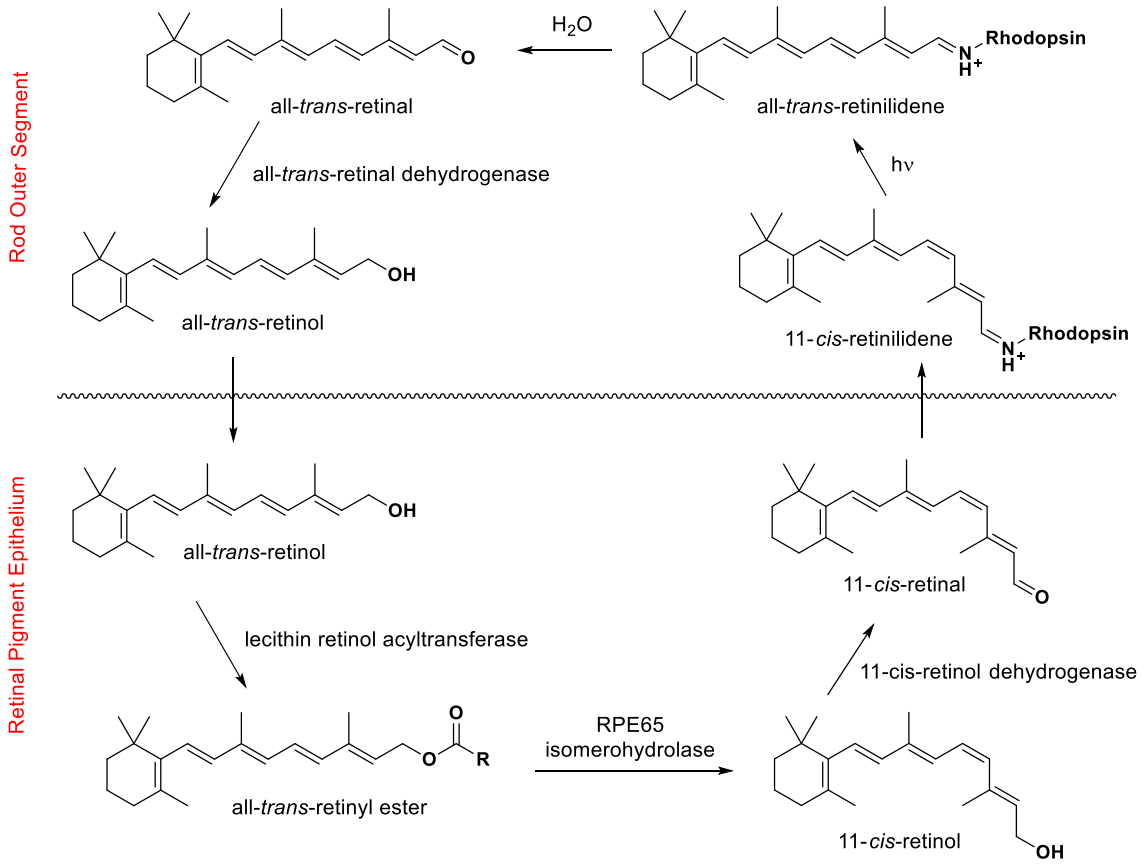

Figure 4 The human vision cycle

1.3 Etiology of AMD

Any damage to the RPE, the photoreceptor cells or the blood vessels that supply blood to these layers (chroricapillaris) could lead to the loss of phototransduction activity.[(10)] Furthermore, the RPE cells, the photoreceptor cells and the choriocapillaris are physically and physiologically interconnected with a loss in any one of them resulting in the loss of

the other two. [11-14] If such degradation occurs in the macula, complete central vision is lost.[1]

Accumulation of cellular by-products arising from the apoptosis or degradation of cellular material (including photoreceptor cells) lead to aggregates of a mixture of lipids, proteins and other cellular elements above the RPE called drusen.[1, 15] The presence of noticeable drusen which does not necessarily affect vision is referred to as 'dry AMD' (Figure 5).

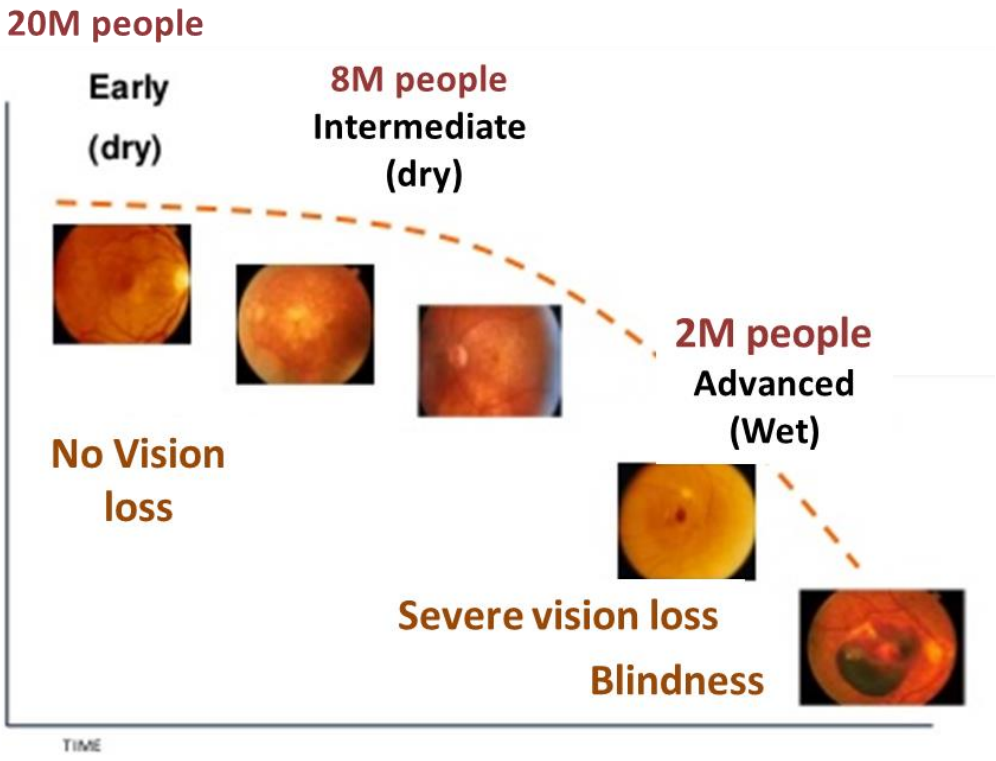

Figure 5 Progression of AMD

The enlargement of drusen can result in a condition called geographic atrophy of the RPE.[5] In such a scenario, the part of the RPE that undergoes atrophy loses its ability to phototransduce. If this affects the center of the macula (fovea), this could seriously impair

vision. If instead of atrophy, there is choroidal neovascularization in the sub-RPE or sub-retinal space, this could lead to severe vision loss and is known as 'wet AMD'.[16] As shown (Figure 5), this only affects about 10% of the total number of patients with AMD but it accounts for nearly 90% of the severe visual loss seen in AMD patients.[11]

1.4 Drusen and lipofuscin, a biochemical analysis

The presence of drusen is often diagnosed as an early stage of AMD.[15] In order to discover the biogenesis of drusen, it has been analyzed to identify the lipids and proteins that constitute this complex mixture. The drusen is a mixture of proteins, lipids, polysaccharides and glycosaminoglycans. Lipids like esterified cholesterol and phosphatidyl choline comprise about 40% of the drusen[17] while more than one hundred proteins have been characterized in the drusen with clusterin, vitronectin and serum albumin being identified as the proteins present in the highest concentration.[17, 18] While most of these characterized proteins are generally found in the RPE, it is noteworthy to mention that β-lactoglobulin (BLG), a bovine milk protein not biosynthesized in humans has also been identified in the drusen of patients affected with AMD.[18]

1.4.1 A2E

The degradation of photoreceptor cells (rods and cones) leads to the formation of lipofuscins (non-degradable fluorophores) in the RPE.[19, 20] A majority of the characterized molecules in lipofuscin are derivatives of ATR.[21] Of these compounds, the one most

studied is the bis-retinoid A2E. Not only does A2E damage cells via detergent action but it also undergoes photo-oxidation leading to the formation of DNA damaging epoxides.[19] A2E is predicted to be biosynthesized from 2 molecules of ATR and a molecule of phosphatidylethanolamine (PE) (Figure 6). The cyclization of PE activated ATR followed by oxidation and dephosphorylation is proposed to generate A2E.[9, 22-24]

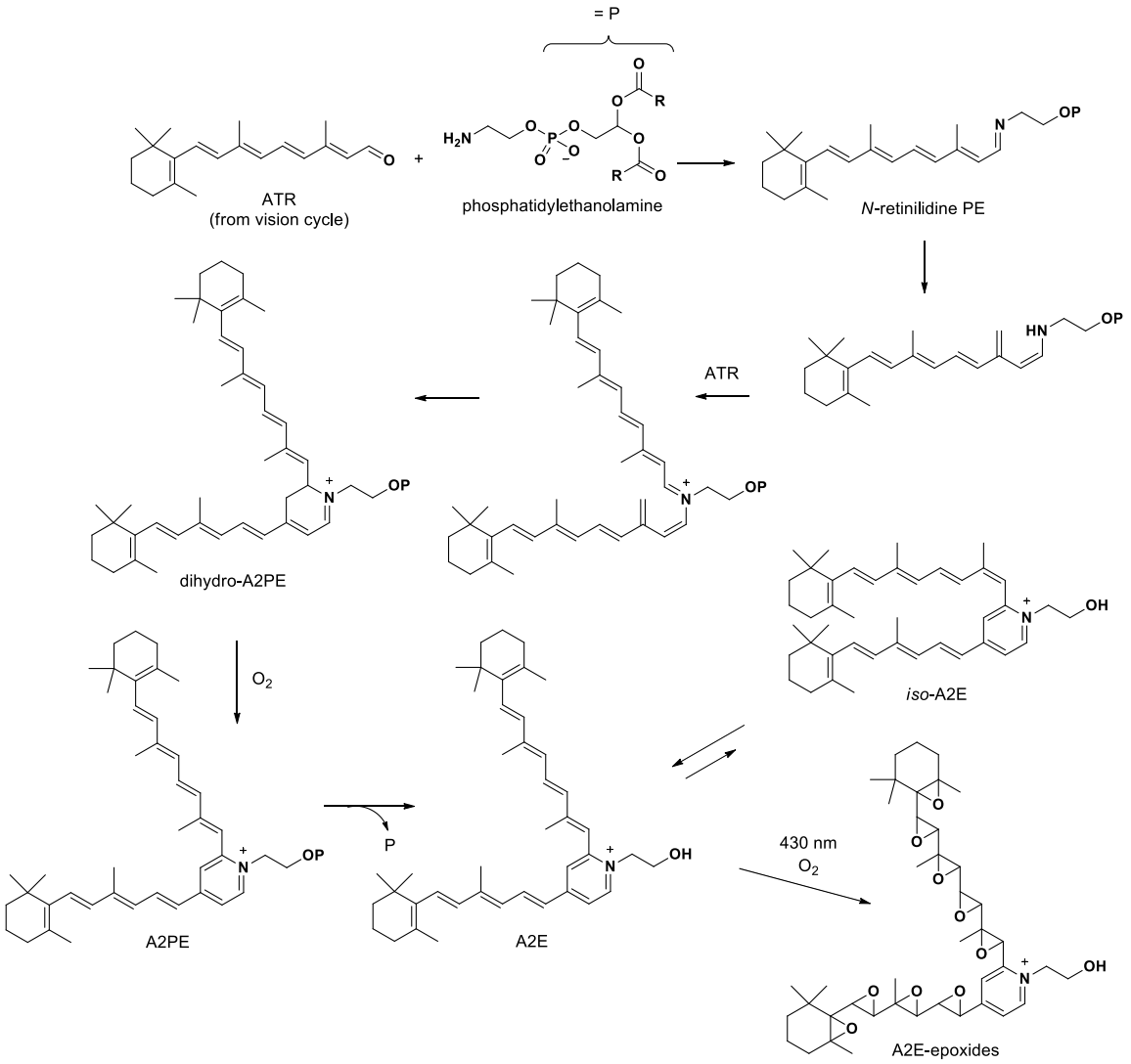

Figure 6 Proposed biosynthesis of retinoid-derived compounds found to accumulate in lipofuscins of the RPE.R groups in phosphatidylethanolamine designate the long alkyl chains.

1.4.2 Cycloretinal

A more recently characterized lipofuscin, ATR dimer or cycloretinal[21-26] is very similar to A2E but lacks the enthanolamine fragment. While the cell-toxicity of cycloretinal is not well studied, it is reasonable to predict that photo-oxidation of cycloretinal could lead to cell damage in a manner similar to A2E.

While cycloretinal could be generated chemically by activating ATR with an amine (like PE or proline) (Figure 7A),[9, 25] such reactions have not been shown to progress *in vitro* at physiological pH.[25, 27] An excess of base (triehylamine) is required for catalysis. Moreover, the identification that the R enantiomer of cycloretinal is preferably biosynthesized indicates the role of a stearic active site in this cyclodimerization.[21, 26] It is therefore proposed that this cyclodimerization could be protein catalyzed (Figure 7B).

1.5 Treatment of AMD

Patients diagnosed with early stage AMD, dry AMD or geographic atrophy have no recourse to therapeutics and are only advised to get regular eye checks, quit smoking and take multi-vitamins so as to prevent wet AMD.[28-30] Wet AMD is treated by injecting vascular endothelial growth factor (VEGF) inhibitors intravitreally at approximately six week intervals.[1] Drugs like pegapatnib (nucleic acid)[31] or bevacizumab (monoclonal antibody)[32, 33] are currently being injected to prevent the growth of blood vessels in the retina, thereby delaying ‘wet’ AMD.

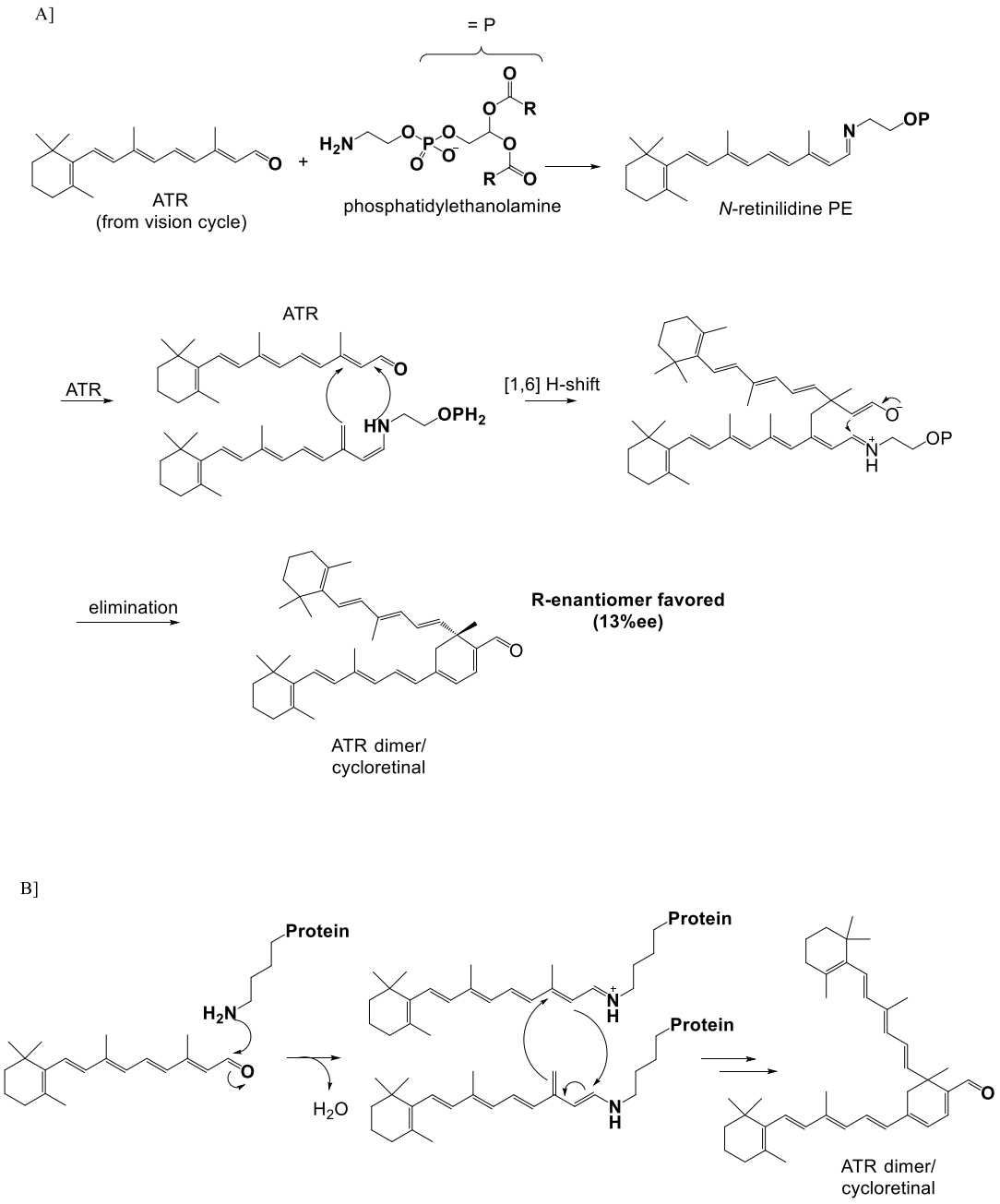

Figure 7 Proposed mechanism for cycloretinal formation mediated by A] phosphatidylethanoloamine B] proteinaceous lysine residues.

1.6 Beta-lactoglobulin and AMD

Investigations into the synthesis and biosynthesis of cycloretinal[21, 27, 34], a component of lipofuscin has led to the discovery that BLG can promote the cyclodimerization of ATR to cycloretinal both *in vitro* and *in vivo*.[35, 36] The identification of BLG in the drusen of people affected with AMD[18] and a study suggesting that milk consumption may lead to an increased likelihood of developing AMD[37] has led to the proposal that BLG may have a role in the biosynthesis of the lipofuscin cycloretinal.

BLG's availability (it can easily be isolated from the whey fraction of milk)[38] has resulted in nearly 300 papers studying the biochemical and biophysical properties of the protein being published yearly since 1996.[39-41] While the role of BLG in milk processing and its role as an allergen[42, 43] have been the target of extensive investigations in the dairy industry,[44-46] its stability at low pH,[47] the presence of a central hydrophobic cavity,[48] the Tanford transition,[49] its ability to bind lipids and retinol[39] and its similarity to retinol binding protein[50-52] have been of particular interest to protein chemists.
Despite all these investigations, a role for this milk protein in humans, if any, has not been identified.

1.7.1 Primary structure

A phylogenetic tree generated by comparing the primary amino acid sequence of bovine beta-lactoglobulin with BLG found in other mammals (Figure 8) shows that the *Bos taurus* protein is most similar to the BLG found in sheep, goats, bison and water buffalo, all members of the family bovidae. Interestingly, the primary amino acid sequence for BLG found in *Orcinus orca* (killer whale) is more similar to that of bovine BLG as compared to the BLG found in *Equus caballus* (horse).[(53)]

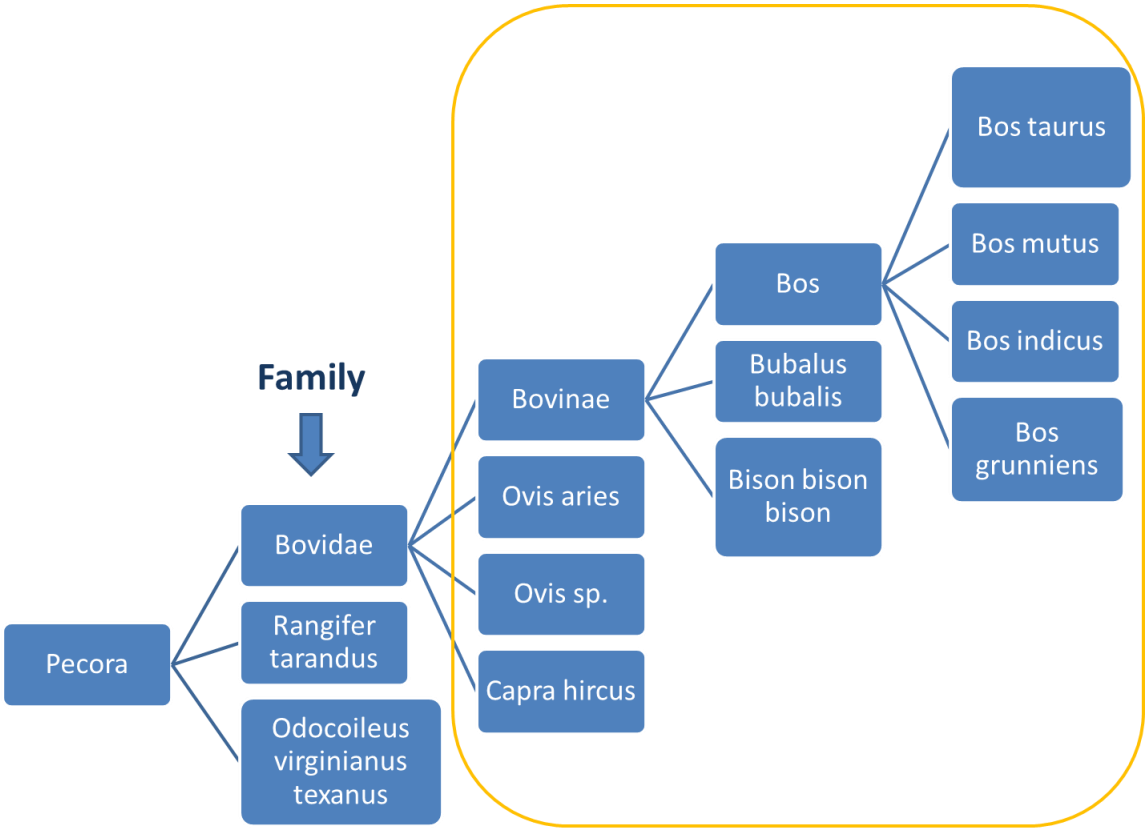

Figure 8 phylogenetic tree generated by comparing bovine BLG to BLG of other species

1.7.2 Tertiary structure

The three-dimensional structure of BLG has been well characterized by X-ray crystallography [38, 39, 41, 54-81] and nuclear magnetic resonance (NMR) spectrometry.[60, 82-85] BLG is an 18.4 kDa protein which contains nine beta strands and a single three-turn alpha helix (Figure 9). Eight of the nine beta strands fold into a beta-barrel that contains the central hydrophobic cavity or calyx. The ninth beta strand is believed to form the dimer interface in the bovine protein.[39]

A representative crystal structure of BLG bound to retinoic acid[62] shows that the beta-ionone ring of BLG is surrounded by hydrophobic residues: Leucine 32, Valine 43, Isoleucine 56, Phenyl alanine 105 and alanine 118. The polar carboxylate terminal of retinoic acid is surrounded by polar residues lysine 60, lysine 69 and glutamate 62 (Figure 10). ATR is postulated to bind similarly in the hydrophobic cavity with the aldehyde group set up to form an imine bond with either lysine.

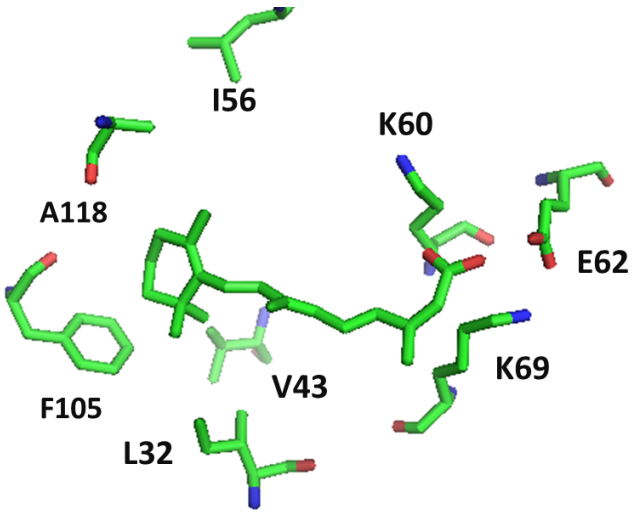

Figure 9 Central hydrophobic cavity of BLG with retinoic acid bound

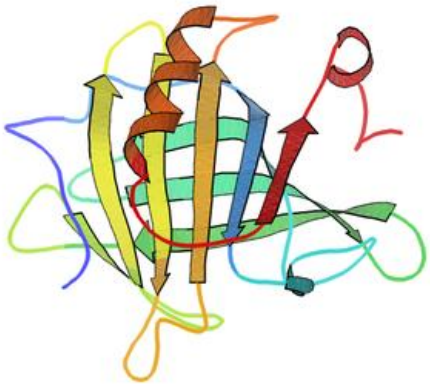

Figure 10 Cartoon of 3-dimensional structure of BLG

Various spectrometric studies support the theory that the EF loop of BLG located at the 'open' end of the central calyx moves to 'close' the calyx when pH is lowered from 7.1 to 6.2. This transition, referred to as the Tanford transition, suggests that the central calyx of the protein can only bind ligands at higher pH while being 'closed' at lower pH.[49, 83, 85, 86] Heteronuclear NMR studies indicate that the regions close to the entrance to the calyx (CD and EF loops) are locally unfolded at neutral pH which could correspond to the open state.[83, 85] There is some crystallographic evidence for this transition.[57, 59] The K_d of retinol with BLG at pH 2 or pH 7.5 is very similar suggesting that the tertiary structure of the protein is stable to acidic conditions.[47]

1.7.3 Quaternary structure

Bovine BLG is believed to exist as a dimer at neutral pH and as a monomer at lower pH.[39, 41] Comparison of crystal structures of goat,[87, 88] sheep[89, 90] and reindeer[91] BLG to

bovine BLG shows that all these proteins exist as dimers at native pH while horse BLG exists as a monomer.[39]

1.8 Ligand binding of BLG

Table 2 Selected ligand binding constants for bovine BLG

Entry	Ligand	K_d (M)	Entry	Ligand	K_d (M)
1	Lauric acid	7.0×10^{-7}	5	Vitamin D_2	4.91×10^{-9}
2	Palmitate	1.0×10^{-7}	6	Stearate	1.2×10^{-7}
3	Retinoic Acid	2.0×10^{-7}	7	Cholesterol	3.49×10^{-8}
4	Retinol	1.5×10^{-7}	8	β-Ionone	6.0×10^{-7}

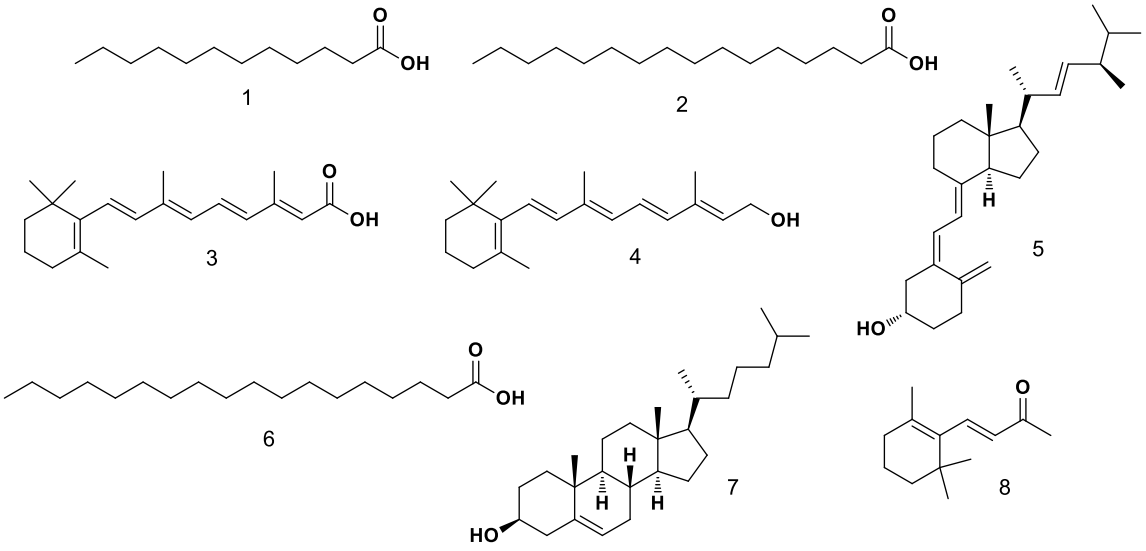

BLG has been crystallized with non-polar ligands including retinol,[62] retinoic acid,[62] vitamin D,[39, 67] dodecyl sulfate,[74, 76] and various fatty acids (stearic acid,[75] palmitic acid,[58] oleic acid,[75] myristic acid,[73] lauric acid,[56, 73, 74, 92] linoleic acid,[75] decanoic acid[55, 71]) bound in its central hydrophobic cavity. The native ligand of BLG has not been conclusively identified since BLG isolated from milk has not been crystallized with any ligands bound.

The binding of ligands to BLG in solution has also been studied by various techniques (Table 2) with fluorescence titration being the most popular one.[39] Since the initial discovery that retinol binds BLG, the energy transfer between a tryptophan residue of BLG (donor) and the ligand (acceptor) has been used to measure the dissociation constants for ligands[47] including sodium dodecyl sulfate, palmitic acid, stearic acid, retinoic acid and retinol.[93, 94] These studies have also reinforced the early observations that the K_d does not change when the pH is lowered from pH 7.5 to pH 2. The presence of a secondary binding site has been predicted with some crystal structures,[67] molecular docking[95] and FRET[96] studies finding evidence for multiple hydrophobic binding sites. An understanding of BLG catalyzed cyclodimerization may also help in the identification of a secondary binding site.

1.9 BLG functional analysis

BLG is classified as a lipocalin due to its eight stranded antiparallel beta barrel three-dimensional structure. Lipocalins are a family of proteins commonly associated with the transport of hydrophobic ligands.[97] BLG's structural similarity to retinol binding protein

(RBP) (Figure 11),another lipocalin, its ability to strongly bind retinol very similarly to RBP (K_d of both is in 10^{-8}M range),[52, 77, 97] its ability to solubilize hydrophobic ligands in aqueous solvents and its presence in human blood[93, 98] has led to the ascription of a transport function for this protein.

The discovery of receptors for BLG in the small intestine has supported the proposal[98] that BLG absorbs into the blood via the small intestine. Even though human blood has

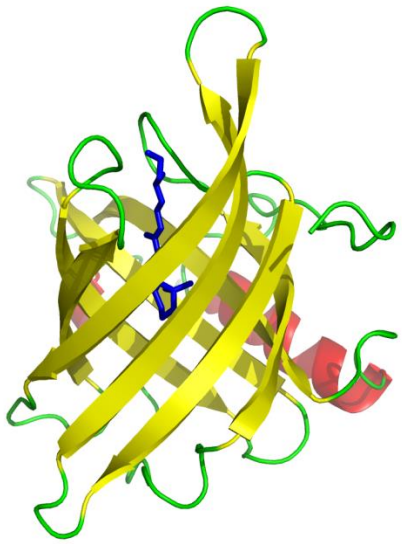

Figure 11 Cartoon of 3-dimensional structure of RBP

micro-molar concentrations of BLG in the human blood, very few studies have been undertaken to identify the fate of this protein. Using radioactive ^{125}I- BLG, researchers were able to show that BLG which was intravenously introduced into blood is secreted into the milk of lactating mice.[99] BLG has been found in the drusen of patients affected with

AMD.[18] Identifying the fate of blood BLG may help in identifying a transport function for this enigmatic milk protein.

While the native function of BLG has remained elusive, it has been a target of various functionalization studies. Two of the important ones to discuss are drug delivery and catalysis.

1.9.1 Applications of BLG in drug delivery

Drug development is prone to failure with many potential drugs being rejected for non-specificity or susceptibility to degradation. To improve specificity and stability, drug delivery systems with the following properties are applied:[100]

- Bio-compatibility: Any drug delivery agent has to be compatible with the living system that it is being applied to. Some of the most preferred targets for drug delivery development are therefore food or plant based compounds that are already regularly consumed or used in daily life and have been shown to be innocuous. Such materials prevent the necessity for costly clinical trials to prove their biocompatibility. Milk proteins are some of the most biocompatible compounds.[100] Despite BLG being an allergen, a vast majority of humans consume milk containing BLG. Therefore, it has been an attractive target for drug delivery development.
- Encapsulation properties: To prevent any active pharmaceutical or other ingredient from degrading, delivery agents are used to encapsulate the molecule. There are varying degrees of encapsulation. While protein binding the API in its cavity

prevents the material from degradation, this limits the choice of delivery agents to those that are naturally available and have the binding properties. Other techniques of encapsulation use the technique of self-assembly and co-assembly of protein nano-particles.[100] Nano-particles of protein isolates (10 to 100nm in size) are prepared and then allowed to assemble into micelles, either by heat induced aggregation or desolvation.[101] These micelles are then used to encapsulate target drug moelcules. Nanoparticles of BLG have been prepared and shown to be structurally stable even at low pH.[102] BLG-pectin nanoparticles have been introduced in acid beverages for delivery of vitamin D and other molecules.[100]

- Bio-accessibility: Drug delivery targets have to be accessible to the tissues or cells that they intend to target. This is especially important in the case of oral drug delivery vehicles. Oral drug delivery vehicles should be resistant to pepsin digestion and tough acidic stomach environment. They should be easily absorbed in the intestines and selectively aggregate in the cells or tissue systems that they intend to target. Therefore, proteins like BLG that are stable at low pH[47] and able to absorb into the blood through the small intestine[98] are special targets for applications as drug delivery agents.
- Bio-degradability: Any good drug delivery agent should be easily degraded and excreted from the body within a short period of time following the completion of its function. Proteins that can be easily degraded and excreted are generally the first targets for drug delivery application development.

Milk proteins other than BLG, mainly BSA are also well studied for drug delivery applications. For example, BSA nanoparticles for the delivery of the chemotherapeutic drug 5-fluorouracil have been developed.[100] Human Serum albumin (HSA) has been shown to accumulate in solid tumours resulting in the development of a methotrexate-albumin drug conjugate to selectively target tumour cells.[103]

1.9.2 BLG's catalytic applications

For a long time, no catalytic function was attributed to BLG. While BLG's native function might be as a carrier protein, like many other proteins,[104, 105] BLG may moonlight as a catalyst promiscuous in its activity. Bovine serum albumin, another milk protein has been shown to catalyze Kemp elimination reactions, thiomichael addition reactions and aldol and knoevenagel condensations.[106]

Even catalysts developed to perform specific functions, like catalytic antibody 38C2 which was raised to catalyze aldol reactions have been shown to catalyze reactions like the Kemp elimination. The enzyme was believed to use its hydrophobic pocket and the active site lysine to perform both aldol condensation and the Kemp elimination.[105]

The de-novo designed and directionally evolved retro-aldolase, RA95.5-8 with activity approaching that of natural class I aldolases [107] is not just capable of retroaldol breakdown of hydrophobic molecules but is also able to catalyze Michael additions[108] and

Knoevenagel condensations[109] indicating that the presence of a hydrophobic cavity and active site lysine introduces promiscuous activity to these enzymes (Scheme 1.1). Similarly, the presence of a pair of lysines in BLG along with its hydrophobic calyx leads to the possibility that BLG can catalyze some of these reactions as well.

Other work to introduce catalytic function to BLG includes the design of artificial metallocatalysts using BLG's hydrophobic cavity (described in detail earlier) to bind diimine ligands carrying various fatty acid substituents and their d6-piano stool Ru/Rh complexes and then applying the complex to perform transfer hydrogenation of an activated aryl ketone in aqueous solvent, thereby affording (R)-enantiomer of the corresponding alcohol with ee up to 32%.[110, 111] Further studies are underway to identify more functions for BLG and evolve its metalloenzymatic functionality.

While enzymes currently do not find widespread use in the manufacture of chemicals, stricter environmental regulations and the cost of metal based catalysts might force the chemical manufacturing industry to direct themselves towards using enzymes in catalysis in which case the widely available milk proteins might be the cheapest starting point. With this in mind and the development of molecular biology techniques to manipulate BLG in cow and goat milk,[112, 113] the exploration of BLG's catalysis functions may be significant.

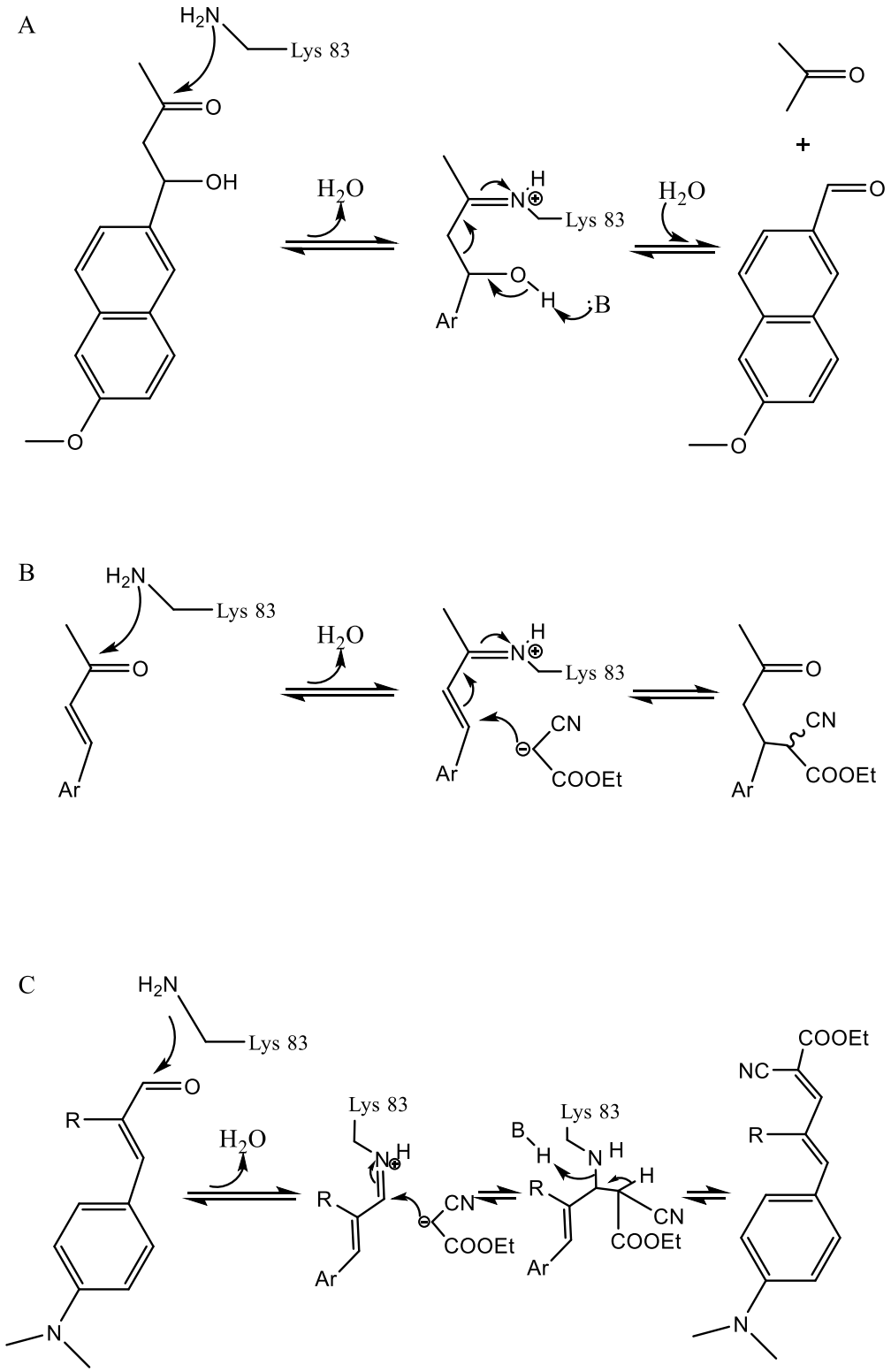

Scheme 1.1 Promiscuous reactions catalyzed by RA95.5-8

1.10 Statement of purpose

In these following chapters, we explain a novel strategy to express and purify recombinant BLG, and apply it to both probe the role of lysines in the cyclodimerization of ATR to cycloretinal as well as study the passage of BLG through the retina of BALB/c mice, all with the hope that these efforts may lead to a better understanding of the cause of AMD. We also demonstrate the retroaldolase activity of BLG and propose that BLG has the potential to be applied as a green catalyst in the chemical industry.

CHAPTER II

EXPRESSION AND PURIFICATION OF BLG

2.1 Introduction

80 years' investigation of BLG has shown that it can bind non-polar molecules,[(39)] is stable to pepsin digestion, can get absorbed into the blood through receptors in the small intestine,[(114)] and is present at micro-molar concentrations in blood serum.[(98)] Due to its presence in whey protein, and ease of isolation from milk, it is being applied as an encapsulation protein for nutraceutical delivery.[(100)]

BLG has been shown to catalyze cyclodimerization of α,β-unsaturated aldehydes to their respective cyclodimers.[(35)] To continue our investigations into BLG catalyzed cyclodimerization, to probe the role of lysines in cyclodimerization and to track the fate of serum BLG in animal models, we needed an efficient technique to express and purify BLG. While BLG has been expressed and purified in *P. pistoris*,[(115)] the added complexity of glycosylation deterred us from following this route. Expression in mammalian cells has been reported, [(116, 117)] but this route was too slow to pursue.

While it would be ideal to express BLG in *E.coli*, this technique has resulted in BLG being expressed in inclusion bodies,[116] likely due to the inability of the reducing environment of *E.coli* cytoplasm to support formation of the two disulfide bonds in BLG.[118] Origami DE3 (Novagen) cells are *E.coli* mutant cells with a cytoplasmic redox potential comparable to mammalian endoplasmic reticulum.[119] By co-expressing disulfide bond isomerase (DsbC) with BLG in Origami DE3 (Novagen), soluble protein was isolated.[119] Since the BLG was not tagged, the purification process included a precipitation step where the host cell protein was salted out by decreasing the pH. Around the same time New England Biolabs made commercially available an *E.coli* mutant that had a cytoplasmic redox potential comparable to mammalian endoplasmic reticulum and overexpressed DsbC (New England Biolabs catalog number C3029J). Other techniques to improve solubility of proteins that express in inclusion bodies include the use of solubility enhancing tags like *E.coli* maltose binding protein (MBP) which are known to promote proper folding and in some cases, even increase yield of their fusion partners.[120]

In this chapter, we detail our laboratory's success in expressing, purifying and characterizing soluble BLG (and its various mutants) using a cleavable, solubility enhancing *E.coli* maltose binding protein (MBP) tag.

2.2 Results and discussion

2.2.1 Expression of His_6 variant of BLG

DsbC expressing mutant of BLG, SHuffle® T7 Express (New England Biolabs) *E.coli* with a cytoplasmic redox potential similar to mammalian endoplasmic reticulum was expected to be capable of expressing BLG in the soluble form. Our attempts to express BLG in this mutant strain of *E.coli* as a His_6 variant failed to produce soluble protein. Other attempts by Dr. Jennifer Foulke-Abel to clone and express *E.coli* codon-optimized BLG variant B in popular pET or pQE vectors employing T7 or lac promoters also failed to produce soluble protein.

2.2.2 Expression of maltose binding protein (MBP) tagged variant of BLG

In our laboratory, the MBP-BLG fusion construct generated soluble fusion protein in excess of 100 mg/L under a *tac* promoter when induced with IPTG at 16°C. However, earlier attempts by Dr. Jennifer Foulke-Abel at cleaving MBP-BLG to obtain pure BLG using Factor Xa proved to be so inefficient a process that it was impractical to carry out at large scale. To explore different protein cleaving enzymes, a tobacco etch virus (TeV) cleavage site was strategically placed between the MBP and BLG proteins by Dr. Hillary Agbo.

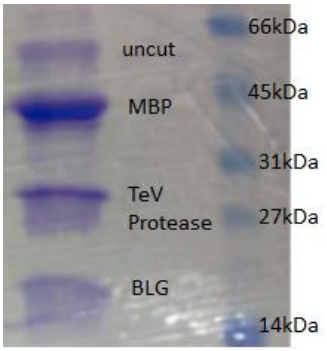

Figure 12 His_6 TeV protease cleavage of MBP-BLG fusion protein

His_6 TeV protease was expressed and purified in our lab. While the TeV protease cleaved our fusion protein efficiently to give BLG (Figure 12), His_6 BLG could not be separated from His_6 TeV protease. A modified strategy to express tag-less BLG and then separate it from His_6 TeV protease using ion-exchange chromatography yielded a mixture of uncut MBP-BLG fusion protein and cleaved BLG.

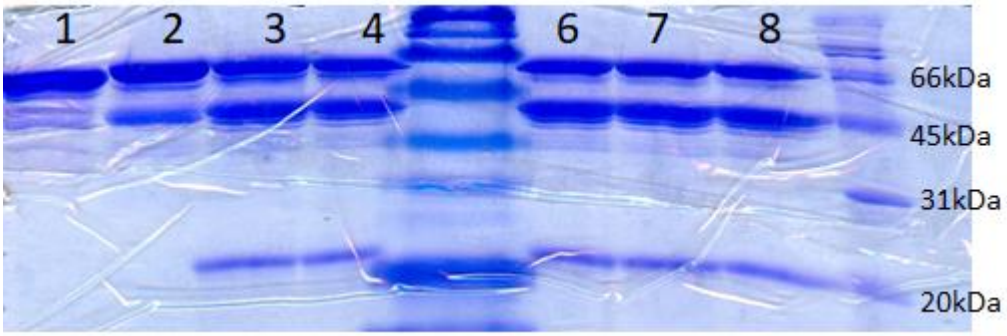

Figure 13 Screening of conditions for MBP-TeV protease catalyzed cleavage of fusion protein: 1] MBP-BLG fusion protein 2]MBP-Tev Protease 3] cleavage with 5mM DTT; 4^0C 4 days 4] cleavage with 20mM DTT; 4^0C 4 days 5] Ladder 6] cleavage with 1mM DTT; 30^0C o/n; 4^0C 3days 7] cleavage with 5mM DTT; 30^0C o/n; 4^0C 3days 8] cleavage with 10mM DTT; 30^0C o/n; 4^0C 3days

Subsequently, we designed a strategy which would use MBP-tagged TeV protease instead of the His_6 variant. Screening of cleavage efficiency indicated that the large MBP tag lowered the efficacy of the TeV protease. Evaluation of multiple cleavage conditions indicated that 30^{o}C overnight was optimal for cleavage (Figure 13). However, this resulted in a significant loss of yield due to protein precipitation. BLG's proven stability, and the need for a large amount of clean BLG, prompted us to cleave at 4 C over a week rather than 30^{o}C overnight. Attempts to purify the protein subsequent to cleavage using Nickel affinity chromatography proved difficult since the uncut fusion protein co-eluted with the cleaved protein. Unsuccessful efforts to remove the uncut fusion protein by trapping it on an amylose resin column could have been due to maltose tightly binding MBP.

To overcome this problem, we designed two strategies:

- 1M Methyl α-D-glucopyranoside has been reported to elute MBP tagged proteins. While this was not as efficient as maltose and did reduce yield, it also dissociated readily from MBP enabling the tagged protein to bind amylose resin on a second pass (Figure 14).
- The second strategy was to mix crude, clarified and filtered lysates of MBP-BLG and MBP-TeV protease together and incubate with 20mM DTT for a week. DTT, a known protease inhibitor does not inhibit TeV protease. Subsequent to cleavage, the mixture is purified by Nickel affinity chromatography to yield a mixture of uncut fusion protein and BLG. The uncut fusion protein is then bound to an amylose resin column resulting in clean BLG flowing through. This technique yielded 7mg/L cell culture of clean, pure BLG.

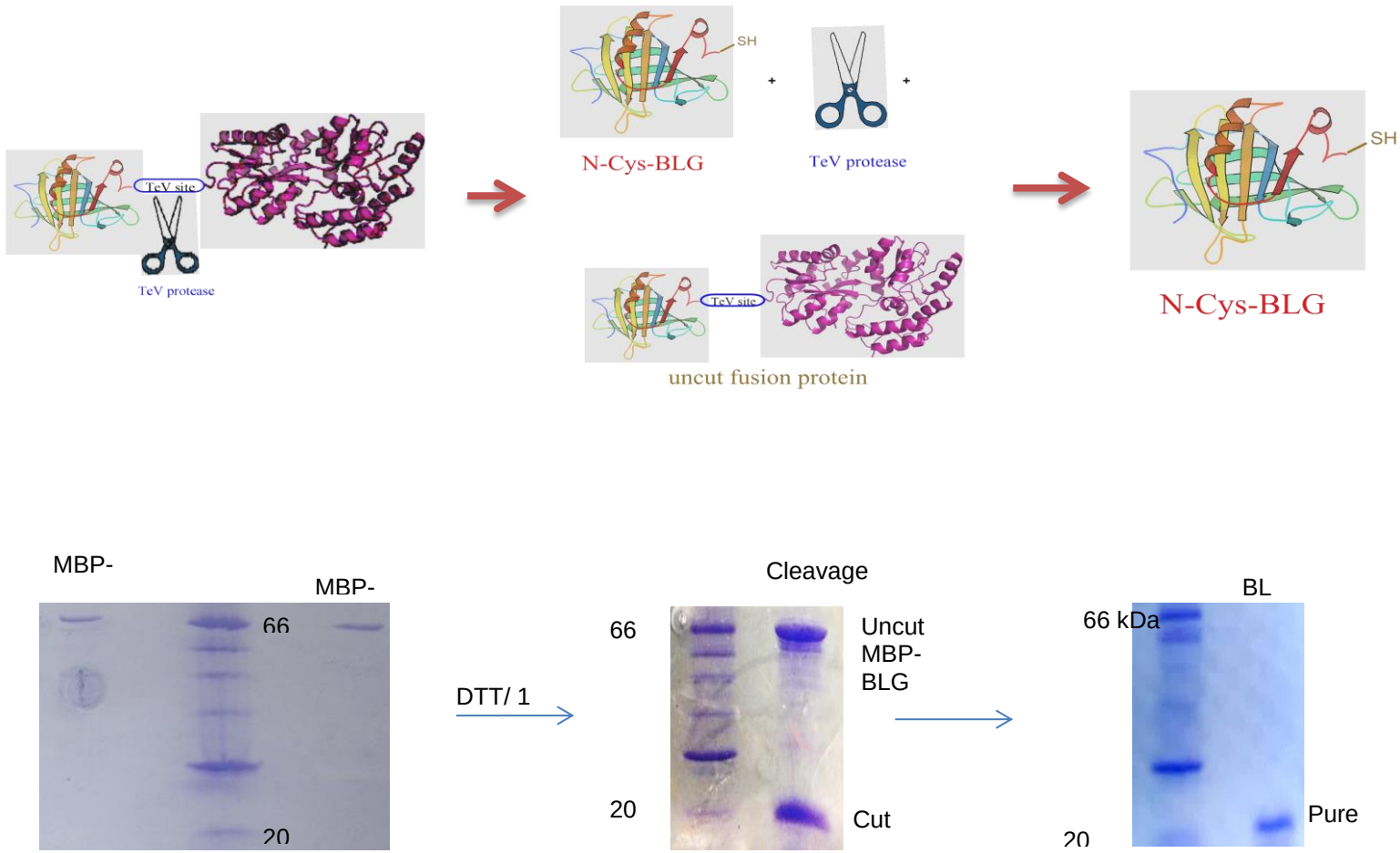

Figure 14 Schematic diagram illustrating the BLG cleavage and purification process

2.2.3 Characterization

The mass of the purified protein was analyzed by SDS-PAGE and ESI-MS. The mass detected by ESI-MS, 19404 Da matched the expected mass. Western blot analysis using anti-his antibody showed a single band corresponding to that of BLG (Figure 15).

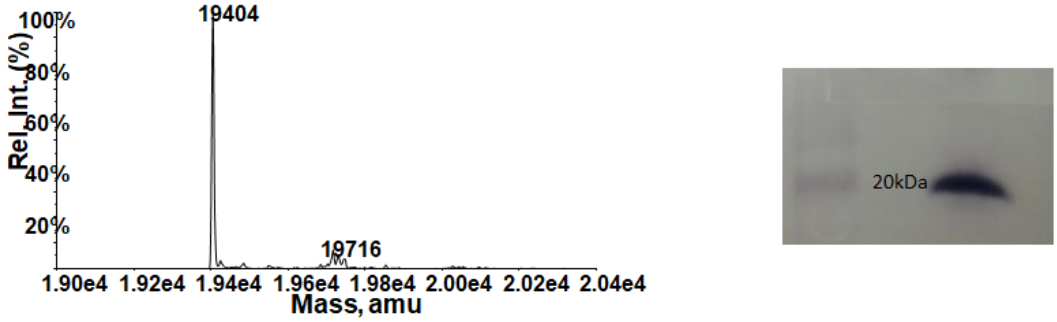

Figure 15 Characterization of purified BLG by mass spectrometry and western blot analysis

2.2.4 Mutagenesis

A mutant of BLG where all the lysines were mutated to alanine (KA-BLG) was generated and overexpressed with a MBP tag. However, since the MBP tag could not be cleaved, possibly due to the inaccessibility of the TeV site, 8 glycines were added at the N-terminal of BLG to introduce a spacer between MBP and BLG. This construct was cloned, overexpressed and purified to obtain KA-BLG protein. Mutants of KA-BLG, A77K,

A60K/A69K and A77K/A91K used in chapter 3 were also cloned, overexpressed and purified using the same strategy (Figure 16). KA-BLG and its mutants were observed to yield far less protein (0.5-2mg/L of cell culture) vs the wild-type variants (7mg/L of cell culture). The reduction in yield could be due to translation of mutants being affected in the absence of lysines.

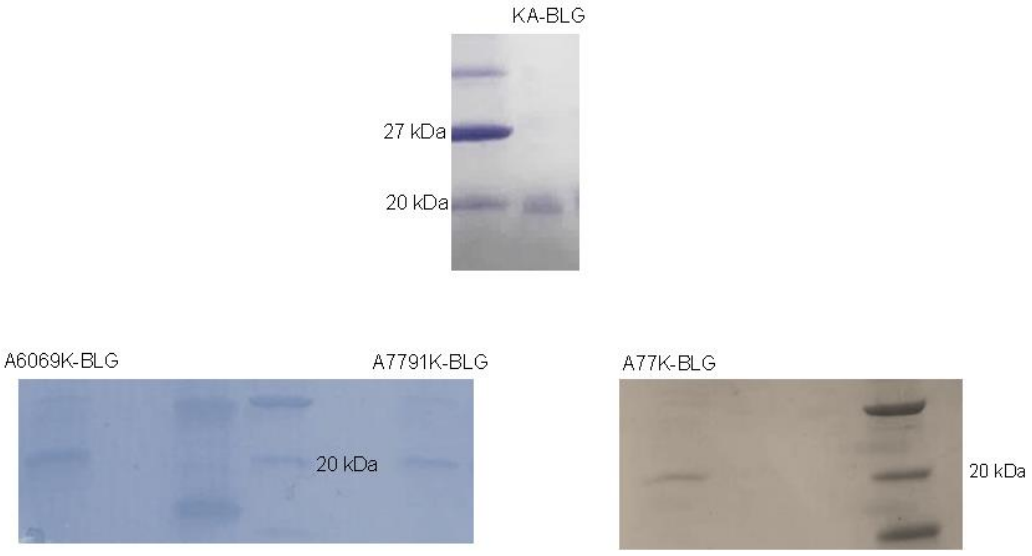

Figure 16 SDS-PAGE gels of purified KA-BLG; A6069K-BLG; A7791K-BLG and A77K-BLG

2.3 Significance

The study of BLG has been limited by the lack of an efficient strategy for its expression and purification in *E.coli*. Our strategy to express and purify BLG using a cleavable, solubility enhancing *E.coli* maltose binding protein (MBP) tag has afforded us not only wild-type BLG but also its various mutants. Optimization of *E.coli* to improve the

expression of disulfide bond containing proteins or the application of *in vivo* cleavage strategies may help in improving the yield of clean protein. While the expression, purification and characterization of BLG and its mutants will allow us to explore the mechanism of BLG catalyzed cyclodimerization as well as track serum BLG in mice, those researchers interested in constructing chimeras of BLG or directionally evolving BLG to improve substrate specificity or kinetics now have access to a competent strategy to obtain catalytically active BLG mutants from *E.coli*.

2.4 Experimental procedures

2.4.1 Cloning of wt-BLG

An *E. coli* codon-optimized version of *Bos taurus* BLG variant B (accession CAA88303) was synthesized and ligated to the TA cloning vector pQE-30UA (Qiagen, Valencia, CA) by GenScript (Piscataway, NJ) to generate the plasmid pQE30-BLG. To generate the maltose binding protein-BLG fusion construct, the BLG fragment was produced by PCR with primers BLG-BamHI-F and BLG-HindIII-R using pUC57-KA-BLG template with 1 Taq MasterMix (M0483). The N-terminal primer introduced a cysteine at the N-terminus of BLG. After agarose gel purification, digestion with *Bam*HI and *Hind*III, the PCR fragment was ligated to the vector pMAL-c4X (New England Biolabs) using T4 DNA ligase at 16 °C to give the vector pMAL-BLG. Following transformation in *E. coli* DH10B, colonies were screened by PCR to identify positive clones and sequenced using pMALseqF and pMALseqR primers.

2.4.2 Cloning of Lys to Ala Mutant of BLG (KA-BLG)

An *E. coli* codon-optimized version of *Bos taurus* BLG variant B with all lysine residues mutated to alanine was synthesized and ligated to the subcloning vector pUC57 by GenScript (Piscataway, NJ), giving plasmid pUC57-KA-BLG. To generate the maltose binding protein-BLG fusion construct, the KA-BLG fragment was produced by PCR with primers KA-BLG-BamHI and BLG-HindIII using pUC57-KA-BLG template with 1 Taq MasterMix (M0483). The N-terminal primer introduced 8 glycines at the N-terminus to facilitate TeV cleavage by introducing a long gap between the TeV site and the BLG protein. After agarose gel purification, digestion with *Bam*HI and *Hind*III, the PCR fragment was ligated to the vector pMAL-c4X (New England Biolabs) using T4 DNA ligase at 16 °C to give the vector pMAL-KA-BLG. Following transformation in *E. coli* DH10B, colonies were screened by PCR to identify positive clones and sequenced using pMALseqF and pMALseqR primers.

2.4.3 Site Directed Mutagenesis of KA-BLG

The QuikChange II Site-Directed Mutagenesis Kit (Agilent Technologies, Inc., Santa Clara, CA) was used to generate mutants A77K; A77&91K and A60&69K of KA-BLG. Primers (Table 3) were generated by the software provided on the Agilent website. Each of the mutants was generated utilizing pUC57-KA-BLG as a template. Double mutants A7791K-BLG and A6069K-BLG were obtained by mutating A77K and A69K, respectively. The mutants were then cloned into pMALC4X (New England Biolabs) using

the primers KA-BLG-BamHI-F and BLG-HindIII. The resulting constructs were sequenced to confirm the correct DNA sequence and the TeV site between MBP and BLG.

2.4.4 General conditions for overexpression and purification of BLG & its mutants

2.4.4.1 Overexpression

KA-BLG was transformed into BL21 DE3 cells by electroporation. The cells were then plated on LB-Agar plates containing ampicillin (100 µg/mL) and incubated overnight (~16 h). An individual colony was then selected and grown overnight in 15 mL of LB medium containing 100 µg/mL ampicillin at 37 °C. This starter culture was used to inoculate 1 L of LB Miller broth containing 0.2% glucose and 100 µg/mL ampicillin. The glucose helps to suppress endogenous amylases thus helping to increase protein expression. The culture was shaken (225 rpm) at 37 °C to an optical density of 0.8 at λ 600 nm. This culture was then cooled to 16 °C and induced with 1 mM isopropyl β-thiogalactopyranoside for 20 h at 16°C with a shaking frequency of 220 rpm. The cells were pelleted (7,000 rpm, 10 min), resuspended in 25 mL of column buffer (50 mM Tris-HCl pH 7.5, 200 mM NaCl, 1 mM EDTA, 10% glycerol) and stored frozen at -80 °C.

Table 3 Primers used in this study

Primer name	Primer sequence
BLG-BamHI-F	5'-GCA**GGATCC**TGTCTGATTGTGACCCA-3'
KA-BLG-G-BamHI-F	5'-GCA**GGATCC**GGCGGCGGCGGCGGCGGCG GCGGCCTGATTGTGACCCAGAC-3'
BLG-HindIII-R	5'-CTGGAAGAACAGTGTCACATTCACCACCAC CACCACCACTAA**AAGCTT**GGC-3'
A77K-F	5'-ATTATCGCGGAAGCAACCAAAATTCCGGCG GTGTTTGC-3'
A77K-R	5'-GCAAACACCGCCGGAATTTTGGTTGCTTCCG CGATAAT-3'
A91K-F	5'-GCAATTGATGCGCTGAATGAAAACAAAGTG CTGGTGCTGGAT-3'
A91K-R	5'-ATCCAGCACCAGCACTTTTCATTCAGCGCATC AATTGC-3'
A60K-F	5'-TCTGGAAATTCTGCTGCAGAAATGGGAAAACG GCGAATGC-3'
A60K-R	5'-GCATTCGCCGTTTTCCCATTTCTGCAGCAGAATT TCCAGA-3'
A69K-F	5'-CGGCGAATGCGCGCAGAAAGCAATTATCGCGG AA-3'
A69K-R	5'-TTCCGCGATAATTGCTTTCTGGCGCATTCGCCG-3'

2.4.4.2 Purification

The cell suspension was thawed at 4 °C. β-Mercaptoethanol and phenylmethylsulfonyl fluoride was then added to the cell suspension (1 mM final concentration). The cell suspension was lysed using a Branson Sonifier 450 fitted with a 5 mm microtip (6 15s pulses at 50% duty cycle, output setting 6, with 3 min cooling intervals). Care was taken to maintain the temperature of the cell suspension at 4 °C by carrying out the sonication in a cold room and keeping the solution on ice. The debris was pelleted at 12,000 rpm for 90 min. The resulting supernatant was diluted with column buffer (1:6 ratio) before applying to a 25 mL amylose resin (New England Biolabs) column (Kontes Flex-Column, 2.5 x 10 cm) that was packed by gravity-flow and equilibrated with column buffer. The column was subsequently washed with 12 column volumes of column buffer and MBP-BLG eluted with column buffer containing 1 M α-methylglucopyranoside (AMG). The purification process was carried out at 4 °C in a chromatography refrigerator. The resulting protein was confirmed by SDS-PAGE and the concentration of the protein determined by Bradford assay using commercial Bovine Serum Albumin (BSA) as a standard. BSA was used as a standard since the size of BSA (66 kDa) is very similar to the size of the fusion protein. All mutants of BLG were expressed and purified as per the protocol detailed above.

2.4.5 Overexpression and Purification of MBP-TeV Protease

2.4.5.1 Overexpression

The construct expressing an autolysis-resistant S219V mutant of MBP tagged TeV protease (addgene Plasmid #8835)[(121)] was transformed into BL21 DE3 cells along with the tRNA accessory plasmid pRIL (from the BL21 CodonPlus strain, Stratagene) by electroporation. The cells were plated on LB-agar medium containing chloramphenicol (30 µg/mL) and ampicillin (100 µg/mL) and incubated overnight. An individual colony was then selected and grown overnight in 15 mL of LB medium containing chloramphenicol (30µg/mL) and ampicillin (100 µg/mL) at 37 °C. This starter culture was used to inoculate 1 L of LB Miller broth containing 0.2% glucose, chloramphenicol (30 µg/mL) and ampicillin (100 µg/mL). The glucose helps suppress endogenous amylases, thus helping increase protein expression. The culture was shaken (225 rpm**)** at 37 °C to an optical density of 0.8 at λ 600 nm. This culture was then cooled to 30 °C and induced with 1 mM isopropyl β-thiogalactopyranoside for 4 h. The cells were pelleted (7,000 rpm, 10 min), resuspended in 25 mL column buffer (50 mM Tris.HCl pH 7.5, 200 mM NaCl, 1 mM EDTA, 10% glycerol), and stored frozen at -80 °C.

2.4.5.2 Purification

The MBP-tagged TeV protease was purified using the protocol that was used to purify the BLG fusion protein. The presence of the protein was confirmed by SDS-PAGE analysis.

The concentration was assessed by Bradford assay using commercial Bovine Serum Albumin (BSA) as a standard.

2.4.6 Cleavage of the BLG Fusion Proteins by MBP tagged TeV Protease

A schematic diagram illustrating the overall cleavage and protein purification process is shown in Figure 1, pg. S11. To achieve cleavage, the purified KA-BLG protein and the MBP-TeV protease were dialyzed by centrifugal ultrafiltration (Amicon Ultra-15 Centrifugal Filter Unit, Millipore, Billerica, MA) to a final concentration of 1 mg/mL in column buffer (50 mM Tris.HCl pH 7.5, 200 mM NaCl, 1 mM EDTA, 10% glycerol). The proteins were mixed and dithiothreitol (DTT) was added to give a final concentration of 20 mM. The cleavage mixture was subsequently incubated at 4 °C for a 1 week period. During screening trials, cleavage conditions were varied by changing the concentration of DTT added after buffer transfer and by varying the incubation temperature and duration. Optimal conditions were found to be 20 mM DTT at 4 °C for 1 week. Cleavage was monitored by SDS-PAGE analysis. Following incubation, the cleavage mixture was dialyzed by centrifugal ultrafiltration with loading buffer (50 mM Tris.HCl pH 7.5, 200 mM NaCl, 5 mM imidazole, 10% glycerol). The protein was diluted to 50 mL and applied to a pre-equilibrated HisTrap FF 5 mL column (GE Healthcare Life Sciences, Piscataway, NJ) using a peristaltic pump at a rate of 0.2 ml/min. The column was washed with 200 mL of wash buffer (50 mM Tris.HCl, pH 7.5, 200 mM NaCl, 20mM imidazole, 10% glycerol) for 16 h. The column was subsequently washed with 25 mL of wash buffer containing 100 mM of imidazole. Clean protein was eluted with elution buffer (50 mM Tris.HCl, pH 7.5,

200 mM NaCl, 250mM imidazole, 10% glycerol) and the resulting protein analyzed by SDS-PAGE. The concentration of the protein determined by Bradford assay using BLG obtained from Davisco as a standard.

2.4.7 Cleavage of wt-BLG Fusion Protein by MBP tagged TeV Protease without intial purification

The cell suspension of wt-BLG and MBP tagged TeV Protease was thawed at 4 °C. β-Mercaptoethanol and phenylmethylsulfonyl fluoride was then added to the cell suspension (1 mM final concentration). The cell suspension was lysed using a Branson Sonifier 450 fitted with a 5 mm microtip (6 15s pulses at 50% duty cycle, output setting 6, with 3 min cooling intervals). Care was taken to maintain the temperature of the cell suspension at 4 °C by carrying out the sonication in a cold room and keeping the solution on ice. The debris was pelleted at 12,000 rpm for 90 min. The resulting supernatants were subsequently filtered by passing through a 0.2 μm filter. 25mL of wt-BLG supernatant and 25mL of MBP-TeV protease supernatant was then mixed together. 1mL of 1M DTT was added to the resulting mixture to give a final concentration of 20mM DTT. This cleavage reaction was incubated at 4^0C for 1 week. Subsequently, the mixture was dialyzed by centrifugal ultrafiltration (Amicon Ultra-15 Centrifugal Filter Unit, Millipore, Billerica, MA) with loading buffer (50 mM Tris.HCl pH 8.0, 200 mM NaCl, 5 mM imidazole, 10% glycerol). The protein was diluted to 50 mL and applied to a pre-equilibrated HisTrap FF 1 mL column (GE Healthcare Life Sciences, Piscataway, NJ) using a peristaltic pump at a rate of 0.2 ml/min. The column was washed with 15 column volumes of wash buffer (50

mM Tris.HCl, pH 8.0, 200 mM NaCl, 20mM imidazole, 10% glycerol) for 16 h. Clean protein was eluted with elution buffer (50 mM Tris.HCl, pH 8.0, 200 mM NaCl, 250mM imidazole, 10% glycerol) and the resulting protein analyzed by SDS-PAGE. The concentration of the protein determined by Bradford assay using BLG obtained from Davisco as a standard.

2.4.8 Mass Spectrometric Analysis

BLG solutions (0.4mg/mL) was dialyzed by centrifugal ultrafiltration (Amicon Ultra-0.5mL 3kDa Centrifugal Filter Unit, Millipore, Billerica, MA) in 50mM ammonium acetate (pH=7.08) to a final concentration of 2mg/mL. This solution was prepped using zip-tip columns from Millipore. The tip was wet by withdrawing 20 µL acetonitrile twice. It was then equilibrated with 0.1% formic acid by pipetting out 20 µL of 0.1% formic acid four times. Sample was then bound to this tip by pipetting 20 µL of the sample ten times. To remove salt, the tip was then washed with 0.1% formic acid by pipetting 20 µL of the formic acid solution ten times. Finally, sample was eluted into a small, clean centrifuge tube by pipetting 15 µL of 7:10 (Acetonitrile/water) with 0.1% formic acid in and out of the loaded pipette tip.

2.4.9 Western blot analysis

After the protein was transferred to PVDF membraine (10V, 165 min), the membrane was incubated in blocking solution (3% bovine serum albumin solution in TBS buffer (50mM

NaCl, 10mM Tris-HCl pH 7.5)) for 60 minutes. Subsequently, the membrane was washed twice with TBSTT buffer (500mM NaCl, 20mM Tris-HCl pH 7.5, 0.2% Triton X-100, 0.05% Tween-20) for 20 minutes. The membrane is then incubated with primary antibody (1μg his-tag monoclonal antibody in 10 mL blocking solution) for 10 minutes after which it was washed with 20mL TBSTT in two washes for a total of 20 minutes. The membrane was then washed with 15 mL TBS buffer for 10 minutes. Afterwards, the membrane was incubated with secondary antibody (2μL goat anti-mouse AP conjugate in 10mL blocking solution) and then washed 4 times for 10 minutes each with 20mL TBSTT buffer. To stain the membrane, AP detection reagent kit (Novagen 69264-3) was used. NBT-BCIP solution (750 μL 20X AP buffer, 60μL NBT, 60μL BCIP made up to 15mL with water) was added to the membrane and allowed to sit without shaking. Once color developed, the membrane is washed in water and air dried.

CHAPTER III

LIPOFUSCIN FORMATION CATALYZED BY THE MILK PROTEIN BETA-LACTOGLOBULIN: LYSINE RESIDUES IN CYCLORETINAL SYNTHESIS

3.1 Introduction

Cycloretinal **3.2**, also referred to as *all-trans* retinal dimer (Figure 17), has been isolated from the human eye and is one of several metabolites associated with age-related macular degeneration (AMD).[19, 22, 25, 26] AMD is the most common cause of blindness affecting adults over the age of 50.[122] In the early stages of the disease, the 'dry' form, this medical condition begins with the accumulation of yellow and white deposits in the macula (the central part of the retina of the eye). These deposits contain lipofuscins, by-products of the visual cycle such as cycloretinal and A2E.[1, 19, 22, 25, 26] In the advanced stage of the disease, the 'wet' form', blood vessel leakage results from vascularization of the macula leading to the loss of central vision.

Parts of this chapter are reprinted with permission from 'Gowda, V., Foulke-Abel, J., Agbo, H., Bench, B. J., Chae, J., Russell, W. K., and Watanabe, C. M. H. (2017) Lipofuscin Formation Catalyzed by the Milk Protein β-Lactoglobulin: Lysine Residues in Cycloretinal Synthesis, *Biochemistry 56*, 5715-5719'. Copyright (2017) American Chemical Society

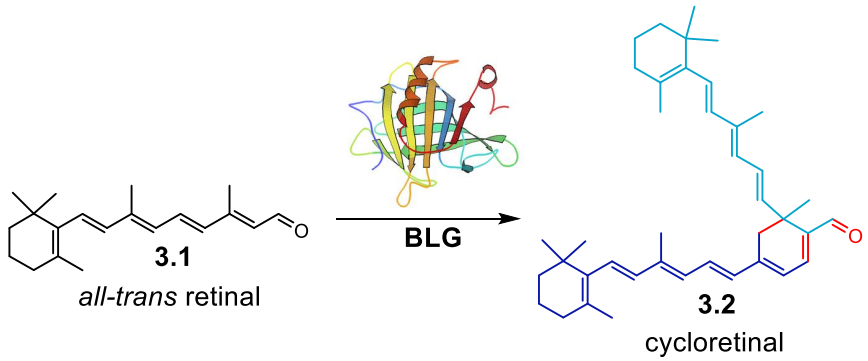

Figure 17 BLG catalyzed cyclodimerization of retinal to cycloretinal

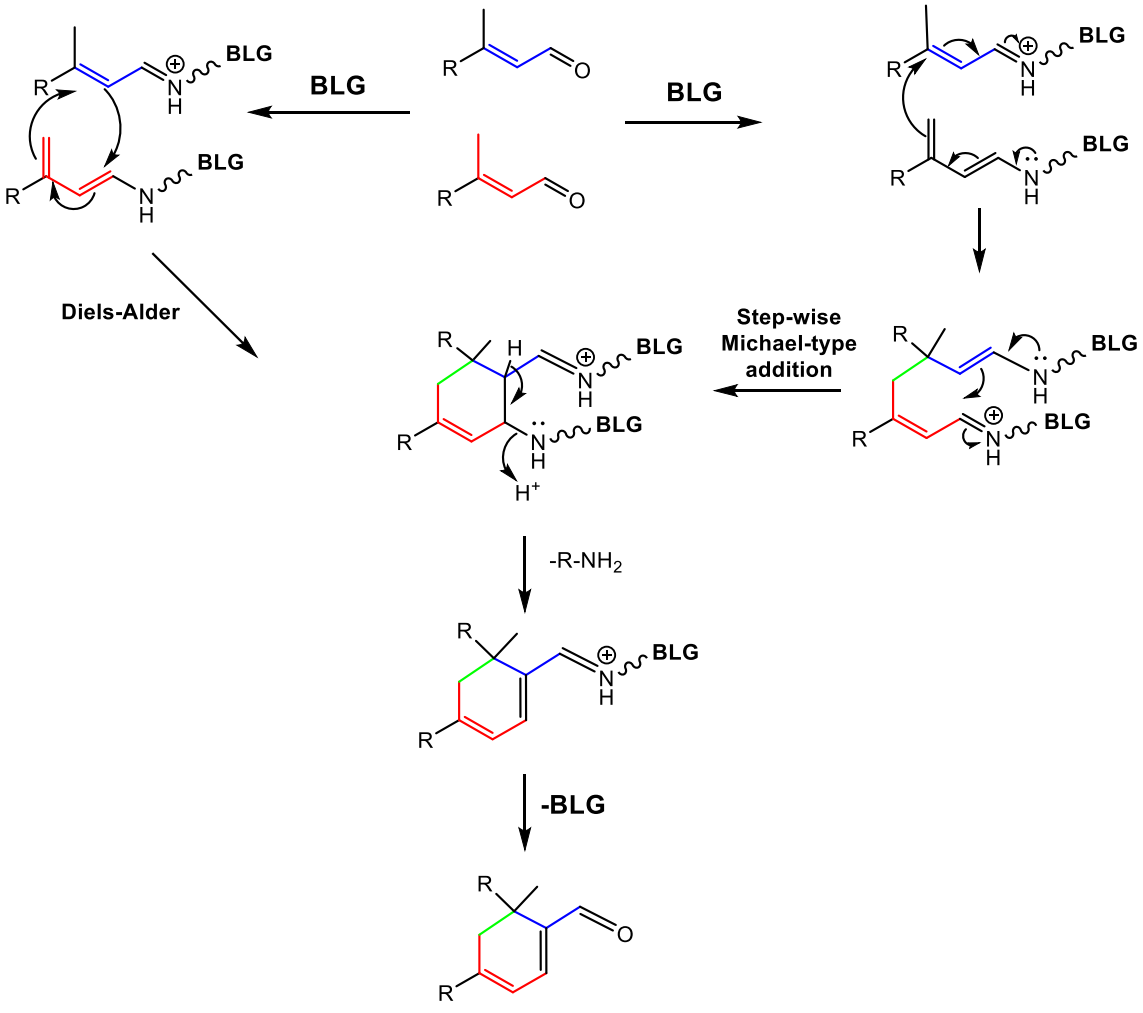

Figure 18 Proposed mechanism for BLG catalyzed cyclodimerization

Bovine β-lactoglobulin (BLG) is a highly stable small protein (18.4 kDa) that constitutes between 12–15% of the protein content of milk. Although the protein has been extensively investigated,[41] its biological function has yet to be assigned. While BLG has been speculated as a transport protein, we have observed that the protein possesses moonlighting activity and is capable of promoting cyclodimerization of α, β-unsaturated terpenals to their respective cycloterpenals (Figure 17). This includes the formation of cycloretinal **3.2**, formed through condensation of *all-trans* retinal **3.1**, *in vitro* and *in vivo*, as has been shown with a rabbit study.[35] The cycloterpenals are a family of natural products of terpenoid biosynthetic origin with a central cyclohexadienal structural motif.[34, 123] It is proposed that BLG can catalyze the condensation of α, β-unsaturated aldehydes through one of two possible pathways: a stepwise Michael-like imine addition or a concerted Diels-Alder-type reaction (Figure 18). For the reaction to proceed, both mechanisms require the activation of aldehyde residues via the formation of a Schiff base with lysine residues of the protein. In this study, we evaluate the involvement of lysine residues via Schiff base formation in facilitating the reaction as well as the need of a physical binding pocket to promote catalysis.

3.2 Results and discussion

BLG contains 15 lysine residues within its primary sequence, 4 of which are contained within binding sites. Analysis of the BLG crystal structure (PDB: 1GX9) reveals a central calyx, which has been reported to bind retinal **3.1**. Lysine residues K60 & K69, which span 4.8 Å, line the active site (Figure 19A). A secondary binding site has been thought to exist

on the β-barrel exterior[67] with lysines K77 and K91 situated within ~12 Å of each other (based on crystal structure 1B8E, Figure 19B). In its native state, BLG exists as a dimer (Figure 19C).

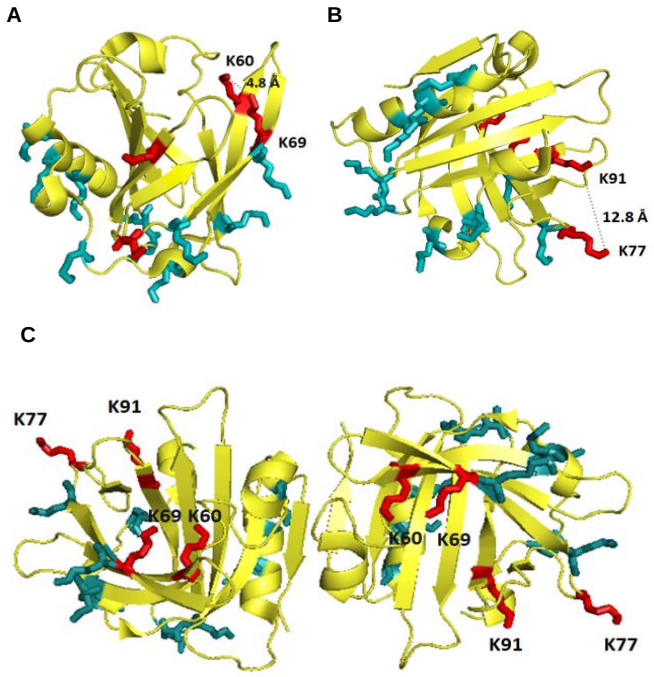

Figure 19 BLG lysine residue pairs postulated to be involved in cycloterpenal catalysis: [A] Residues K60 and K69 on the β-barrel wall interior, [B] Residues K77 on the flexible loop and K91 on the β-barrel exterior, (1GX9), Lysine side chains are highlighted in red (1B8E), [C] Native dimer structure of BLG (1B8E)

To evaluate the involvement of Schiff base formation and the role of lysine residues in cyclodimer formation, the reaction mixture was treated with sodium cyanoborohydride. This serves to trap the Schiff base intermediate (formed between the lysine and its aldehyde substrate and/or product) and reduces the imine bond to its corresponding amine. Since retinal and cycloretinal display light and temperature sensitivity, we employed the substrate analog citral to explore the BLG chemistry. Following reduction, the protein-

bound complexes were fragmented by trypsin digest and the resulting short peptides analyzed by ESI-MS. MS/MS analysis was performed, which enabled MASCOT-assisted prediction of peptide sequences. Mining of fragment signatures revealed peptides containing residues K77 and K91 with citral substrate bound, and residue K91 with the product cyclocitral bound (Figure 20). Residues K77 and K91 are situated within reasonable proximity of one another, 12.8 Å (Figure 19B). While K91 would be considered fairly immobile on the outer wall of the β-barrel, K77 resides on a flexible loop and could facilitate the reaction. However, time-course analysis revealed additional fragments of citral bound lysine residues, distributed in a randomized fashion, throughout the protein. This is perhaps not surprising as the reaction is carried out with excess citral to achieve target residue saturation. In a standard extraction of BLG incubated with citral, the aqueous phase retains a deep orange color (indicative of a citral-protein Schiff base) even after exposure to organic solvent. While no additional lysine residues other than K91 showed product bound, this raised some degree of ambiguity in the results.

The generation and evaluation of BLG lysine mutants was the logical next step. As the purified MBP-BLG fusion was shown to retain its activity to support cycloterpenal formation, site-directed mutagenesis was performed, generating lysine to alanine mutants at each of the fifteen positions. However, as these mutants were not inactivating cycloterpenal formation as shown by HPLC, we modified the strategy whereby BLG was expressed as its MBP fusion and subsequently cleaved using a tobacco etch virus (TeV) cleavage site that was strategically placed between the MBP and BLG proteins. A C-terminal His-tag on BLG was used to aid in the isolation of BLG. Circular dichroism (CD)

analysis of BLG showed no discernible change while monitoring the course of the reaction, which suggested no to minimal conformational change during the catalytic process and formation of cycloretinal (Figure 21).

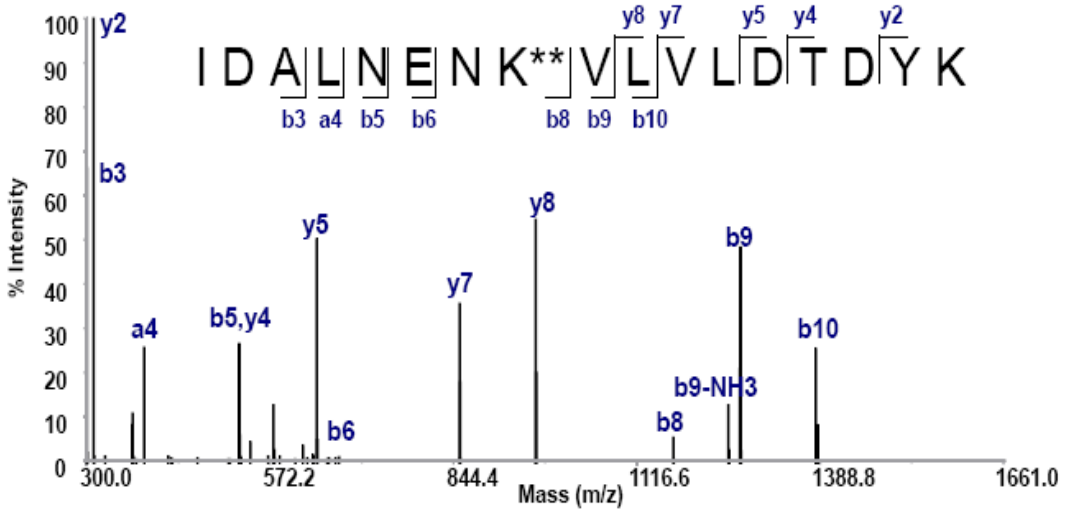

Figure 20 Mass spectrometric results obtained after trypsin digestion of BLG showing cyclocitral (homodimer product) bound to K91

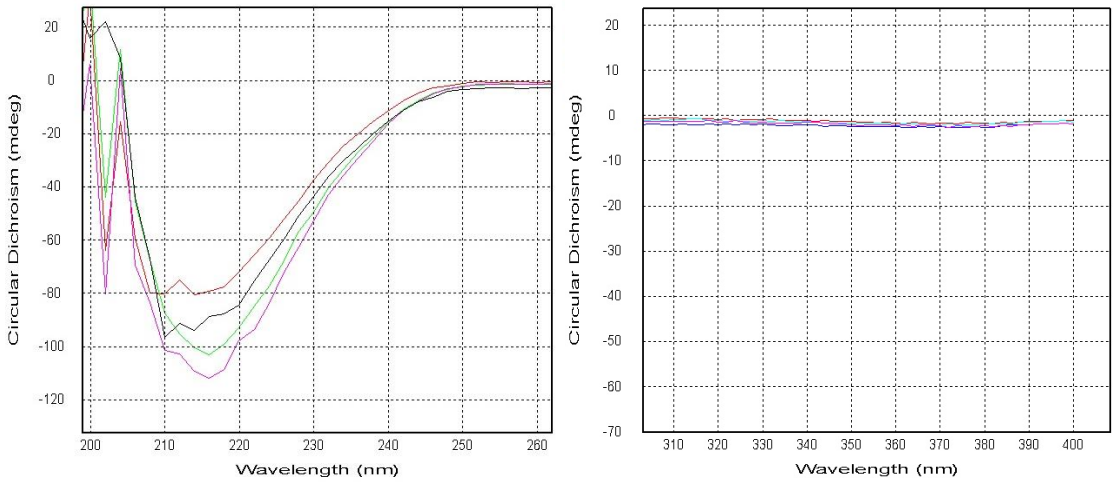

BLG and retinal over 1] 17hours 2] 41 hours 3] 72 hours 4] 90 hours

Figure 21 CD analysis of BLG catalyzed cyclodimerization of all-trans retinal

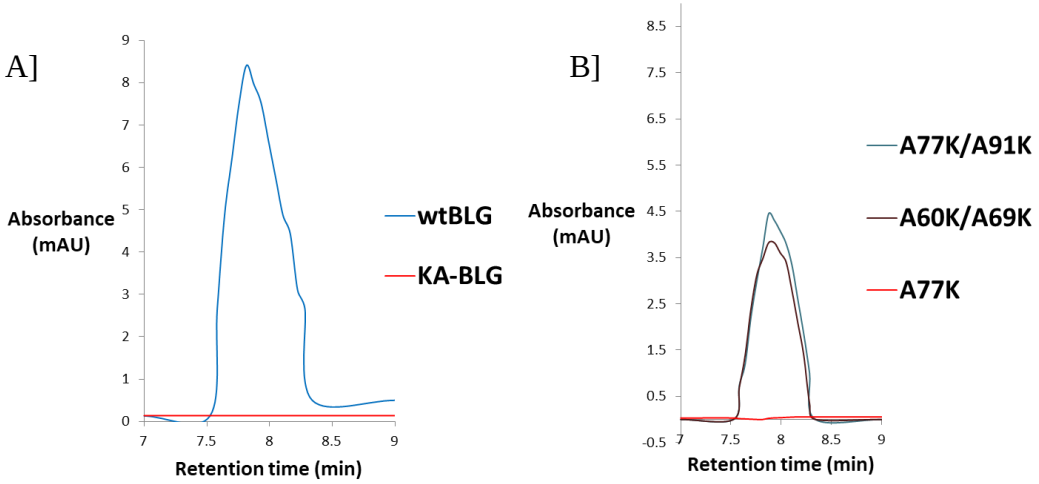

Figure 22 HPLC analysis of cyclodimerization activity of BLG and mutants: A] wtBLG, KA-BLG B] A77K/A91K-BLG, A60K/A69K-BLG, A77K-BLG

To evaluate the role of lysines in cyclodimerization, we mutated each of the lysine residues of BLG to alanine (KA-BLG), to effectively "blank" the activity, with the idea of adding back specific lysine residues for evaluation. The KA-BLG construct was cloned, overexpressed and shown to generate soluble protein. We evaluated the ability of KA-BLG to promote cycloretinal formation utilizing an HPLC assay (Figure 22A). The crude product was derivatized with 2, 4-dinitrophenylhydrazine (DNPH), analyzed by HPLC and quantified using a standard curve generated using a DNPH derivatized synthetic cycloretinal standard.

With this assay, the KA-BLG mutant was shown to inactivate cyclodimerization (Figure 22A), negating cycloretinal formation. We, therefore, generated two sets of mutants. We re-introduced the central calyx lysines K60 and K69 into KA-BLG giving A60K/A69K-BLG and the secondary binding site lysines K77 and K91 giving A77K/A91K-BLG (Figure 22B). Both sets of mutants restored activity, demonstrating that each pair of lysine residues is catalytically active. Total turnover number is defined as the ratio of moles of product generated divided by the moles of biocatalyst used in a reaction and is used to quantify activity of enzymes involved in non-native catalysis.[124, 125] Comparison of total turnover number of both mutants (1.7 ± 0.1 μM per mM for A77K/A91K-BLG and 1.5 ± 0.1 μM per mM A60K/A69K-BLG) showed that they were not as active as wild-type BLG (4.3 ± 0.2 μM per mM protein), which is consistent with the wild-type protein having more than one catalytic site. To evaluate whether a single lysine residue is capable of catalyzing the reaction, we generated BLG with a single mutation, giving A77K-BLG (Figure 22B).

The single mutant was incapable of promoting the reaction, which is suggestive that two lysine residues are required for catalysis.

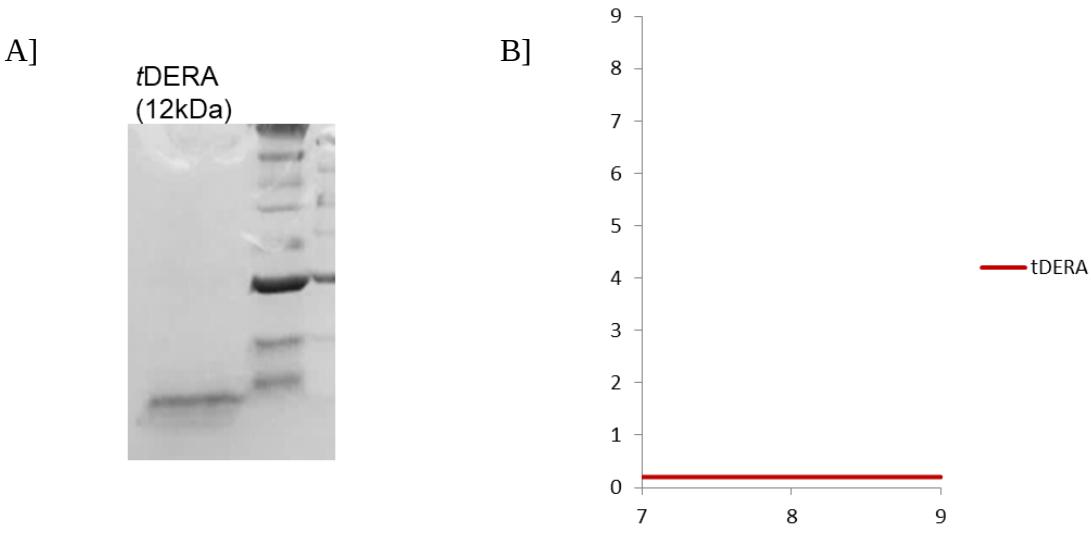

Figure 23 SDS-PAGE analysis [A] and HPLC analysis of cyclodimerization activity [B] of tDERA

To further corroborate these results, a 100-amino acid long truncated peptide mutant of DERA (deoxyribose 5-phosphate aldolase is a well-expressed *E. coli* protein), tDERA, was cloned, overexpressed and assayed for activity (Figure 23A). Despite having six lysines, tDERA was also shown to be catalytically inactive (Figure 23B), and demonstrates the importance of having a binding site to promote catalysis. SDS-treatment of BLG inactivates activity (Figure 24), which further reflects the importance of BLG's tertiary structure and hydrophobic binding sites in the condensation process and formation of cycloretinal.

.

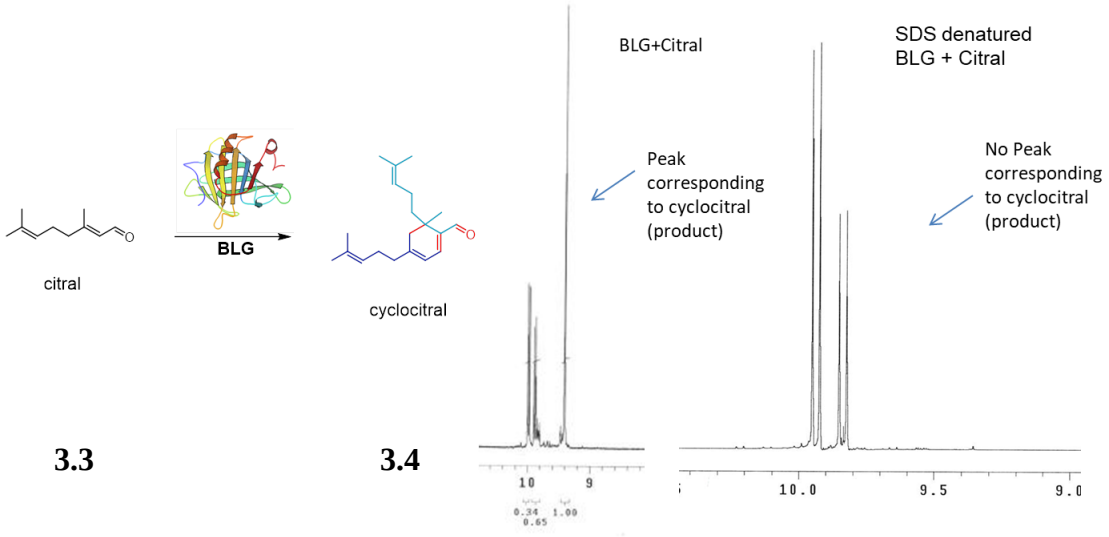

Figure 24 1H-NMR analysis showing that SDS treated BLG does not catalyze cyclodimerization

Homology studies on BLG and a phylogenic analysis (Appendix figure 6 & 7, Page 119-120) show that lysines 60, 69, 77 and 91 are highly conserved within members of the *Bovidae* family (cattle, bison, buffalo, sheeps and goats). However, in comparison to other families that make up the order *Cetartiodactyla* including the *Cevidae* family (white-tailed deer and reindeer), the *Delphinidae* family (killer whales), the *Physeteridae* family (sperm whales) or the *Balaenopteridae* family (minke whales), lysine residues are shown to be mutated to glutamate. Based on the literature, it is unclear as to what extent these animals suffer from AMD or whether the protein is present in the eye. While humans have no BLG homolog, BLG is transported to human serum from our diet[(98)] and proteomic studies on both normal individuals and those with AMD have identified BLG as one of the major proteins in the eye.[(18)]

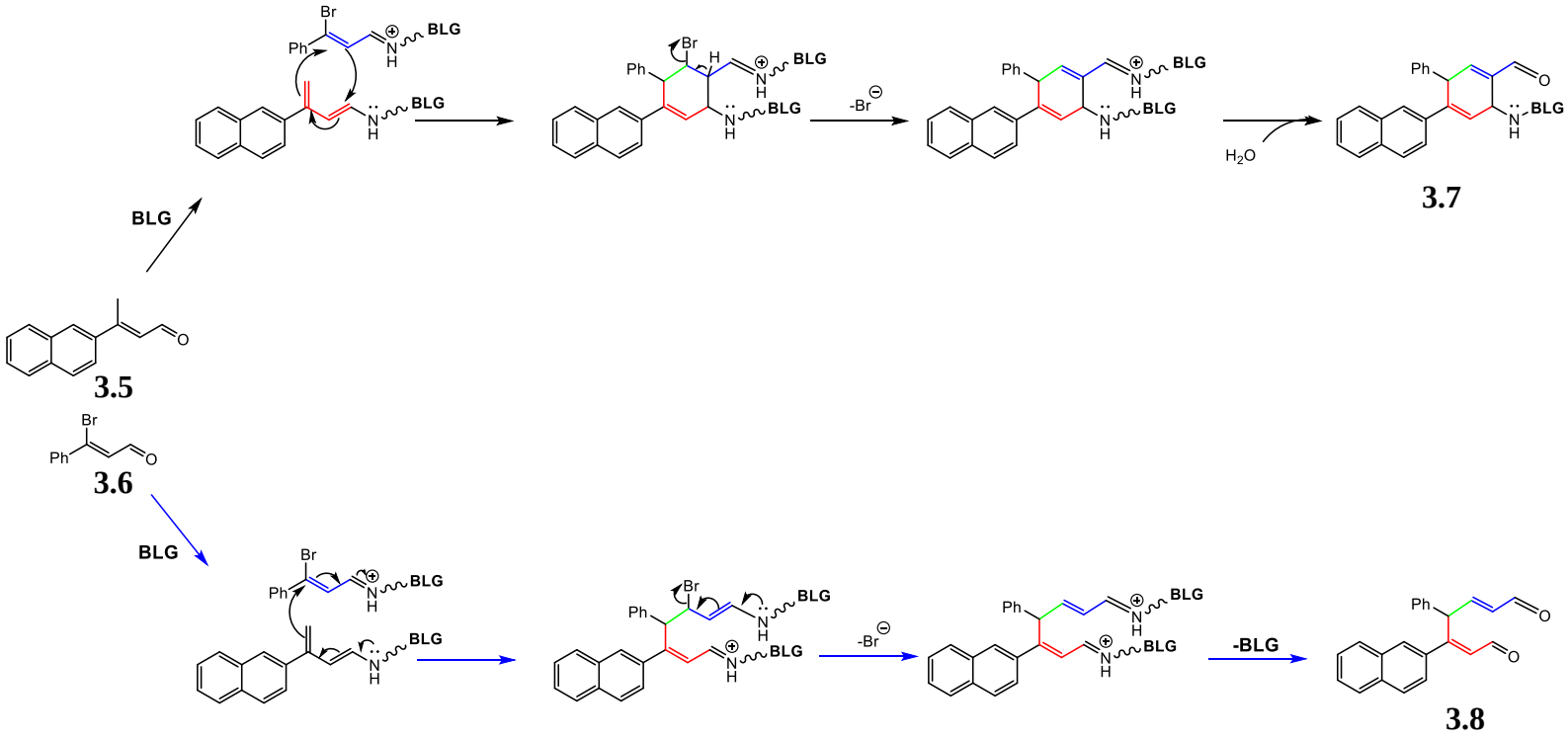

Figure 25 Evaluation of the mechanism with substrates analogs: condensation reaction with compounds 5 and 6

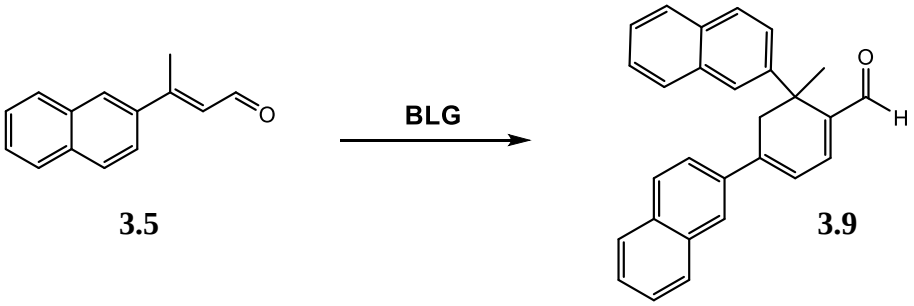

Figure 26 Control reaction with compound 3.5

BLG has been shown to catalyze the cyclodimerization of a variety of aromatic substrates including cross condensation reactions in the formation of mixed dimers[(35)]. In order to gain further insight into the mechanism of the BLG catalyzed cyclodimerization reaction, we designed an experiment to evaluate trapping of a reaction intermediate on the protein active site residue, utilizing compound **3.5** and brominated derivative **3.6** (Figure 25). Our rationale was that if cyclodimerization proceeded through a concerted Diels-Alder mechanism, deprotonation would result in the elimination of bromide resulting in the formation of a stable covalent amine bond between the protein's active site lysine and reaction intermediate **3.7**. Conversely, if the reaction proceeded through a stepwise mechanism, product **3.8** (Figure 25) would be formed. Trypsin digestion and ESI-MS analysis of the control reaction (BLG incubated with **3.5)**, revealed product **3.9** (Figure 26) bound to lysine K91; a result which is consistent with our Schiff base trapping experiments with $NaCNBH_3$. Mass spectrometric analysis of the reaction incubating both compounds **3.5** and **3.6** with BLG did not reveal compound **3.7** bound to the protein. Moreover, extraction of the reaction with ethyl acetate and its subsequent analysis by H-NMR

spectroscopy did not reveal the formation of compound **3.8**. However, compound **3.9** was also not isolated from the reaction mixture. Hence, while reaction of **3.5** and **3.6** with BLG did not proceed as designed, compound **3.6** did appear to be serving as an inhibitor of the reaction.

Trypsin digestion and subsequent peptide analysis by ESI-MS revealed lysines K91 and K60 bound to debrominated **3.6,** shown as species **3.10**, (Appendix Table 1, Page 118). Two other surface lysines (K135 & K8) also revealed labeling. These results are consistent with our mutagenesis studies and support the notion that inactivating single lysines of the lysine pair K60/K69 or K77/K91 eliminates cyclodimerization activity in BLG.
Trypsin digestion and subsequent peptide analysis by ESI-MS revealed lysines K91 and K60 bound to debrominated **3.6,** shown as species **3.9 (**Figure 26). Two other surface lysines (K135 & K8) also revealed labeling. These results are consistent with our mutagenesis studies and support the notion that inactivating single lysines of the lysine pair K60/K69 or K77/K91 eliminates cyclodimerization activity in BLG.

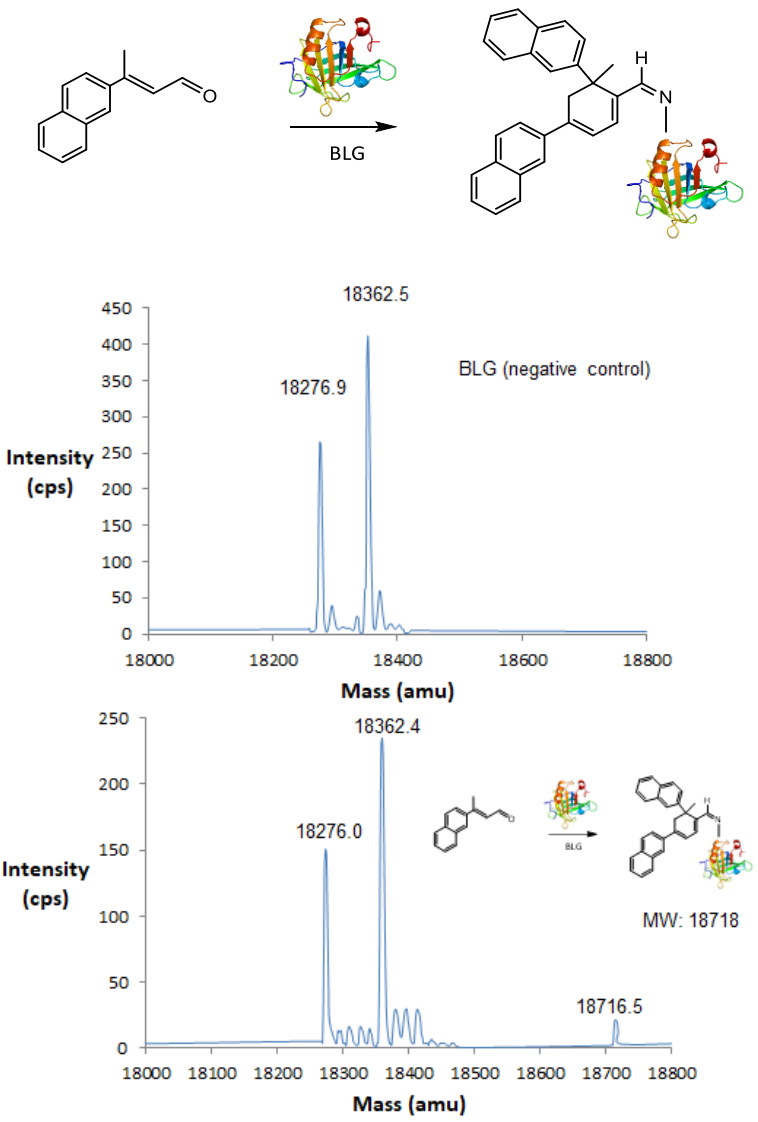

Figure 27 Mass spectrometric results obtained before trypsin digestion of BLG showing product bound to BLG

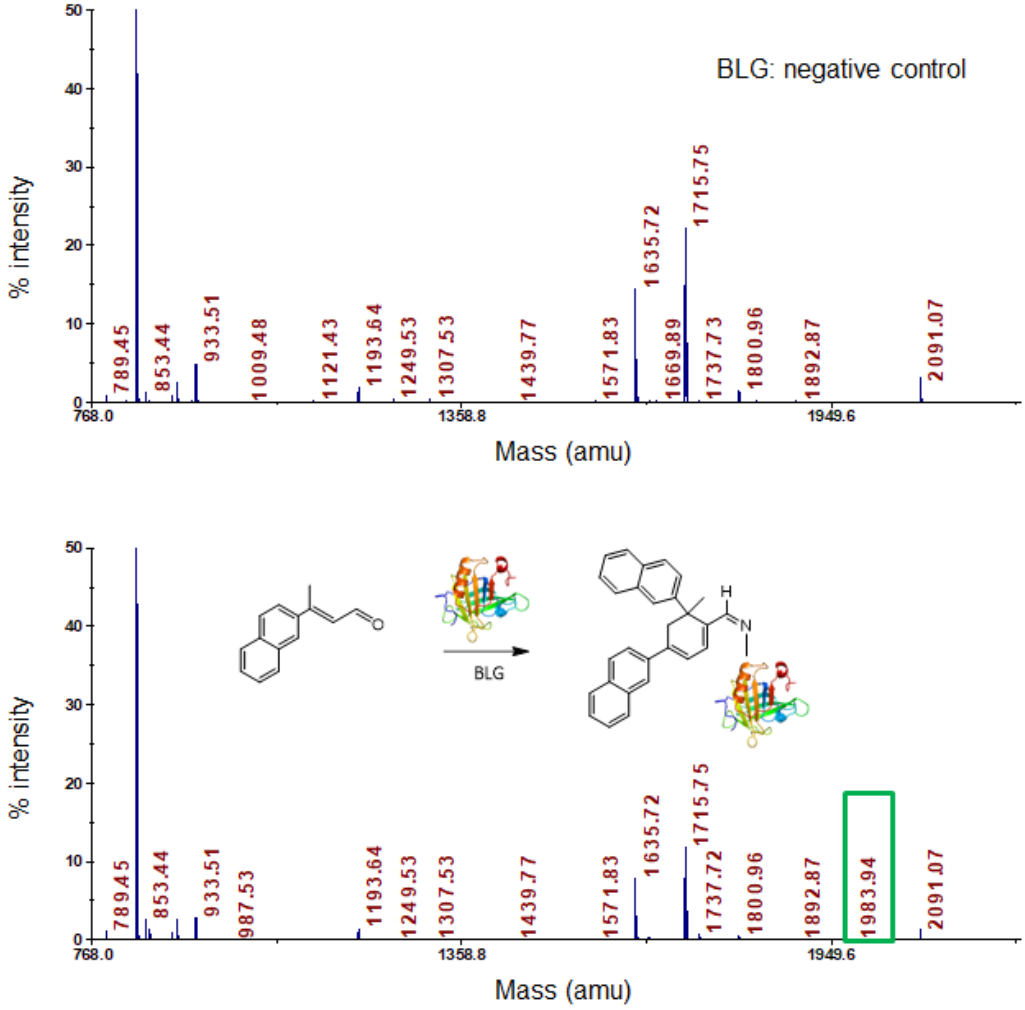

Figure 28 Mass spectrometric results obtained after trypsin digestion of product-bound BLG

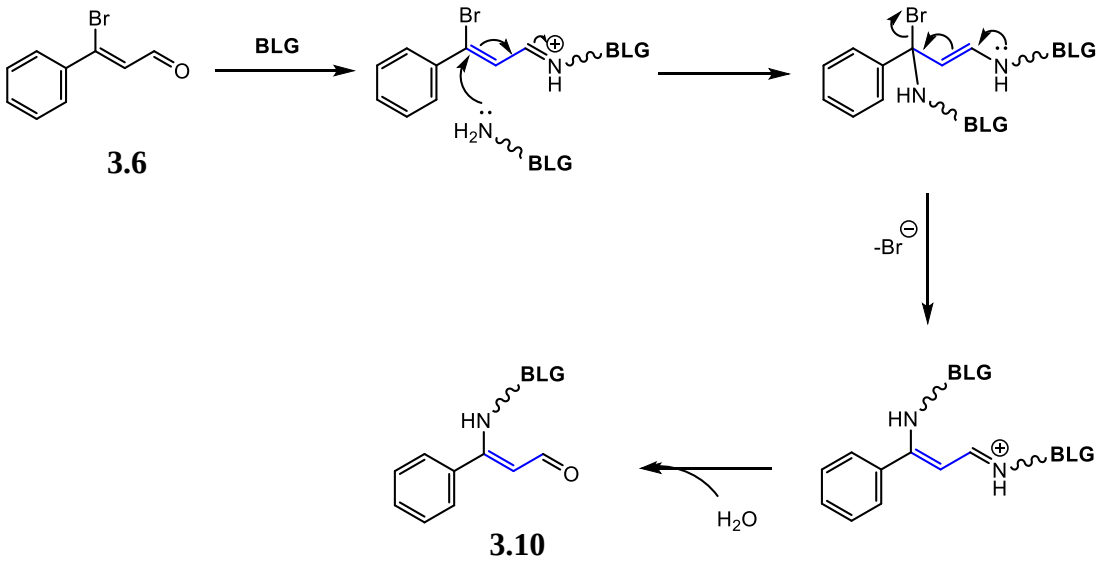

Figure 29 Proposed mechanism for covalent labelling of BLG by 3.6

3.3 Significance

Understanding the mechanism of lipofuscin formation like cycloretinal, may contribute toward the development of therapies that control the progression of AMD. Proteomic studies on both normal individuals and those with AMD have identified BLG as one of the major proteins in the eye. [(18)] Humans have no BLG homolog, hence, the protein is derived from our diet. Moreover, BLG has been shown to support cycloretinal formation *in vivo*, as revealed by a rabbit study. [(35)] It has been suggested that the biosynthesis of cycloretinal might involve proteinaceous acid-base catalysis and a chiral protein environment.[(25)] Our findings here on the BLG promoted cyclodimerization of retinal to cycloretinal demonstrate the key role that Schiff base formation plays in catalysis, specifically that between the retinal aldehyde and lysine residues of the protein. Moreover, the reaction

necessitates the involvement of two lysine residues (A60K/A69K or A77K/A91K), as opposed to one and a physical binding pocket. A single lysine residue or a peptide chain does not support the reaction. BLG provides as a model system toward understanding how cycloretinal is formed and may lead to the identification of other endogenous proteins with similar properties that play a significant role in lipofuscin formation.

3.4 Experimental procedures

3.3.1 Instrumentation and General Methods

NMR spectra were acquired on a Bruker Avance III 500 MHz spectrometer equipped with a 5 mm H-C-N cryoprobe (Bruker Corporation, Billerica, Massachusetts, USA) at 500 MHz for ^{1}H NMR and 125 MHz for ^{13}C NMR in $CDCl_3$. Mass spectra (ESI) were obtained at the Laboratory for Biological Mass Spectrometry at the Department of Chemistry, Texas A&M University, with an API QStar Pulsar, MDS Sciex (Toronto, ON, Canada) Quadrupole-TOF hybrid spectrometer.

3.3.2 General methods for trypsin digestion and mass spectrometric analysis

Trypsin digest, liquid chromatography-mass spectrometry (LC-MS) and the associated data mining procedures were each carried out at the Laboratory for Biological Mass Spectrometry at Texas A&M University. Aliquots (75 μL) of each sample were desalted using a Micro Bio-Spin P30 column (BioRad, Hercules, CA). Protein concentration was

adjusted to 0.1 mg/mL with $(NH_4)_2HCO_3$ buffer and reduced with 5 mM dithiothreitol at 60 °C for 1 h. Subsequent protein alkylation was achieved using 20 mM iodoacetamide at room temperature for 10 min. Protein samples were then digested with trypsin overnight (protein:enzyme ratio of 1:50) at 37 °C. Separation and mass spectrometry were carried out on a NanoFrontier LC-MS (Hitachi High Technologies, Dallas, TX) equipped with a nanospray ESI source. A 200 ng peptide sample was separated on a Vydac C18 capillary column (Grace Davison Discovery Sciences, 150 x 0.075 mm) at a flow rate of 200 nL/min under the following gradient routine employing water/acetonitrile and 0.1% formic acid in all conditions: 2% water/acetonitrile for 5 min, 2-10% over 0.1 min, 10-40% over 29.9 min, 40-60% over 10 min, 60-98% over 5 min, 98% for 6 min, 98-2% over 1 min, 2% for 13 min. MASCOT-assisted predictions for modified lysine and carboamidomethyl groups on peptide fragments were used in manual examination of tandem MS/MS data. Final spectra were produced by deconvolution to show the m/z +1 peaks and labeled to indicate the ion fragments resulting from b and y-type peptide cleavage.

3.3.3 HPLC Analysis Conditions

All samples in this study were analyzed using a Varian ProStar Liquid Chromatography system with a Luna 5 silica column (10 x 250 mm, 5 µm, 100 Å, Phenomenex) and a mobile phase gradient of 40% hexane in ethyl acetate to 20% hexane in ethyl acetate over 30 min. with a 2 mL/min flow rate. A wavelength of 290 nm was used as it afforded the best signal to noise ratio for derivatized cycloretinal.

3.3.4 Cyclodimerization Assay Conditions

Wild-type BLG or mutants of BLG (150 μM) was solubilized in 5 mL of PBS (10 mM phosphate buffer, 27 mM potassium chloride and 137 mM sodium chloride, pH 7.4) to which *all-trans* retinal (450 μM) was added. The reaction tube was covered with foil and incubated in a shaker (250 rpm) at 37 °C for 4 days[(35)]. The reaction was subsequently quenched by adding 5 mL of water and the solution extracted with ethyl acetate multiple times. The ethyl acetate fraction was dried over sodium sulfate and concentrated *in vacuo*. The resulting residue was stored at -80 °C until analysis. Prior to analysis by HPLC the organics were dissolved in 43.5 μL 0.07% HCl in methanol and the mixture derivatized with 16.5 μL of 2 mg/mL 2, 4-dinitrophenyl hydrazine. The resulting mixture was analyzed by HPLC according to methods detailed on page S3. The HPLC peak (Appendix Figure 1, Page 113) corresponding to cycloretinal was characterized by co-injection of 2,4-dinitrophenyl hydrazine derivatized with synthetic cylocretinal.

3.3.5 Cyclodimerization with SDS Denatured BLG

Wild-type BLG (150 μM) was solubilized in 500 mL of PBS to which citral (450 μM) and 50 g of SDS was added. The mixture was shaken at 250 rpm for 4 days at 37 °C. The BLG mixture was subsequently extracted with 2*500mL ethyl acetate and centrifuged to separate the organic layer. The organics were concentrated *in vacuo* and analyzed by NMR using $CDCl_3$ as solvent.

3.3.6 Total Turnover Number (TTN) Analysis

The amount of cycloretinal produced using wtBLG and its mutants was quantified using a standard curve generated with 2,4-DNP derivatized synthetic cycloretinal (Appendix Figure 2, Page 114). The amount of cycloretinal in micromoles was then divided by the number of millimoles of protein added to the reaction mixture to obtain TTN in terms of μM per mM of protein.

3.3.7 Cloning of Truncated DERA

The DERA gene was ordered from Genscript. The DERA gene was generated by amplifying the nucleotides coding for the first 100 amino acids of DERA using the primers mentioned in Table 1. The PCR product was purified and ligated into pET24b using the restriction enzymes *Nde*I and *Xho*I.

3.3.8 Overexpression and purification of truncated DERA

3.3.8.1 Overexpression

The construct containing the truncated DERA was transformed into BL21 DE3 cells by electroporation and plated on LB-Agar plates containing kanamycin **(**50 μg/mL**)** and incubated overnight (~16 h). An individual colony was selected and grown overnight in 15 mL LB media containing kanamycin **(**50 μg/mL) at 37 °C. This starter culture was used to

inoculate 1 L LB Miller broth containing kanamycin **(**50 µg/mL**).** The culture was shaken (225 rpm) at 37 °C to an optical density at of 0.8 at λ 600 nm. The culture was cooled to 16 °C and induced with 1 mM isopropyl β-thiogalactopyranoside for 20 h. The cells were pelleted (7,000 rpm, 10 min), resuspended in 25 mL loading buffer (20 mM NaH_2PO_4, pH 7.5, 200 mM NaCl, 5mM imidazole, 10% glycerol), and stored frozen at -80 °C.

3.3.8.2 Purification

The cell suspension was thawed at 4 °C and β-mercaptoethanol and phenylmethylsulfonyl fluoride added to the cell suspension (1 mM final concentration). The cell suspension was lysed using a Branson Sonifier 450 fitted with a 5 mm microtip (6 15s pulses at 50% duty cycle, output setting 6, with 3 min cooling intervals). Care was taken to maintain the temperature of the cell suspension at 4 °C by carrying out the sonication in a cold room and keeping the solution on ice. The cellular debris was pelleted at 12,000 rpm for 90 min. The resulting supernatant was diluted with loading buffer (20 mM NaH_2PO_4, pH 7.5, 200 mM NaCl, 5 mM imidazole, 10% glycerol) in a 1:2 ratio, and applied to a pre-equilibrated HisTrap FF 5 mL column (GE Healthcare Life Sciences, Piscataway, NJ) with a peristaltic pump at a rate of 0.2 ml/min. The column was washed with 200 mL of wash buffer (20 mM NaH_2PO_4, pH 7.5, 200 mM NaCl, 20 mM imidazole, 10% glycerol) for ~16 h, followed by a second wash with 25 mL of wash buffer containing 100 mM imidazole. Clean protein was eluted with elution buffer (20 mM NaH_2PO_4, pH 7.5, 200 mM NaCl, 250 mM imidazole, 10% glycerol) and the protein subsequently analyzed by SDS-PAGE. The concentration of the protein was assessed by Bradford assay. Commercially available

BLG was used as a standard for Bradford assay as it was closer in size to the truncated DERA than Bovine Serum Albumin (BSA). Subsequently, tDERA was assayed for cyclodimerization activity utiliizing the same conditions used to assay BLG catalyzed cyclodimerization.

3.3.9 BLG-Citral Trapping Experiment with $NaCNBH_3$

Samples of BLG (1 mL, 1% w/v in PBS: 10 mM phosphate buffer, 2.7 mM potassium chloride and 137 mM sodium chloride, pH 7.4) were incubated with 4 molar equivalents of citral and 10 molar equivalents of $NaCNBH_3$ at 37 °C for periods of 6, 24, 48, 72, and 96 h. A second set of BLG samples was set up in an identical fashion to which $NaCNBH_3$ (10 molar equivalents prepared in PBS) was added following each incubation period (6, 24, 48, 72, and 96 h). After 2 h, the reaction mixture was dialyzed into 10 mM PBS, pH 7.4 using a millipore centrifugal filter (3 kDa). Two 75 μL aliquots of each time point were subsequently analyzed by trypsin digestion as detailed on page S3.

3.3.10 BLG Reaction with 3-(naphthalene-2-yl)-but-2-enal

Wild-type BLG was solubilized in 5 mL PBS (PBS: 10 mM phosphate buffer, 2.7 mM potassium chloride and 137 mM sodium chloride, pH 7.4) to give a 150 μM solution to which 3-(naphthalene-2-yl)-but-2-enal was added (450 μM). The reaction tube was covered in foil and incubated at 250 rpm for 4 days at 37 °C. The sample (100 μL) was dialyzed with 400 μL of 50 mM ammonium acetate using a Millipore 3 kDa centrifugal

filter (10,000 rpm, 10 min). The retentate was washed with 50 mM ammonium acetate and submitted for mass spectrometric and peptide analysis as detailed previously.

~Note: Due to the harsh conditions of trypsin digestion and analysis, the expected protein-homodimer adduct will not be directly observed. However, if the homodimer is indeed bound to the protein, trypsin will not cleave at the labeled lysine site. For example, we would expect to see the peptide 'IDALNENKVLVLDTDYK' in the reaction but not in the negative control. *(126)*

3.3.11 CD Analysis of BLG Promoted Cyclodimerization of *All-Trans* Retinal

Wild-type BLG was solubilized in 5 mL PBS **(**PBS: 10 mM phosphate buffer, 2.7 mM potassium chloride and 137 mM sodium chloride, pH 7.4) to give a 150 μM solution to which *all-trans* retinal was added (450 μM). The reaction tube was covered in foil and shaken at 250 rpm for 4 days at 37 °C. Aliquots (500μL) were taken daily and transferred to water using a Millipore 3 kDa centrifugal filter. The sample was then analyzed on a CD spectrometer (Chirascan) over the wavelength range of 200−400 nm for 5 min at 20 °C.

CHAPTER IV

BIOCATALYSIS WITH THE MILK PROTEIN BETA-LACTOGLOBULIN: PROMOTING RETROALDOL CLEAVAGE OF CONJUGATED ALDEHYDES

4.1 Introduction

Enzymes that are versatile in their activity and substrate tolerance can be commercially applied to the production of chemicals and pharmaceuticals thereby increasing efficiency of manufacturing plants while reducing environmentally harmful waste.[127] Natural enzymes, while highly proficient in the catalysis of their native substrates are not very versatile. Aldolases are a characteristic example of such enzymes with high activity towards their native polar substrates but very low tolerance towards hydrophobic ones.[128, 129] Various strategies including directed evolution,[130] catalytic antibodies,[131, 132] and computational design[133] have been explored to design an aldolase with high activity towards non-polar molecules. The de-novo design and directed evolution of a retro-aldolase, RA95.5-8 with activity approaching that of natural class I aldolases has made the most progress toward this goal.[107] Further investigations of RA95.5-8 indicate that this enzyme is not only promiscuous in substrate selectivity, but also in catalytic activity. Studies into the enzyme's ability to catalyze Michael additions[108] and Knoevenagel condensations[109] indicate that the minimum requirement for promiscuity in catalyzing C-C bond generating reactions is an active site capable of binding hydrophobic molecules and an active site lysine to form iminium ions or enamines.

Bovine β-lactoglobulin (BLG) constitutes between 12–15% of the protein content of milk. Despite extensive investigations into its physical and biochemical properties for approximately 80 years, the protein's function remains unassigned.[41] Its size, stability, bioavailability and capacity to bind hydrophobic molecules in its central calyx have resulted in applications including encapsulation and nutraceutical delivery.[134] The presence of an active site lysine capable of activating aldehydes by imine formation and a hydrophobic cavity led us to propose that BLG, like RA95.5-8, could also serve as an effective retroaldolase. Previously, we have shown that BLG can promote condensation of α, β-unsaturated aldehydes, to their respective cyclodimers through C-C bond formation.[35, 135] For example, condensation of *all-trans* retinal **4.1** yields the formation of *all-trans* retinal dimer, cycloretinal **4.2** (Figure 30).

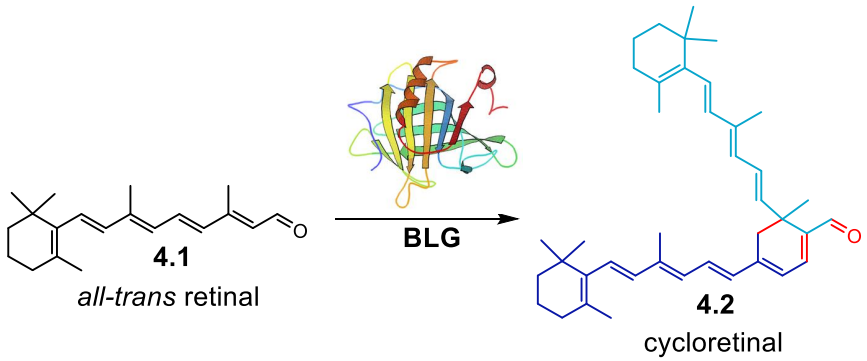

Figure 30 BLG catalyzed cyclodimerization of all-trans retinal to cycloretinal

Here, we report on the results of our investigations, which suggest that BLG is able to catalyze the retro-aldol breakdown of α, β-unsaturated aldehydes. Exploration of the

substrate scope of BLG's retroaldolase activity revealed that substrates with aromatic, non-polar side chains are preferred to aliphatic or polar head groups.

4.2 Results and discussion

Synthesis of the α,β-unsaturated substrates was achieved by invoking a Horner-Wadsworth-Emmons reaction to give the E-alkene ii, followed by DIBAL reduction of the nitrile, as shown for the formation of β-methyl naphthene aldehyde **4.5** (Figure 31A)**.**[(136)] Due to the similarity between compound **4.5** and methodol, a compound used to study retroaldol reactions, we initially chose this compound to evaluate the cleavage products of the reaction.

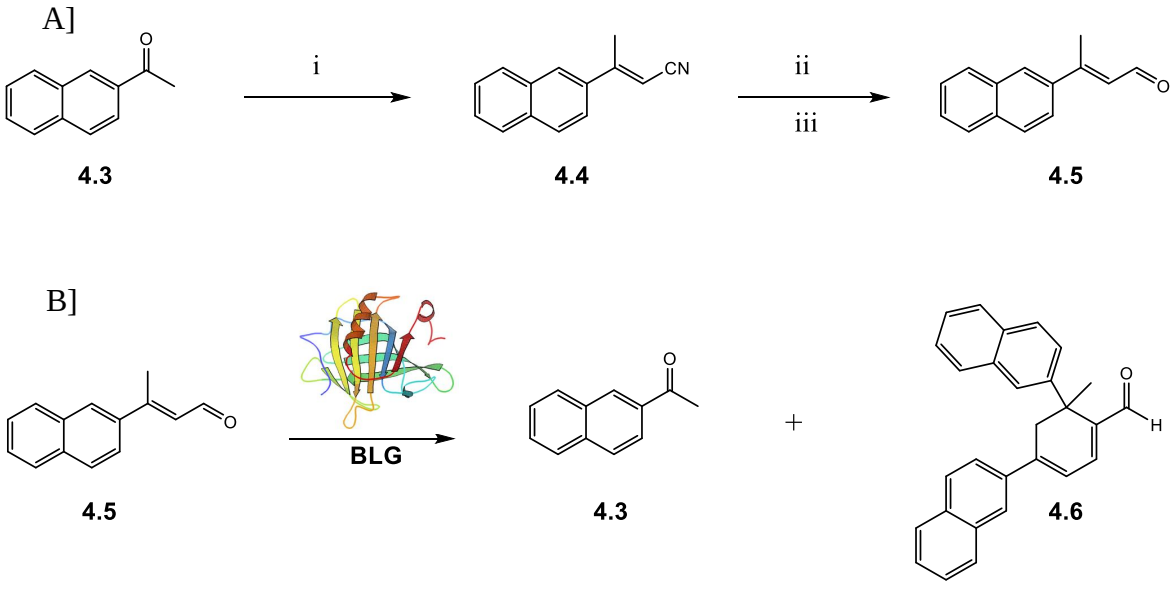

Figure 31Oxidative cleavage as mediated by BLG: A] Synthesis of β-methyl naphthene aldehyde 4.5: i NaH, DCM; ii DIBAL-H, -60 °C; iii H2O; B] BLG catalyzed oxidative cleavage of β-methyl naphthene aldehyde 4.5

Compound **4.5** was incubated with BLG in PBS buffer at 37 °C and the organics subsequently extracted with ethyl acetate. Analysis by HPLC, revealed the formation of four peaks (Figure 32A). Each peak was collected and analyzed by NMR spectroscopy.

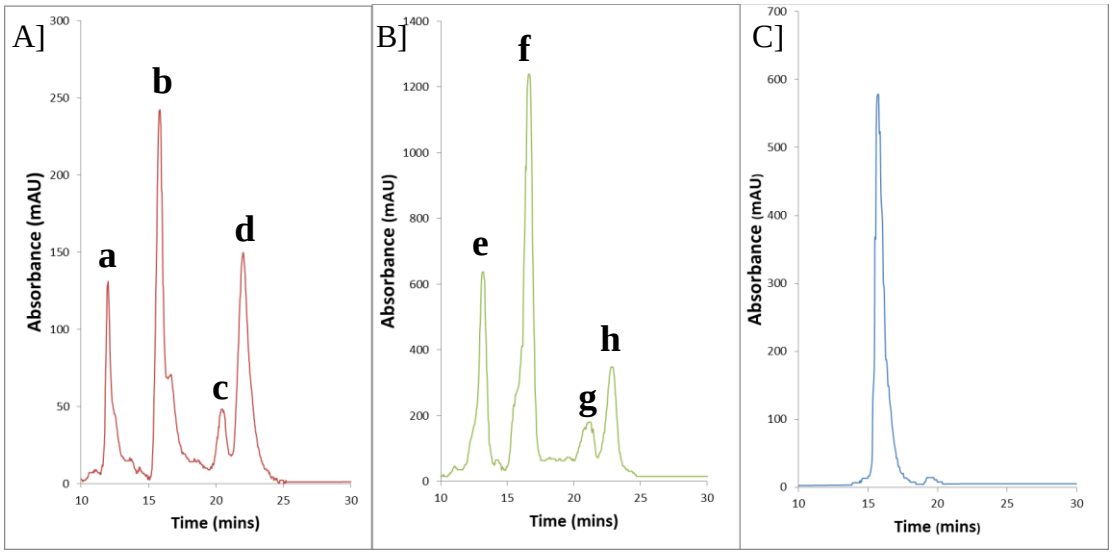

Figure 32 Evaluation of BLG reaction by HPLC analysis: A] BLG reaction with compound 4.5, B] BLG reaction with compound 4.13, C] acetonaphthone 4.3 synthetic standard

The expected homodimer **4.6** was observed in peak **a**. Peak **b** was structurally characterized as acetonaphthone **4.3**, which was also validated by comparison with acetonaphthone **4.3** standard (Figure 32C). Peak **d** was identified as starting material **4.5** by H-NMR spectroscopy and Peak **c** was shown to be a compound closely related to the starting material; however, it wasn't isolated in sufficient quantities to fully characterize it.

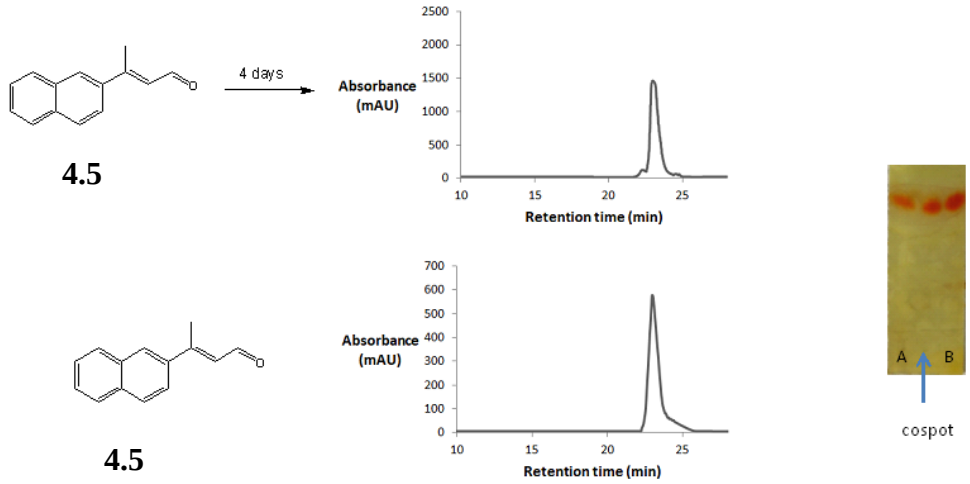

Figure 33 Control reaction showing that in the absence of protein, compound 3 does not non-enzymatically break down into acetonaphthone

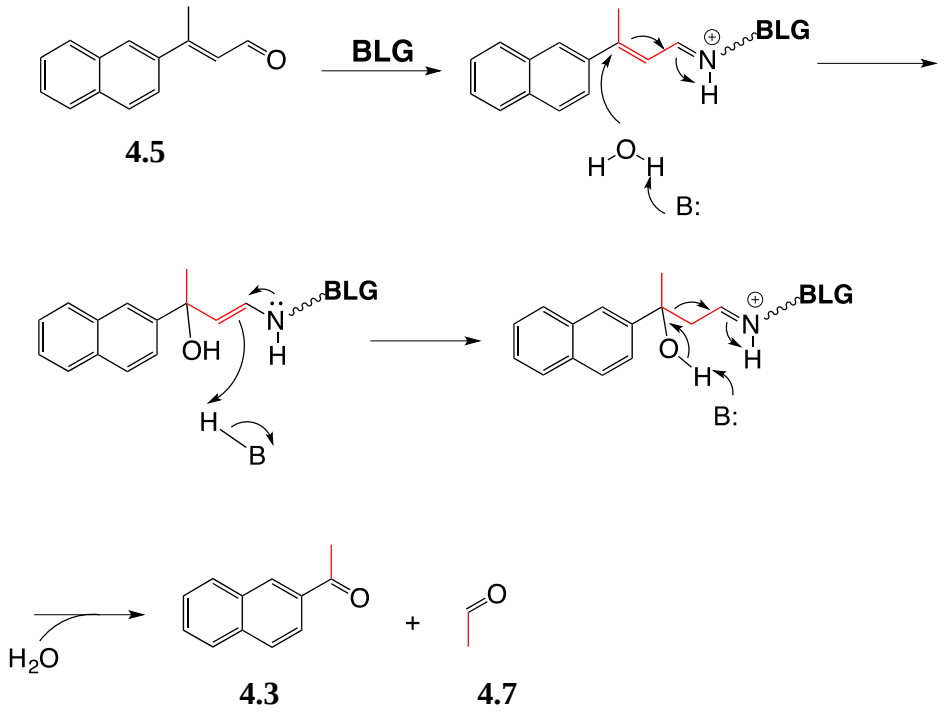

Figure 34 Proposed mechanism for BLG catalyzed retroaldol cleavage

A control reaction where **4.5** was incubated with PBS over 4 days resulted in the retrieval of only starting material (Figure 33).

The scope of the reaction was evaluated with a series of α, β-unsaturated aldehyde substrates, Table 4. The retro-aldol breakdown product for each was characterized by HPLC co-injection with synthetic standards and the total turnover number (TTN) for each substrate was evaluated as shown in Table 4. BLG was shown to be most effective in the retroaldol cleavage of compounds with aromatic, phenyl **4.10** or naphthyl **4.5** side chains. Extending the side chain to that of a biphenyl- **4.11** or fluorene **4.12** groups resulted in a 3- to 10-fold reduction in retroaldolase activity, respectively. Likewise, the more polar aromatic substrate, 2-methyl furanyl **4.9** moiety and the aliphatic substrate **4.8** showed very little to no retroaldolase activity. This is thus suggestive that the retroaldolase activity favors that of a hydrophobic binding cavity that most effectively accommodates phenyl and naphthyl sidechains.

The proposed route for cleavage of the α, β-unsaturated double bond of **4.5** to generate acetonaphthone **4.3** is depicted in Figure 34. Hydrolysis of the imine activated double bond (via a lysine residue within the BLG binding pocket) initiates the process followed by a retro-aldol like cleavage of the C—C single bond. The preference for aromatic groups over aliphatic side-chains is likely due to resonance stabilization of a transition state C-3 carbocation during C-C bond cleavage.

Table 4 Evaluation of scope of the retroaldol reaction using a series of substrates

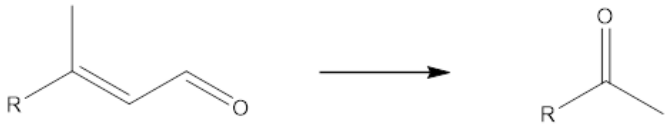

R group	Compound	TTN (μM product/ mM BLG)
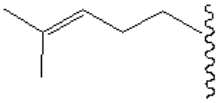	4.8	0
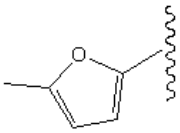	4.9	0.003
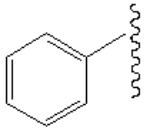	4.10	8.80
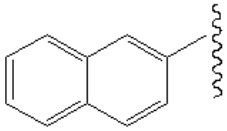	4.5	6.93
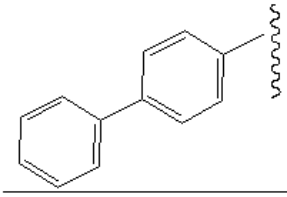	4.11	0.67
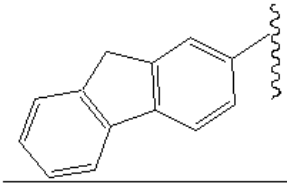	4.12	2.27

In light of this mechanism, we evaluated whether a cyclodimerization inhibitor, 3-bromocinnamaldehyde **4.13** (Figure 35A),[(53)] could effect an enhancement in retro-aldol activity. Brominated **4.13** has been previously shown to inactivate key lysine residues (Figure 29) as validated by trypsin digestion and ESI/MS analysis.[(53)]

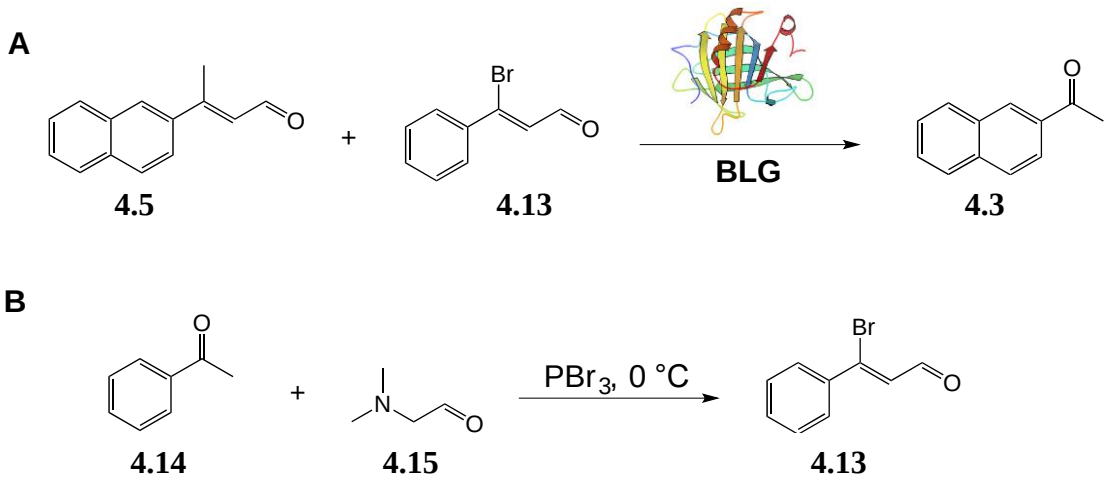

Figure 35 Effect of substrate analog 4.13 on retroaldol cleavage: [A] BLG catalyzed retroaldol cleavage of β-methyl naphthene aldehyde 3 in the presence of inhibitor 8; [B] Synthesis of substrate analog 4.13

The cyclodimerization process necessitates the involvement of two BLG lysine residues[(53)] as opposed to one for the retroaldol cleavage. Hence, inhibitor **4.13** is expected to have a more substantive effect on the dimerization reaction as opposed to that of the oxidative cleavage. Compound **4.13** was synthesized from acetophenone **4.14** using the Vilsmeier-Haack reaction according to Figure 35B.[(137)] BLG was incubated with a 1:1.5 ratio of **4.5** to **4.13** in PBS buffer at 37 °C. The reaction mixture was subsequently quenched and extracted with ethyl acetate. HPLC analysis showed 4 peaks (Figure 32B) that were

collected and characterized by H-NMR spectroscopy. Peak **f** was confirmed as acetonaphthone **4.3**. Cyclodimer **4.6** was not observed indicating that treatment with **4.13** eliminated cyclodimerization activity of BLG. While peak **e** eluted at about the same retention time as the homodimer **4.6**, it was structurally characterized as **4.13**. Peak **h** was confirmed as **4.5** and peak **g** was also not isolated in sufficient quantities for accurate characterization.

The amount of acetonaphthone **4.3** formed in each experiment was quantified by HPLC analysis utilizing a standard curve (Appendix Figure 16, Page 129). Addition of cyclodimerization inhibitor **4.13** more than doubled the yield of acetonaphthone (0.45 mg/L) compared to incubation of BLG with **4.5** alone, which yielded only 0.18 mg/L of the acetonaphthone cleavage product.

Control experiments with **4.5** or **4.16** (Figure 36)**,** which differ only by the presence of a bromo- or methyl-group at C-3, were carried out. Synthesis of **4.16** was achieved in the same manner as the synthesis of **4.13.** ESI-MS analysis showed lysine labeling with **4.16** while no labeling was observed with **4.5**, which further substantiates that the bromo-group is critical for covalent labelling (Table 5).

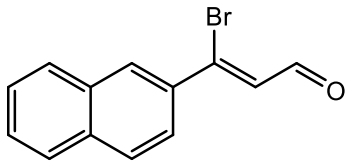

4.16

Figure 36 Brominated analog of compound 4.5

Table 5 Labelling of BLG with brominated substrate analogs

	Expected mass	Observed mass
BLG + 1 molecule of compound **4.13**	18407.16 & 18492.759	18407.1992 & 18494.1992
BLG + 2 molecules of compound **4.13**	18538.32 &18623.919	18538.900 & 18628.5996
BLG + 1 molecule of compound **4.16**	18458 &18639	18457.5000 &18639.1992
BLG + 2 molecules of compound **4.16**	18543.5996 &18724.5996	18545.3008 & 18726.6992

4.3 Significance

Although the TTN for BLG catalyzed retroaldol cleavage is much lower than de-novo designed proteins, the ready availability of BLG makes it a viable choice for biocatalytic investigations. Davisco Foods International alone produces over 10 million pounds of whey protein isolates annually. Here, we have shown that β-lactoglobulin has the capability to catalyze retro-aldol cleavage of the α, β-unsaturated aldehydes. Catalysis is proposed to proceed through initial hydrolysis of the α, β-unsaturated imine followed by a retro-aldol cleavage of the alcohol (Figure 34). Use of a cyclodimerization inhibitor, disables this competing reaction and enhances the retroaldol process. We have demonstrated that BLG is a versatile protein with the ability to not only promote condensation reactions but also, a retroaldol type cleavage reaction. Evolution of these enzymes and/or further understanding of the mechanism of these reactions might lead to the development of BLG variants with higher catalytic efficiency and/or adaptable biocatalysts for commercial use.

4.4 Experimental procedures

4.4.1 Instrumentation and general methods

All reactions were carried `out in flame-dried glassware unless otherwise noted. All non-enzymatic reactions were magnetically stirred and monitored by thin layer chromatography (TLC), performed using glass-backed silica gel plates Analtech (#47011). Flash column

chromatography was performed using 60Å Silica Gel (Silacycle, 230-400 mesh) as a stationary phase. ^{1}H & ^{13}C NMR spectra for synthesized compounds were recorded on a Varian Inova 300 unless otherwise noted. ^{1}H NMR chemical shifts are reported as δ values in ppm relative to $CDCl_3$ (7.26 ppm), coupling constants (*J*) are reported in Hertz (Hz). Compounds obtained from enzymatic reactions using substrate **3** were purified on a Varian ProStar chromatography system and analyzed by NMR spectrometry. NMR spectra were acquired on a Bruker Avance III 500 MHz spectrometer equipped with a 5 mm H-C-N cryoprobe (Bruker Corporation, Billerica, Massachusetts, USA) at 500 MHz for ^{1}H NMR and 125 MHz for ^{13}C NMR in $CDCl_3$. Mass spectra (ESI) were obtained at the Laboratory for Biological Mass Spectrometry at the Department of Chemistry, Texas A&M University, with API QStar Pulsar, MDS Sciex (Toronto, ON, Canada) Quadrupole-TOF hybrid spectrometer.

4.4.2 Materials

Commercial solvents, reagents, Phosphate Buffer Saline (PBS) salts and acetonaphthone standards were used as received from Sigma-Aldrich. β-lactoglobulin was obtained from Davisco Foods International,Inc. (JE-003-6-922, La Sueur, MN, 93.6% BLG).

4.4.3 General methods for trypsin digestion and mass spectrometric analysis

Trypsin digest, liquid chromatography-mass spectrometry (LC-MS) and the associated data mining procedures were each carried out at the Laboratory for Biological Mass

Spectrometry at Texas A&M University. Aliquots (75 μL) of each sample were desalted using a Micro Bio-Spin P30 column (BioRad, Hercules, CA). Protein concentration was adjusted to 0.1 mg/mL with $(NH_4)_2HCO_3$ buffer and reduced with 5 mM dithiothreitol at 60 °C for 1 h. Subsequent protein alkylation was achieved using 20 mM iodoacetamide at room temperature for 10 min. Protein samples were then digested with trypsin overnight (protein:enzyme ratio of 1:50) at 37 °C. Separation and mass spectrometry were carried out on a NanoFrontier LC-MS (Hitachi High Technologies, Dallas, TX) equipped with a nanospray ESI source. A 200 ng peptide sample was separated on a Vydac C18 capillary column (Grace Davison Discovery Sciences, 150 x 0.075 mm) at a flow rate of 200 nL/min under the following gradient routine employing water/acetonitrile and 0.1% formic acid in all conditions: 2% water/acetonitrile for 5 min, 2-10% over 0.1 min, 10-40% over 29.9 min, 40-60% over 10 min, 60-98% over 5 min, 98% for 6 min, 98-2% over 1 min, 2% for 13 min. MASCOT-assisted predictions for modified lysine and carboamidomethyl groups on peptide fragments were used in manual examination of tandem MS/MS data.

4.4.4 General methods for mass spectrometric analysis of BLG

Protein samples were dialyzed into 50mM Ammonium acetate using millipore centrifugal filters. The samples were then analyzed by injecting 30 μL of each sample onto API QStar Pulsar, MDS Sciex (Toronto, ON, Canada) Quadrupole-TOF hybrid spectrometer. The obtained spectra was deconvoluted to obtain mass spectra as a function of intensity vs m/z.

4.4.5 HPLC analysis conditions

All samples except the reaction with **4.5** were analyzed on Thermo Scientific™ UltiMate™ 3000 Rapid Separation HPLC system with a Prodigy 5µm ODS-2 150 Å, LC column 250 mm×4.6 mm(Phenomenex) and a mobile phase comprising water (with 0.1% formic acid) as inlet A and 75%:25% Methanol:Isopropanol (with 0.1% formic acid) as inlet B. The conditions used were: 0-1 min: 80%A; 1-23 min: gradient change to 0% A; 23-33 min: maintain 0%A. A wavelength of 280 nm was used as it afforded the best signal to noise ratio.

The reaction assay of compound **3** with BLG was analyzed using a Varian ProStar Liquid Chromatography system with a Luna 5 silica column (10 x 250 mm, 5 µm, 100 Å, Phenomenex) and a mobile phase gradient of 40% hexane in ethyl acetate to 20% hexane in ethyl acetate over 30 min. with a 2 mL/min flow rate. A wavelength of 280 nm was used as it afforded the best signal to noise ratio.

4.4.6 Generic assay of BLG with α,β unsaturated aldehydes

Assays with BLG were carried out according to procedures reported by Bench, et.al [(35)]. BLG (150 µM) was added to 500 mL of PBS (10 mM phosphate buffer, 27 mM potassium chloride and 137 mM sodium chloride, pH 7.4) along with the α,β unsaturated aldehyde (450 µM). The 1L flask was covered in foil and shaken at 250 rpm, 37 °C in an incubator shaker for 4 days. The reaction was quenched by adding 500 mL of water and the solution extracted twice with 250 mL of ethyl acetate. The ethyl acetate fraction was dried over

sodium sulfate and concentrated *in vacuo*. The resulting compound was stored at -80 °C until further analysis. Prior to analysis by HPLC the organics were dissolved in 200 µL methanol.

Assay with brominated compound **8** was repeated in the same manner except that 35.5 mg of compound **8** was added to the reaction mixture.

4.4.7 Total Turnover Number (TTN) analysis

The amount of ketone product produced using wtBLG was quantified using a standard curves generated with synthetic standards. The amount of ketone product in micromoles was then divided by the number of millimoles of protein added to the reaction mixture to obtain TTN in terms of µM per mM of protein.

4.4.8 Synthesis of α,β unsaturated aldehydes

The α,β unsaturated aldehydes used in this study were synthesized according to previously reported procedures. They were characterized by comparing H-NMR to previously reported H-NMR data.[27, 34]

4.4.8.1 Synthesis of (Z)-3-bromo-3-naphthylacrylaldehyde

Compound **11** was synthesized similarly to the synthesis of compound 4.13. A solution of dimethylformamide (15 mmol, 3.0 equiv) in $CHCl_3$ (10 ml) was cooled to 0 ^oC and PBr_3

(13.5 mmol, 2.7 equiv) was added to the solution over 15 min. The reaction mixture was stirred at room temperature for 1 h. Acetonaphthone (5 mmol, 1 equiv.) was added to the solution and was allowed to stir overnight. The reaction mixture was then poured into ice water, neutralized with K_2CO_3 to a pH of 8 and extracted with Et_2O (20 ml x 3). The organic phase was washed with brine, dried over $MgSO_4$, and concentrated *in vacuo*. The compound was purified by flash column chromatography (1:30, EtOAc: hexanes). ^{1}H NMR (300 MHz, CDCl3) δ 9.96 (d, 1H), 8.05 (s, 1H), 7.75-7.62(m, 4H), 7.51-7.46(m, 2H), 6.73(d, 2H) 13C NMR (300 MHz, CDCl3) δ 193.6, 144.9, 134.6, 134.4, 132.7, 129.5, 129.1, 128.6, 128.2, 127.7, 127.6, 127.2, 124.0 HRMS (ESI) calcd for C13H9BrO [M+Na] 282.97346 and 284.97141, found 282.97040 and 284.96837 Since this compound has not been characterized before, we have also included DEPT, COSY, HMBC, HSQC and MS/MS analysis.

CHAPTER V

APPLICATION OF CONFOCAL FLUORESCENCE MICROSCOPY TO TRACK THE PASSAGE OF BLOOD-BORNE BLG IN MOUSE EYE

5.1 Introduction

Bovine BLG is a lipocalin being investigated as a drug delivery system since it is resistant to pepsin digestion in the stomach, is absorbed into blood through special receptors in the small intestine[35, 93, 98, 114] and has been shown to bind various non-polar ligands. The fate of the micromolar amounts of BLG observed in blood is not known. It has been shown that ^{125}I labelled BLG introduced intravenously was secreted into the milk of lactating mice indicating that BLG can pass across the mammary epithelial cell barrier by exploiting the immunoglobulin transport pathway.[99]

BLG's similarity to RBP,[52] its ability to bind retinol[39] and its detection in the retina of people affected with AMD[18] could mean that its native function is the transport of retinol to the retina. BLG may also be transported across the blood-retina barrier in a manner similar to the transport of immunoglobulins.[138] Once in the retina, it is possible that BLG moonlights as an enzyme that promotes the formation of cycloretinal, a component of lipofuscin.

Confocal fluorescence microscopy allows for images of thin sections of a tissue to be obtained (without the need for mounting or processing the tissue in any way) which can be

assembled into a three-dimensional image of the sample.[139] This technique can be applied to track the passage of a BLG-fluorescent molecule conjugate through the retina of a live mouse in real time to confirm whether BLG is actively transported across the blood-retina barrier.

In this study, we overexpress a BLG mutant with an extra cysteine at its N-terminal, couple it to a fluorescent molecule functionalized with a maleimide group, characterize the BLG conjugate and use it to study the passage of blood borne BLG through the retina.

5.2 Results and discussion

5.2.1 Over-expression and purification of N-Cys-BLG mutant

Since it has been shown that the only cysteine in BLG that is not involved in a disulfide bond is not accessible to solvent,[64] a mutant of BLG with an extra N-terminal cysteine (N-Cys-BLG) was cloned, overexpressed and purified to afford clean protein characterized by SDS-PAGE and mass spectrometric analysis.

5.2.2 Coupling N-Cys-BLG to N-hydroxyethylmaleimide

Initial optimization of coupling conditions was carried out using a cheap alternative maleimide compound: N-hydroxyethylmaleimide (NEM). Screening studies helped discover that phosphate buffered saline (PBS) at pH=8.1 was the best buffer for the

maleimide coupling. The significant difference in coupling efficiency between pH 7.5 (0% by mass spectrometric analysis) and 8.1 (100% by mass spectrometric analysis) (Figure 37) could be due to the slightly basic conditions helping deprotonate the cysteine side-chain (pK_a= ~8.3). The optimal concentration for DMSO, used to solubilize NEM was found to be 1% as any increase in DMSO concentration beyond that resulted in protein precipitation. Trypsin digestion and mass spectrometric analysis revealed that the two labelled cysteines were cysteines 4 (N-terminal cysteine inserted in the mutant, Figure 38) and 164 (C-terminal cysteine, Figure 39) were binding NEM. The exposure of BLG to DTT during purification may have resulted in the reduction of the Cys_{70}-Cys_{164} disulfide bond making cysteine 164 accessible to disulfide bond formation.

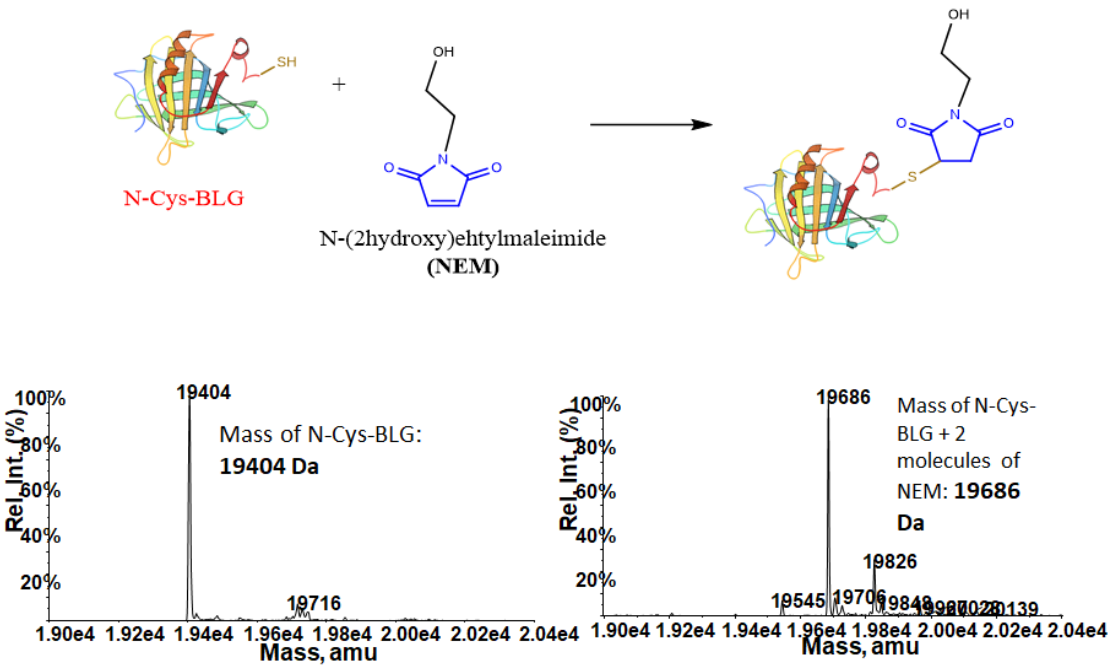

Figure 37 When treated with NEM, the peak for N-Cys-BLG (mass=19404 a.m.u.) disappeared and a new peak corresponding to BLG+ 2 moles of NEM (mass= 19686 a.m.u.) was seen

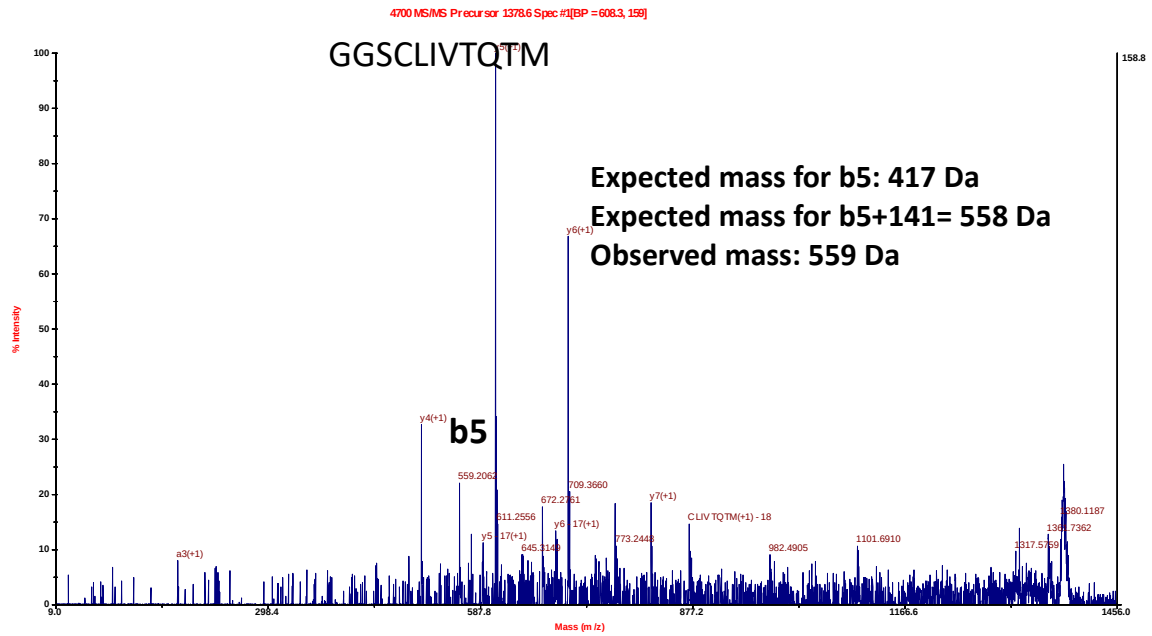

Figure 38 Cysteine-4 containing peptide labeled with NEM analyzed by trypsin digestion and mass spectrometry

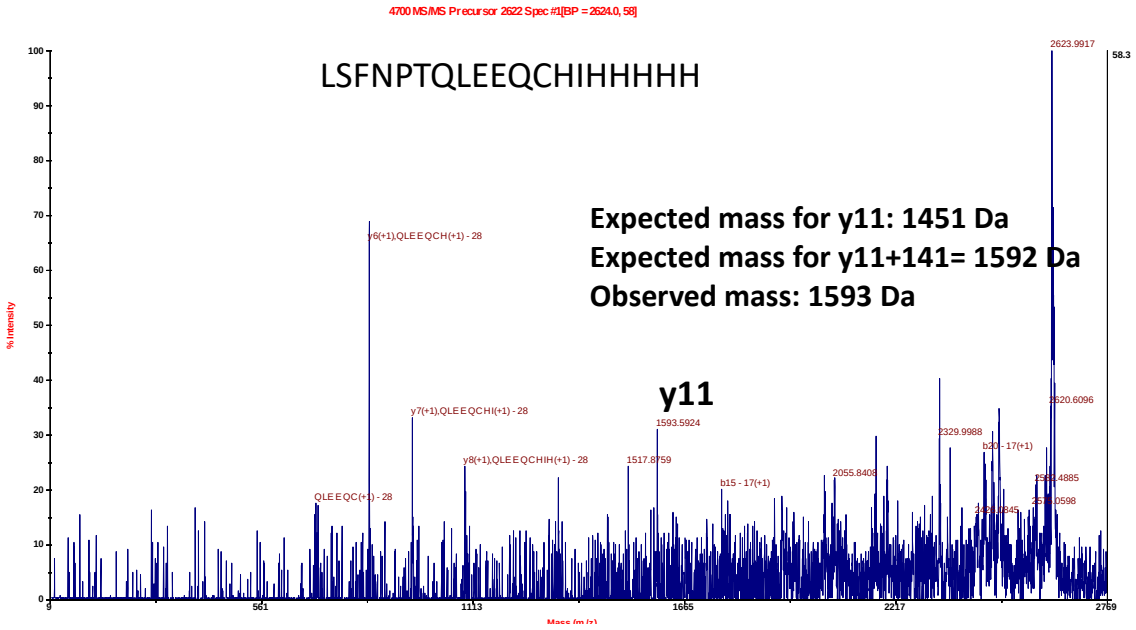

Figure 39 Trypsin digestion and peptide analysis showing cysteine-164 containing peptide labeled with NEM

5.2.3 Coupling N-Cys-BLG to ATTO532

Similar conditions to that used for NEM was used to couple BLG to ATTO532. However, the BLG-ATTO532 conjugate could not be analyzed by mass spectrometry. This could be due to ATTO532 (whose complete structure was not provided by ATTOTec) affecting the ionization of the protein conjugate. While the digestion of N-Cys-BLG or BLG-NEM conjugate had unveiled all the expected peptide sequences, attempts to digest BLG-ATTO532 conjugate using trypsin and subsequently analyze by mass spectrometry did not divulge the N-terminal and C-terminal sequences hinting that these peptides had been modified in a way that they could not be detected.

To verify that the dye had indeed coupled covalently to the protein and was not just bound in the hydrophobic cavity, we purified the coupled protein by passing it through a Nickel affinity column. After binding the protein, it was washed until the flow-through did not have any absorbance at 532 nm. During elution fractions which showed absorbance at 532nm were collected, treated with a protein denaturant, sodium dodecyl sulfate (SDS) and dialyzed with PBS for a week to allow for any non-covalently bound dye to dialyze out. Subsequently, the protein was concentrated and analyzed by SDS-PAGE. SDS and DTT treatment would denature the protein and any molecule bound in the hydrophobic cavity would be released into the surrounding solvent. However, SDS-PAGE analysis showed that the protein corresponding to the size of BLG was fluorescent suggesting that the dye may be covalently bound to BLG (Figure 40).

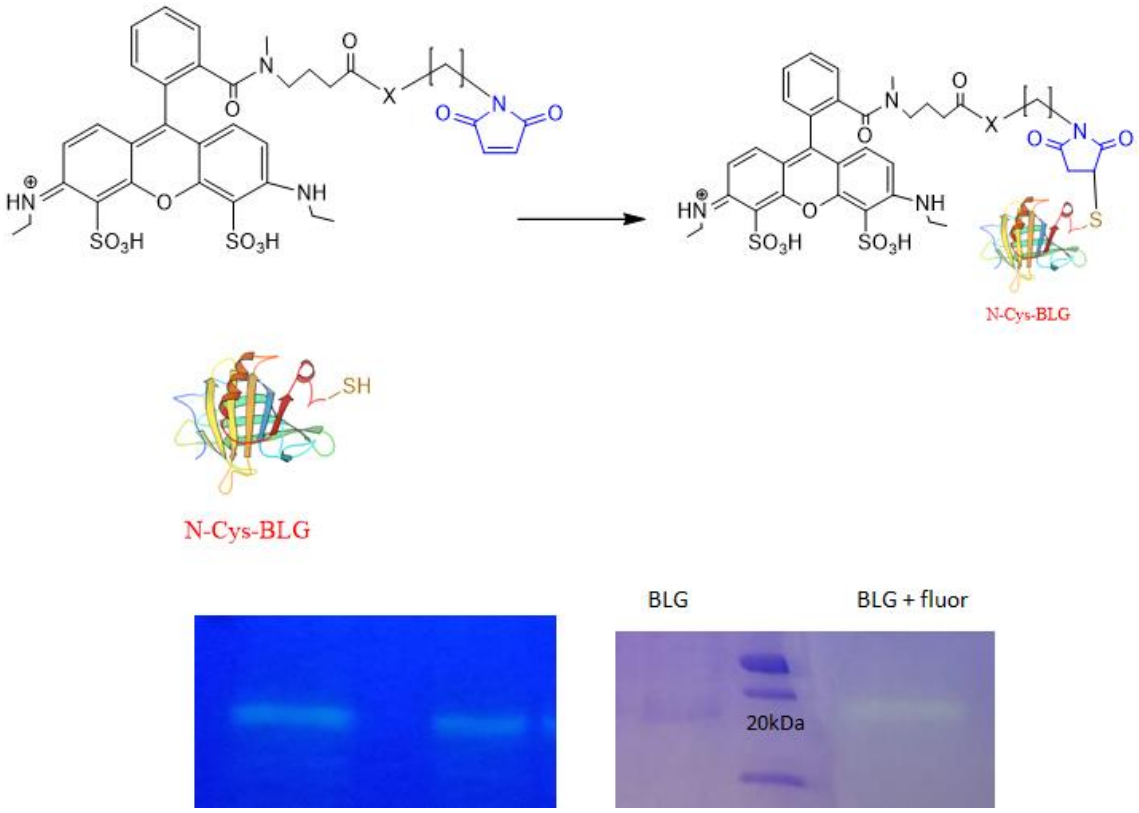

Figure 40 Characterization of BLG-ATTO532 conjugate by SDS-PAGE analysis

The number of dye molecules bound to 1 molecule of BLG, calculated by estimating the concentration of BLG-ATTO532 conjugate (by amino acid analysis) and the concentration of fluorescent molecule (from absorbance at 532nm), showed that 4 molecules of dye was bound to each molecule of BLG. This high number could be due to the cleavage of disulfide bonds by DTT resulting in the increased access of cysteines to coupling.

5.2.4 Imaging mouse retina

The retina of BALB/c mice that were intravenously introduced with BLG-ATTO532 conjugate, ATTO532 dye and saline was observed by fluorescence microscopy. While injection of saline showed only the autofluorescence of the retinal region (Figure 41A), injection of ATTO532 showed images (Figure 41B) resembling an angiogram of mouse retina (Figure 41C).[(140)] The retina of mice injected BLG-ATTO532 conjugate was very similar to those injected just ATTO532 (Figure 42A). An hour after injection, there was no marked decrease in fluorescence (Figure 42B) but 48 hours after injection, no fluorescence was observed (Figure 42C). Repeated injections every 48 hours did not reveal any fluorescence beyond the blood vessels suggesting that there was no build-up of BLG-ATTO532 conjugate in the retina. These results suggest that either the BLG-ATTO532 conjugate is not transported across the blood-retina barrier in young mice or that the amounts being transported are not within our detection limits. Repeating the experiment with older mice may help us study the effect of age on coherence of the blood-retina barrier.

A] B]

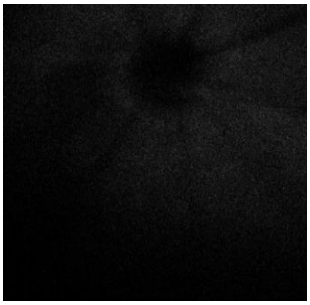

C]

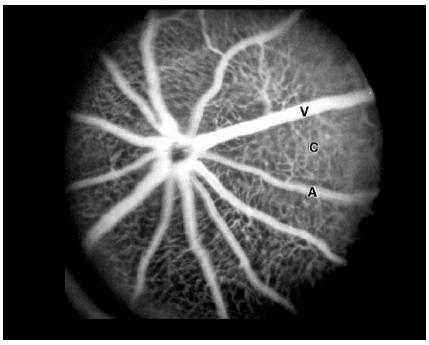

Figure 41 Confocal images of retina of mouse A] saline injection B] ATTO532 injection C] Angiogram of mouse retina

A] B] C]

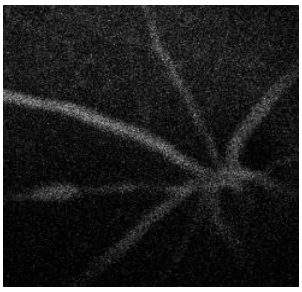

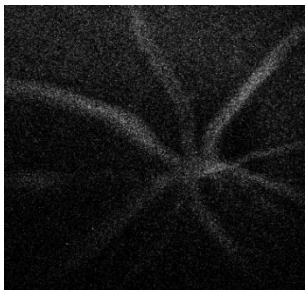

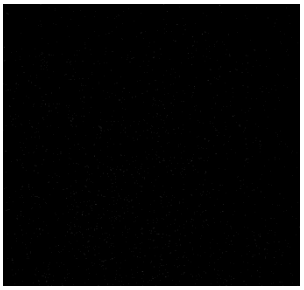

Figure 42 Confocal fluorescence image of mouse retina after A] 15 minutes B] 1 hour C] 48 hours

5.3 Significance

In these studies, we have reported an effective method to couple BLG to a fluorescent molecule using cysteine-maleimide coupling, thus yielding a conjugate that can be applied to discover the fate of blood borne BLG. Our studies to trace BLG in mice suggested that the blood-retina barrier in young mice is impervious to BLG (within the detection limits of confocal fluorescence microscopy). Since BLG was detected in drusen of a 93 year old man affected with AMD, it is possible that our mouse model, using young mice, does not accurately simulate a potentially weaker blood-retina barrier of older humans. Future studies using older mice may help discover the origin of BLG in the drusen of patients affected with AMD and thereby lead to a better understanding of the cause of this debilitating eye disease.

5.4 Experimental procedures

5.4.1 Overexpression and purification of N-Cys-BLG

N-Cys-BLG was overexpressed and purified as described in Chapter 2.

5.4.2 Coupling of BLG to N-hydroxyethylmaleimide

The BLG purified from his-trap column was dialyzed by centrifugal ultrafiltration (Amicon Ultra-15 Centrifugal Filter Unit, Millipore, Billerica, MA) to a final concentration of 2mg/mL in phosphate buffered saline (PBS) **(**10 mM phosphate buffer, 2.7 mM potassium chloride and 137 mM sodium chloride, pH 8.1 at 4^{o}C). This BLG solution was divided into 100µL aliquots in clean autoclaved microcentrifuge tubes.
5mg of N-hydroxyethylmaleimide was dissolved in 140 µL dimethyl sulphoxide biotechnology performance certified (DMSO) purchased from Sigma (D2438) in a clean, autoclaved microcentrifuge tube. 1µL of this solution was added to each of the 100µL aliquots of BLG. The resultant solution was gently mixed by pipetting with 100µL pipette. The reaction tubes were then covered with foil and incubated at 4^{o}C for 20 hours.
The solution was then dialyzed by centrifugal ultrafiltration (Amicon Ultra-0.5mL 3kDa Centrifugal Filter Unit, Millipore, Billerica, MA) in 50mM ammonium acetate (pH=7.08) to a final concentration of 2mg/mL. This sample was used for further mass spectrometric analysis.

5.4.3 Trypsin digestion and mass spectrometric analysis of coupled BLG

BLG solutions (0.4mg/mL) was dialyzed by centrifugal ultrafiltration (Amicon Ultra-0.5mL 3kDa Centrifugal Filter Unit, Millipore, Billerica, MA) in 50mM ammonium acetate (pH=7.08) to a final concentration of 2mg/mL. This solution was prepped using zip-tip columns from Millipore. The tip was wet by withdrawing 20 µL acetonitrile twice.

It was then equilibrated with 0.1% formic acid by pipetting out 20 μL of 0.1% formic acid four times. Sample was then bound to this tip by pipetting 20 μL of the sample ten times. To remove salt, the tip was then washed with 0.1% formic acid by pipetting 20 μL of the formic acid solution ten times. Finally, sample was eluted into a small, clean centrifuge tube by pipetting 15 μL of 7:10 (Acetonitrile/water) with 0.1% formic acid in and out of the loaded pipette tip.

Trypsin digest, liquid chromatography-mass spectrometry (LC-MS) and the associated data mining procedures were each carried out at the Laboratory for Biological Mass Spectrometry at Texas A&M University. Protein concentration was adjusted to 1 mg/mL with $(NH_4)_2HCO_3$ buffer and reduced with 2 mM dithiothreitol at 25 °C for 1 h. Subsequent protein alkylation was achieved using 20 mM iodoacetamide at room temperature for 10 min. Protein samples were then digested with trypsin overnight (protein:enzyme ratio of 1:50) at 37 °C. Separation and mass spectrometry were carried out at the Laboratory for Biological Mass Spectrometry at the Department of chemistry, Texas A&M University, with API QStar Pulsar, MDS Sciex (Toronto, ON, Canada) Quadrupole-TOF hybrid spectrometer. Final spectra were produced by deconvolution to show the m/z +1 peaks and labeled to indicate the ion fragments resulting from b and y-type peptide cleavage.

5.4.4 Coupling of BLG to ATTO-532

The BLG purified from his-trap column was dialyzed by centrifugal ultrafiltration (Amicon Ultra-15 Centrifugal Filter Unit, Millipore, Billerica, MA) to a final

concentration of 2mg/mL in phosphate buffered saline (PBS) **(**10 mM phosphate buffer, 2.7 mM potassium chloride and 137 mM sodium chloride, pH 8.1 at 4^{o}C). This BLG solution was divided into 100µL aliquots in clean autoclaved microcentrifuge tubes.
1mg of ATTO-532 (ATTO-TEC GmbH, Germany) was dissolved in 20µL in phosphate buffered saline (PBS) **(**10 mM phosphate buffer, 2.7 mM potassium chloride and 137 mM sodium chloride, pH 8.1 at 4^{o}C) in a clean, autoclaved microcentrifuge tube. 2µL of this solution was added to each of the 100µL aliquots of BLG. The resultant solution was gently mixed by pipetting with 100µL pipette. The reaction tubes were then covered with foil and incubated at 4^{o}C for 20 hours. The ratio of protein to dye is 1:12.
The solution was then dialyzed by centrifugal ultrafiltration (Amicon Ultra-0.5mL 3kDa Centrifugal Filter Unit, Millipore, Billerica, MA) in 50mM ammonium acetate (pH=7.08) to a final concentration of 2mg/mL. This sample was used for further mass spectrometric analysis and is referred to as BLG-ATTO532 conjugate.

5.4.5 Purification and SDS-PAGE characterization of BLG coupled to ATTO532

Coupled BLG was dialyzed by centrifugal ultrafiltration (Amicon Ultra-0.5mL 3kDa Centrifugal Filter Unit, Millipore, Billerica, MA) in loading buffer (50 mM Tris.HCl pH 8.0, 200 mM NaCl, 5 mM imidazole, 10% glycerol). Fractions that absorbed at 532nm was pooled together and separated into 3 aliquots. One aliquot was treated with sodium dodecyl sulfate (SDS) and then dialyzed into phosphate buffered saline (PBS) **(**10 mM phosphate buffer, 2.7 mM potassium chloride and 137 mM sodium chloride, pH 8.1 at 4^{o}C) over a week using dialysis bag. Once all the unreacted dye was removed, the protein was

concentrated and analyzed by SDS-PAGE. One half of the gel was stained with Coomassie blue stain and then compared against a ladder and the unstained gel.

5.4.6 Determining concentration of BLG-ATTO532 conjugate by amino-acid analysis

5.4.6.1 Instrumentation

Hydrolysis of samples is performed in a PicoTag Workstation. Amino acids are derivatized and separated on an Agilent 1260 liquid chromatograph with" Chemstation" software that controls the LC and collects, analyzes and reports the data. The G1367E autosampler performs pre-column derivatization and multiple sample handling.

Derivatized amino acids are eluted from a narrow bore, (2.1 x 200 mm), (Hypersil AA-ODS), 5 um reverse phase column purchased from Thermo Fisher (part # 30105-202130). Solvent A consists of a 20mM Na acetate buffer with 0.018% v/v triethylamine (Fluka 90338), 0.05mM EDTA, (Sigma E4884) and 0.3% tetrahydrofuran (Fluka 87363) adjusted to pH 7.2 with weak acetic acid. Solvent B is a 20% 100 mM Na acetate buffer (pH 7.2) with 40% acetonitrile and 40% methanol. The working gradient begins at 0 minutes at 100% A at 0.45 ml/min and goes to 60% B over 17 minutes.

Primary amino acids (tagged with OPA, Agilent Item # 5061-3335) are detected at 338/390 nm by the Variable Wavelength (UV) detector (G1365D) and secondary amino acids (tagged with FMOC, Agilent Item #5061-3337) at 266/324 nm.

5.4.6.2 Assay description

Protein samples (both unreacted BLG and BLG-ATTO532 conjugate) were aliquoted and mixed with internal standards (Norvaline, Sigma # N7502 for primary amino acids and Sarcosine, Sigma S7672 for secondary amino acids), dried in glass tubes (6 x 50 mm, Fisher PN 14-957AA) in a vacuum concentrator and subjected to vapor phase hydrolysis by 6N HCl (Thermo Sci # 24308) at 150ºC for 1.5 hours under argon atmosphere in the presence of phenol (2%, Sigma #P5566) which limits the halogenation of Tyrosine residues. The samples were subsequently reconstituted in 0.4 N Borate Buffer (Agilent # 5061-3339) to bring the eventual pH to 10 for optimum derivatization and transferred to the Agilent G1367E autosampler for automated derivatization and loading. Standard amino acids eluted at discrete retention times in the working portion of the chromatogram and the ChemStation® software integrated the area under the peak of the amino acid and compared it to the area under the peak of its internal standard. A line was generated by linear regression.

Note: Since hydrolysis is used, Asparagine and Glutamine are deamidated to their respective acids. Results for these residues are reported as ASX and GLX to denote that these data contain the combined amounts from both the amide and the acid. Acid hydrolysis also destroys Tryptophan. The assay is controlled by a known protein, a recombinant Human Serum Albumin (Pro-Spec-TanyTechnoGene #pro-595). An aliquot from the same batch of HSA was run with every assay. The data from these controls was used to calculate the inter-assay error of all the amino acids.

5.4.7 Determining concentration of ATTO-532 dye by Absorbance Spectroscopy

The concentration of the ATTO-532 dye in the BLG-ATTO532 conjugate was determined by absorbance scanning in a Genesys 2 UV-Vis spectrophotometer (ThermoFisher Scientific, Waltham, MA) at 532nm with PBS serving as the absorbance blank and using the absorptivity co-efficient of 115000 $M^{-1}cm^{-1}$ provided by the vendor.

5.4.8 Imaging mouse retina

The following protocol (IACUC 2016-0168) was approved by the Texas A&M University Institutional Animal Care and Use Committee (IACUC). The mice (BALB/c) were purchased from Charles River (USA). All adult mice were housed separately in standard cages in the Laboratory Animal Resources and Research (LARR) facility at Texas A&M University and maintained under standard conditions.

The mice were initially anesthetized using ketamine:dexmitomodene (25mg/mL:0.25mg/mL) cocktail. Coupled BLG was dialyzed by centrifugal ultrafiltration (Amicon Ultra-0.5mL 3kDa Centrifugal Filter Unit, Millipore, Billerica, MA) into phosphate buffered saline (PBS) **(**10 mM phosphate buffer, 2.7 mM potassium chloride and 137 mM sodium chloride, pH 8.1 at $4^{o}C$) to give a final protein concentration of 2.5mg/mL. 200 microliter of this solution was intravenously introduced into the mice (n=2). Control injections with either saline or ATTO532 was also performed.

Imaging analysis

The mouse retina was imaged on an inverted Nikon confocal scanning microscope. The imaging objective was a Nikon CFI 10X with a 0.30 NA. This objective is to be used in free space air, something that contributed to less optimal imaging quality, and will be discussed later. Three lasers were used as excitation sources. Their center wavelengths are 488 nm, 543 nm, and 632 nm, respectively. The three emission filters used were a 540/30 nm, a 590/50 nm, and a 650 nm longpass, with each corresponding to in order to their respective laser above. The dye used is most efficiently excited and detected using the 543 nm laser and 590/50 nm filter combination.

After anesthetization and injection of saline, ATTO532 dye or BLG-ATTO532 conjugate, the non-imaged mouse eye was covered using a gel lubricant. Likewise, the imaged eye was covered using an optically clear ultrasound gel with the same refractive index as water and a pupil dilating agent: Opcon-A (Bausch and Lomb, active pharmaceutical ingredient-naphazoline HCl and pheniramine maleate). The mouse eye was then placed on a cover slip and "coupled" to the surface via the ultrasound gel. This coupling made a homogenous medium between the coverslip and the mouse eye. The gel for both eyes was necessary because of the effects of anesthesia on the mouse. Prolonged exposure to air without the ability to blink will dry the cornea, cause damage, and make imaging more difficult. The reasons ultrasound gel was used in particular are that it is optically clear and possess a similar refractive index to water, i.e. tissue and the eye. The idea behind this is that the medium changes between the objective and the eye would reduce the effects of index mismatch, such as aberrations.

After the mouse was correctly positioned, axial translation was used to find the interface between the cornea and glass. This was set as the zero positon for imaging. The stage

axially was translated roughly 3-4 mm into the eye. However, because the lens of the mouse eye itself has a focal length of about ~2.6 mm on average, the distance into the eye is not the same as the focal spot translation.[(141)] Simple geometric optics suggest that the axial focal spot inside the eye would non-linearly relate to the axial translation of the stage. A simple simulation using raytracing software reveals this to be true. Note that this was assuming only the lens of the eye affected the light rays. Regardless, the effective focal distance was roughly 2 mm into the eye where an offset of 1 mm in either direction translates to ~.2 mm. These are rough estimations as a rigorous examination to determine the exact focal position within the eye was not done. The axial resolution of the microscope in optimal conditions is 11.2 μm. Aberrations caused by refractive index mismatch between the air objective and water imaging environment as well as additional mouse eye lens would likely degrade this. Z-stacks, or volumetric three dimensional stacks, were acquired at two different positions. One stack was taken at the focal plane of the retina and another at 1 mm superficial to this. The axial spacing of the Z-stack was set so that each image in the stack was 15 μm apart from one another and covered anywhere from 1 mm to 0.2 mm.

CHAPTER VI

CONCLUSIONS

Dry form of age-related macular degeneration, a neurodegenerative disease proposed to affect five million people by 2050 is characterized by the deposition of drusen and lipofuscins in the retina. The biosynthesis of lipofuscin is poorly understood. Bovine BLG is an enigmatic protein whose native function, if any, has been hard to unravel. Its similarity to RBP, its detection in the drusen of patients affected with AMD and its ability to cyclodimerize ATR to cycloretinal both *in vitro* and *in vivo* leads to the belief that this protein may be one of the proteins responsible for the biosynthesis of the lipofuscin cycloretinal. Our results lead us to believe that a hydrophobic cavity and two lysines relatively proximal to each other are necessary for the cyclodimerization of retinal to cycloretinal. While mutagenesis studies support the initial proposal that this catalysis happens in the central hydrophobic cavity of BLG, mass spectrometric and other mutagenesis studies support the theory that a secondary binding site of BLG with lysines 77 and 91 may also be involved. Further studies utilizing BLG from other animals that may not contain secondary binding sites could lead to better understanding of this cyclodimerization mechanism.

During these studies, we discovered that BLG can catalyze the retro-aldol cleavage of α, β unsaturated aldehydes on hydrophobic substrates. Retroaldolase activity, only the second enzymatic activity discovered for BLG, was seen to be most effective on substrates with phenyl or naphthyl side-chains. Retroaldolase activity of BLG, when combined with an

efficient purification technique for BLG reported in this dissertation could lead to the development of a cheap, commercial catalyst.

While our results also suggest that the blood-retina barrier in mice is not permeable to BLG-ATTO532 dye conjugate, it could be possible that a potentially weak blood-retina barrier in older patients may be permeable to this protein. Computational analysis of the one hundred and thirty other proteins found in the drusen may also discover that some of these have two proximal lysines along with a hydrophobic cavity and thus be capable of cyclodimerizing ATR to cycloretinal.

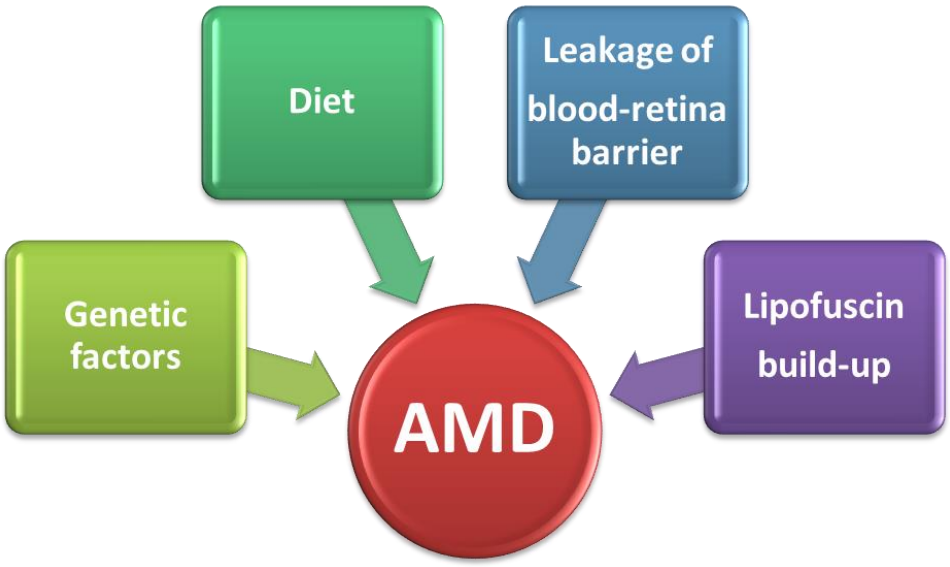

Figure 43 Various factors could potentially contribute to the progression of AMD

Therapeutics to prevent drusen formation will need to include not only a cocktail of drugs that can inhibit lipofuscin formation and strengthen the blood-retina barrier but also gene editing agents to negotiate the genetic causes of AMD. Discovering enzymes that break-down lipofuscins into easily execrable by-products might be a preferable alternative therapy. Delivering these enzymes through means other than injections to the eye would further help alleviate the discomfort that people with AMD would need to go through. Better healthcare which has nearly doubled life expectancy in less than a hundred years from less than 50 to more than 80 years has also led to the increased prevalence of age-related diseases. Protein mediated biosynthesis of the lipofuscin cycloretinal is probably only one musician in a whole orchestra of factors (from dietary to genetic) involved in the development of AMD, a neurodegenerative disease. While dietary intake of milk does lead to increased chance of developing AMD[(37)], our experiments and a survey of literature have not revealed any conclusive evidence for a direct correlation between dietary intake of BLG and AMD progression. However, our studies into BLG mediated catalysis reported in this dissertation have provided insight on the role of lysines in the biosynthesis of cycloretinal *in vivo*.

REFERENCES

1. Stone, E. M. (2007) Macular Degeneration, *Annual Review of Medicine 58*, 477-490.
2. Roberts, H., Ni, M., and O'Brart, D. (2017) Financial modelling of femtosecond laser-assisted cataract surgery within the National Health Service using a ‘hub and spoke’model for the delivery of high-volume cataract surgery, *BMJ open 7*, e013616.
3. Farrand, K. F., Fridman, M., Stillman, I. Ö., and Schaumberg, D. A. (2017) Prevalence of diagnosed dry eye disease in the united states among adults aged 18 years and older, *American Journal of Ophthalmology 182*, 90-98.
4. Klein, R., and Klein, B. E. K. (2013) The Prevalence of Age-Related Eye Diseases and Visual Impairment in Aging: Current Estimates, *Investigative Ophthalmology & Visual Science 54*, ORSF5-ORSF13.
5. The Eye Diseases Prevalence Research, G. (2004) Prevalence of age-related macular degeneration in the united states, *Archives of Ophthalmology 122*, 564-572.
6. Wong, T. Y., Loon, S. C., and Saw, S. M. (2006) The epidemiology of age related eye diseases in Asia, *British Journal of Ophthalmology 90*, 506.
7. Campo, I. S., and Beghin, J. C. (2005) Dairy food consumption, production, and policy in Japan.
8. Kolb, H. (2011) Simple Anatomy of the Retina by Helga Kolb.

9. Kiser, P. D., Golczak, M., and Palczewski, K. (2014) Chemistry of the retinoid (visual) cycle, *Chemical reviews 114*, 194-232.

10. Korte, G. E., Reppucci, V., and Henkind, P. (1984) RPE destruction causes choriocapillary atrophy, *Investigative Ophthalmology & Visual Science 25*, 1135-1145.

11. Ferris, F. L., Fine, S. L., and Hyman, L. (1984) Age-related macular degeneration and blindness due to neovascular maculopathy, *Archives of ophthalmology 102*, 1640-1642.

12. Winkler, B. S., Boulton, M. E., Gottsch, J. D., and Sternberg, P. (1999) Oxidative damage and age-related macular degeneration, *Molecular vision 5*, 32.

13. Dunaief, J. L., Dentchev, T., Ying, G.-S., and Milam, A. H. (2002) The role of apoptosis in age-related macular degeneration, *Archives of ophthalmology 120*, 1435-1442.

14. Chong, N. V., Keonin, J., Luthert, P. J., Frennesson, C. I., Weingeist, D. M., Wolf, R. L., Mullins, R. F., and Hageman, G. S. (2005) Decreased thickness and integrity of the macular elastic layer of Bruch's membrane correspond to the distribution of lesions associated with age-related macular degeneration, *The American journal of pathology 166*, 241-251.

15. Klein, R., Myers, C. E., Lee, K. E., Gangnon, R. E., Sivakumaran, T. A., Iyengar, S. K., and Klein, B. E. (2015) Small drusen and age-related macular degeneration: The Beaver Dam Eye Study, *Journal of clinical medicine 4*, 425-440.

16. Campochiaro, P. A., Soloway, P., Ryan, S. J., and Miller, J. W. (1999) The pathogenesis of choroidal neovascularization in patients with age-related macular degeneration, *Mol Vis 5*, 34-38.

17. Wang, L., Clark, M. E., Crossman, D. K., Kojima, K., Messinger, J. D., Mobley, J. A., and Curcio, C. A. (2010) Abundant Lipid and Protein Components of Drusen, *PLoS One 5*, e10329.

18. Crabb, J. W., Miyagi, M., Gu, X., Shadrach, K., West, K. A., Sakaguchi, H., Kamei, M., Hasan, A., Yan, L., Rayborn, M. E., Salomon, R. G., and Hollyfield, J. G. (2002) Drusen proteome analysis: An approach to the etiology of age-related macular degeneration, *Proceedings of the National Academy of Sciences of the United States of America 99*, 14682-14687.

19. Sparrow, J. R., Vollmer-Snarr, H. R., Zhou, J., Jang, Y. P., Jockusch, S., Itagaki, Y., and Nakanishi, K. (2003) A2E-epoxides Damage DNA in Retinal Pigment Epithelial Cells: Vitamin E and Other Antioxidants Inhibit A2E Formation, *Journal of Biological Chemistry 278*, 18207-18213.

20. Anderson, O. A., Finkelstein, A., and Shima, D. T. (2013) A2E induces IL-1ss production in retinal pigment epithelial cells via the NLRP3 inflammasome, *PloS one 8*, e67263.

21. Fishkin, N. E., Sparrow, J. R., Allikmets, R., and Nakanishi, K. (2005) Isolation and characterization of a retinal pigment epithelial cell fluorophore: an all-trans-retinal dimer conjugate, *Proceedings of the National Academy of Sciences of the United States of America 102*, 7091-7096.

22. Kim, S. R., Jang, Y. P., Jockusch, S., Fishkin, N. E., Turro, N. J., and Sparrow, J. R. (2007) The all-trans-retinal dimer series of lipofuscin pigments in retinal pigment epithelial cells in a recessive Stargardt disease model, *Proceedings of the National Academy of Sciences 104*, 19273-19278.

23. Kaufman, Y., Ma, L., and Washington, I. (2011) Deuterium Enrichment of Vitamin A at the C20 Position Slows the Formation of Detrimental Vitamin A Dimers in Wild-type Rodents, *Journal of Biological Chemistry 286*, 7958-7965.

24. Ma, L., Kaufman, Y., Zhang, J., and Washington, I. (2011) C20-D3-vitamin A Slows Lipofuscin Accumulation and Electrophysiological Retinal Degeneration in a Mouse Model of Stargardt Disease, *Journal of Biological Chemistry 286*, 7966-7974.

25. Fishkin, E. N., Sparrow, J. R., Allikmets, RA., Nakanishi, K. (2005) Isolation and Characterization of a Retinal Pigment Epithelial Cell Fluorophore: An All-Trans-Retinal Dimer Conjugate, *Proceedings of the National Academy of Sciences 102*, 7091-7096.

26. Fishkin, N., Pescitelli, G., Sparrow, J. R., Nakanishi, K., and Berova, N. (2004) Absolute Configurational Determination of an All-Trans-Retinal Dimer Isolated from Photoreceptor Outer Segments, *Chirality 16*, 637-641.

27. Bench, B. J., Liu, C., Evett, C. R., and Watanabe, C. M. H. (2006) Proline Promoted Synthesis of Ring-Fused Homodimers: Self-Condensation of α,β-Unsaturated Aldehydes, *The Journal of Organic Chemistry 71*, 9458-9463.

28. Eisenhauer, B., Natoli, S., Liew, G., and Flood, V. M. (2017) Lutein and Zeaxanthin—Food Sources, Bioavailability and Dietary Variety in Age-Related Macular Degeneration Protection, *Nutrients 9*, 120.

29. Broadhead, G. K., Grigg, J. R., Chang, A. A., and McCluskey, P. (2015) Dietary modification and supplementation for the treatment of age-related macular degeneration, *Nutrition reviews 73*, 448-462.

30. Gorusupudi, A., Nelson, K., and Bernstein, P. S. (2017) The Age-Related Eye Disease 2 Study: Micronutrients in the Treatment of Macular Degeneration, *Advances in Nutrition: An International Review Journal 8*, 40-53.

31. Gragoudas, E. S., Adamis, A. P., Cunningham Jr, E. T., Feinsod, M., and Guyer, D. R. (2004) Pegaptanib for neovascular age-related macular degeneration, *New England Journal of Medicine 351*, 2805-2816.

32. Yoganathan, P., Deramo, V. A., Lai, J. C., Tibrewala, R. K., and Fastenberg, D. M. (2006) Visual improvement following intravitreal bevacizumab (Avastin) in exudative age-related macular degeneration, *Retina 26*, 994-998.

33. Arevalo, J. F., Maia, M., Flynn, H., Saravia, M., Avery, R. L., Wu, L., Farah, M. E., Pieramici, D. J., Berrocal, M. H., and Sanchez, J. G. (2008) Tractional retinal detachment following intravitreal bevacizumab (Avastin) in patients with severe proliferative diabetic retinopathy, *British Journal of Ophthalmology 92*, 213-216.

34. Bench, B. J., Tichy, S. E., Perez, L. M., Benson, J., and Watanabe, C. M. H. (2008) Synthesis and Cellular Effects of Cycloterpenals: Cyclohexadienal-Based Activators of Neurite Outgrowth, *Bioorgan Med Chem 16*, 7573-7581.

35. Bench, B. J., Foulke-Abel, J., and Watanabe, C. M. (2011) Milk, revealed "silent" chemistry: new mode of cycloretinal synthesis, *Molecular bioSystems 7*, 162-168.

36. Asato, A. E., Watanabe, C., Li, X. Y., and Liu, R. S. H. (1992) The Proline and Beta-Lactoglobulin Mediated Asymmetric Self-Condensation of Beta-Ionylideneacetaldehyde, Retinal and Related-Compounds, *Tetrahedron Letters 33*, 3105-3108.

37. Seddon, J. M., Rosner, B., Sperduto, R. D., Yannuzzi, L., Haller, J. A., Blair, N. P., and Willett, W. (2001) Dietary fat and risk for advanced age-related macular degeneration, *Archives of ophthalmology 119*, 1191-1199.

38. Palmer, A. H. (1934) The Preparation of a Crystalline Globulin from the Albumin Fraction of Cow's Milk, *Journal of Biological Chemistry 104*, 359-372.

39. Kontopidis, G., Holt, C., and Sawyer, L. (2004) Invited Review: β-Lactoglobulin: Binding Properties, Structure, and Function, *Journal of Dairy Science 87*, 785-796.

40. Sawyer, L., Brownlow, S., Polikarpov, I., and Wu, S.-Y. (1998) β-Lactoglobulin: Structural Studies, Biological Clues, *International Dairy Journal 8*, 65-72.

41. Sawyer, L., and Kontopidis, G. (2000) The core lipocalin, bovine β-lactoglobulin, *Biochimica et Biophysica Acta (BBA) - Protein Structure and Molecular Enzymology 1482*, 136-148.

42. Goldman, A., Anderson, D., Sellers, W., Saperstein, S., Kniker, W., and Halpern, S. (1963) Milk allergy, *Pediatrics 32*, 425-443.

43. Wal, J. M. (1998) Cow's milk allergens, *Allergy 53*, 1013-1022.

44. Fox, P. F. (1995) Heat-induced changes in milk. 2.

45. Relkin, P., and Mulvihill, D. (1996) Thermal unfolding of β-lactoglobulin, α-lactalbumin, and bovine serum albumin. A thermodynamic approach, *Critical Reviews in Food Science & Nutrition 36*, 565-601.

46. De Jong, P. (1997) Impact and control of fouling in milk processing, *Trends in Food Science & Technology 8*, 401-405.

47. Fugate, R. D., and Song, P.-s. (1980) Spectroscopic characterization of β-lactoglobulin-retinol complex, *Biochimica et Biophysica Acta (BBA) - Protein Structure 625*, 28-42.

48. Cho, Y., Batt, C. A., and Sawyer, L. (1994) Probing the retinol-binding site of bovine beta-lactoglobulin, *Journal of Biological Chemistry 269*, 11102-11107.

49. Tanford, C., Bunville, L. G., and Nozaki, Y. (1959) The reversible transformation of β-lactoglobulin at pH 7.51, *Journal of the American Chemical Society 81*, 4032-4036.

50. Sawyer, L., Papiz, M. Z., North, A. C., and Eliopoulos, E. E. (1985) Structure and function of bovine β-lactoglobulin, Portland Press Limited.

51. Godovac-Zimmermann, J., Conti, A., Liberatori, J., and Braunitzer, G. (1985) Homology between the Primary Structures of β-Lactoglobulins and Human Retinol-Binding Protein: Evidence for a Similar Biological Function?, *Biological Chemistry 366*, 431-434.

52. Pervaiz, S., and Brew, K. (1985) Homology of beta-lactoglobulin, serum retinol-binding protein, and protein HC, *Science 228*, 335-338.

53. Gowda, V., Foulke-Abel, J., Agbo, H., Bench, B. J., Chae, J., Russell, W. K., and Watanabe, C. M. H. (2017) Lipofuscin Formation Catalyzed by the Milk Protein β-

Lactoglobulin: Lysine Residues in Cycloretinal Synthesis, *Biochemistry 56*, 5715-5719.

54. Brownlow, S., Morais Cabral, J. H., Cooper, R., Flower, D. R., Yewdall, S. J., Polikarpov, I., North, A. C., and Sawyer, L. (1997) Bovine beta-lactoglobulin at 1.8 A resolution--still an enigmatic lipocalin, *Structure (London, England : 1993) 5*, 481-495.

55. Qin, B. Y., Creamer, L. K., Baker, E. N., and Jameson, G. B. (1998) 12-Bromododecanoic acid binds inside the calyx of bovine β-lactoglobulin, *FEBS Letters 438*, 272-278.

56. Qin, B. Y., Creamer, L. K., Baker, E. N., and Jameson, G. B. (1998) 12-Bromododecanoic acid binds inside the calyx of bovine beta-lactoglobulin, *FEBS Lett 438*, 272-278.

57. Qin, B. Y., Bewley, M. C., Creamer, L. K., Baker, H. M., Baker, E. N., and Jameson, G. B. (1998) Structural basis of the Tanford transition of bovine beta-lactoglobulin, *Biochemistry 37*, 14014-14023.

58. Wu, S. Y., Perez, M. D., Puyol, P., and Sawyer, L. (1999) beta-lactoglobulin binds palmitate within its central cavity, *The Journal of biological chemistry 274*, 170-174.

59. Qin, B. Y., Bewley, M. C., Creamer, L. K., Baker, E. N., and Jameson, G. B. (1999) Functional implications of structural differences between variants A and B of bovine beta-lactoglobulin, *Protein science : a publication of the Protein Society 8*, 75-83.

60. Uhrinova, S., Smith, M. H., Jameson, G. B., Uhrin, D., Sawyer, L., and Barlow, P. N. (2000) Structural changes accompanying pH-induced dissociation of the beta-lactoglobulin dimer, *Biochemistry 39*, 3565-3574.

61. Oliveira, K. M., Valente-Mesquita, V. L., Botelho, M. M., Sawyer, L., Ferreira, S. T., and Polikarpov, I. (2001) Crystal structures of bovine beta-lactoglobulin in the orthorhombic space group C222(1). Structural differences between genetic variants A and B and features of the Tanford transition, *European journal of biochemistry 268*, 477-483.

62. Kontopidis, G., Holt, C., and Sawyer, L. (2002) The Ligand-binding Site of Bovine β-Lactoglobulin: Evidence for a Function?, *Journal of molecular biology 318*, 1043-1055.

63. Kontopidis, G., Holt, C., and Sawyer, L. (2002) The ligand-binding site of bovine beta-lactoglobulin: evidence for a function?, *Journal of molecular biology 318*, 1043-1055.

64. Jayat, D., Gaudin, J. C., Chobert, J. M., Burova, T. V., Holt, C., McNae, I., Sawyer, L., and Haertle, T. (2004) A recombinant C121S mutant of bovine beta-lactoglobulin is more susceptible to peptic digestion and to denaturation by reducing agents and heating, *Biochemistry 43*, 6312-6321.

65. Adams, J. J., Anderson, B. F., Norris, G. E., Creamer, L. K., and Jameson, G. B. (2006) Structure of bovine beta-lactoglobulin (variant A) at very low ionic strength, *Journal of structural biology 154*, 246-254.

66. Niemi, M., Jylha, S., Laukkanen, M. L., Soderlund, H., Makinen-Kiljunen, S., Kallio, J. M., Hakulinen, N., Haahtela, T., Takkinen, K., and Rouvinen, J. (2007)

Molecular interactions between a recombinant IgE antibody and the beta-lactoglobulin allergen, *Structure (London, England : 1993) 15*, 1413-1421.

67. Yang, M.-C., Guan, H.-H., Liu, M.-Y., Lin, Y.-H., Yang, J.-M., Chen, W.-L., Chen, C.-J., and Mao, S. J. T. (2008) Crystal structure of a secondary vitamin D_3 binding site of milk beta-lactoglobulin, *Proteins: Structure, Function, and Bioinformatics 71*, 1197-1210.

68. Vijayalakshmi, L., Krishna, R., Sankaranarayanan, R., and Vijayan, M. (2008) An asymmetric dimer of β-lactoglobulin in a low humidity crystal form—Structural changes that accompany partial dehydration and protein action, *Proteins: Structure, Function, and Bioinformatics 71*, 241-249.

69. Yang, M. C., Guan, H. H., Liu, M. Y., Lin, Y. H., Yang, J. M., Chen, W. L., Chen, C. J., and Mao, S. J. (2008) Crystal structure of a secondary vitamin D3 binding site of milk beta-lactoglobulin, *Proteins 71*, 1197-1210.

70. Vijayalakshmi, L., Krishna, R., Sankaranarayanan, R., and Vijayan, M. (2008) An asymmetric dimer of beta-lactoglobulin in a low humidity crystal form--structural changes that accompany partial dehydration and protein action, *Proteins 71*, 241-249.

71. Loch, J., Polit, A., Gorecki, A., Bonarek, P., Kurpiewska, K., Dziedzicka-Wasylewska, M., and Lewinski, K. (2011) Two modes of fatty acid binding to bovine beta-lactoglobulin--crystallographic and spectroscopic studies, *Journal of molecular recognition : JMR 24*, 341-349.

72. Ohtomo, H., Konuma, T., Utsunoiya, H., Tsuge, H., and Ikeguchi, M. (2011) Structure and stability of Gyuba, a beta-lactoglobulin chimera, *Protein science : a publication of the Protein Society 20*, 1867-1875.

73. Loch, J. I., Polit, A., Bonarek, P., Olszewska, D., Kurpiewska, K., Dziedzicka-Wasylewska, M., and Lewinski, K. (2012) Structural and thermodynamic studies of binding saturated fatty acids to bovine beta-lactoglobulin, *International journal of biological macromolecules 50*, 1095-1102.

74. Loch, J. I., Bonarek, P., Polit, A., Swiatek, S., Dziedzicka-Wasylewska, M., and Lewinski, K. (2013) The differences in binding 12-carbon aliphatic ligands by bovine beta-lactoglobulin isoform A and B studied by isothermal titration calorimetry and X-ray crystallography, *Journal of molecular recognition : JMR 26*, 357-367.

75. Loch, J. I., Bonarek, P., Polit, A., Ries, D., Dziedzicka-Wasylewska, M., and Lewinski, K. (2013) Binding of 18-carbon unsaturated fatty acids to bovine beta-lactoglobulin--structural and thermodynamic studies, *International journal of biological macromolecules 57*, 226-231.

76. Gutierrez-Magdaleno, G., Bello, M., Portillo-Tellez, M. C., Rodriguez-Romero, A., and Garcia-Hernandez, E. (2013) Ligand binding and self-association cooperativity of beta-lactoglobulin, *Journal of molecular recognition : JMR 26*, 67-75.

77. Nossoni, Z., Assar, Z., Yapici, I., Nosrati, M., Wang, W., Berbasova, T., Vasileiou, C., Borhan, B., and Geiger, J. (2014) Structures of holo wild-type human cellular retinol-binding protein II (hCRBPII) bound to retinol and retinal, *Acta Crystallographica Section D 70*, 3226-3232.

78. Loch, J. I., Bonarek, P., Polit, A., Jablonski, M., Czub, M., Ye, X., and Lewinski, K. (2015) beta-Lactoglobulin interactions with local anaesthetic drugs - Crystallographic and calorimetric studies, *International journal of biological macromolecules 80*, 87-94.

79. Loch, J. I., Bonarek, P., Tworzydło, M., Polit, A., Hawro, B., Łach, A., Ludwin, E., and Lewiński, K. (2016) Engineered β-Lactoglobulin Produced in E. coli: Purification, Biophysical and Structural Characterisation, *Molecular Biotechnology 58*, 605-618.

80. Loch, J. I., Bonarek, P., Tworzydlo, M., Polit, A., Hawro, B., Lach, A., Ludwin, E., and Lewinski, K. (2016) Engineered beta-Lactoglobulin Produced in E. coli: Purification, Biophysical and Structural Characterisation, *Mol Biotechnol 58*, 605-618.

81. Kurpiewska, K., Biela, A., Loch, J. I., Swiatek, S., Jachimska, B., and Lewinski, K. (2017) Investigation of high pressure effect on the structure and adsorption of beta-lactoglobulin, *Colloids and surfaces. B, Biointerfaces 161*, 387-393.

82. Kuwata, K., Era, S., Hoshino, M., Forge, V., Goto, Y., and Batt, C. A. (1999) Solution structure and dynamics of bovine β-lactoglobulin A, *Protein Science 8*, 2541-2545.

83. Sakurai, K., and Goto, Y. (2006) Dynamics and mechanism of the Tanford transition of bovine beta-lactoglobulin studied using heteronuclear NMR spectroscopy, *Journal of molecular biology 356*, 483-496.

84. Konuma, T., Sakurai, K., and Goto, Y. (2007) Promiscuous Binding of Ligands by β-Lactoglobulin Involves Hydrophobic Interactions and Plasticity, *Journal of molecular biology 368*, 209-218.

85. Sakurai, K., Konuma, T., Yagi, M., and Goto, Y. (2009) Structural dynamics and folding of β-lactoglobulin probed by heteronuclear NMR, *Biochimica et Biophysica Acta (BBA) - General Subjects 1790*, 527-537.

86. Blanch, E. W., Hecht, L., and Barron, L. D. (1999) New insight into the pH-dependent conformational changes in bovine β-lactoglobulin from Raman optical activity, *Protein Science 8*, 1362-1367.

87. Crowther, J. M., Lassé, M., Suzuki, H., Kessans, S. A., Loo, T. S., Norris, G. E., Hodgkinson, A. J., Jameson, G. B., and Dobson, R. C. J. (2014) Ultra-high resolution crystal structure of recombinant caprine β-lactoglobulin, *FEBS Letters 588*, 3816-3822.

88. Loch, J. I., Bonarek, P., Polit, A., Jabłoński, M., Czub, M., Ye, X., and Lewiński, K. (2015) β-Lactoglobulin interactions with local anaesthetic drugs – Crystallographic and calorimetric studies, *International journal of biological macromolecules 80*, 87-94.

89. Kontopidis, G., Nordle Gilliver, A., and Sawyer, L. (2014) Ovine beta-lactoglobulin at atomic resolution, *Acta crystallographica. Section F, Structural biology communications 70*, 1498-1503.

90. Loch, J. I., Molenda, M., Kopec, M., Swiatek, S., and Lewinski, K. (2014) Structure of two crystal forms of sheep beta-lactoglobulin with EF-loop in closed conformation, *Biopolymers 101*, 886-894.

91. Oksanen, E., Jaakola, V. P., Tolonen, T., Valkonen, K., Akerstrom, B., Kalkkinen, N., Virtanen, V., and Goldman, A. (2006) Reindeer beta-lactoglobulin crystal structure with pseudo-body-centred noncrystallographic symmetry, *Acta crystallographica. Section D, Biological crystallography 62*, 1369-1374.

92. Bello, M., and García-Hernández, E. (2014) Ligand entry into the calyx of β-lactoglobulin, *Biopolymers 101*, 744-757.

93. Caillard, I., and Tome, D. (1994) Modulation of Beta-Lactoglobulin Transport in Rabbit Ileum, *Am J Physiol 266*, G1053-G1059.

94. Foulke-Abel, J. D. (2010) *Natural product biosynthesis: Friend or foe? From anti-tumor agent to disease causation*, Texas A&M University.

95. Evoli, S., Guzzi, R., and Rizzuti, B. (2014) Molecular simulations of β-lactoglobulin complexed with fatty acids reveal the structural basis of ligand affinity to internal and possible external binding sites, *Proteins: Structure, Function, and Bioinformatics 82*, 2609-2619.

96. Lange, D. C., Kothari, R., Patel, R. C., and Patel, S. C. (1998) Retinol and retinoic acid bind to a surface cleft in bovine β-lactoglobulin: a method of binding site determination using fluorescence resonance energy transfer, *Biophysical Chemistry 74*, 45-51.

97. Pervaiz, S., and Brew, K. (1987) Homology and structure-function correlations between alpha 1-acid glycoprotein and serum retinol-binding protein and its relatives, *The FASEB journal 1*, 209-214.

98. Lovegrove, J. A., Osman, D. L., Morgan, J. B., and Hampton, S. M. (1993) Transfer of cow's milk beta-lactoglobulin to human serum after a milk load: a pilot study, *Gut 34*, 203-207.

99. Harmatz, P. R., Hanson, D. G., Walsh, M. K., Kleinman, R. E., Bloch, K. J., and Walker, W. A. (1986) Transfer of protein antigens into milk after intravenous injection into lactating mice, *American Journal of Physiology - Endocrinology And Metabolism 251*, E227-E233.

100. Livney, Y. D. (2010) Milk proteins as vehicles for bioactives, *Current Opinion in Colloid & Interface Science 15*, 73-83.

101. Gülseren, İ., Fang, Y., and Corredig, M. (2012) Whey protein nanoparticles prepared with desolvation with ethanol: Characterization, thermal stability and interfacial behavior, *Food Hydrocolloids 29*, 258-264.

102. Sagalowicz, L., and Leser, M. E. (2010) Delivery systems for liquid food products, *Current Opinion in Colloid & Interface Science 15*, 61-72.

103. Kratz, F. (2008) Albumin as a drug carrier: Design of prodrugs, drug conjugates and nanoparticles, *Journal of Controlled Release 132*, 171-183.

104. Jeffery, C. J. (2003) Moonlighting proteins: old proteins learning new tricks, *Trends in Genetics 19*, 415-417.

105. Copley, S. D. (2003) Enzymes with extra talents: moonlighting functions and catalytic promiscuity, *Current opinion in chemical biology 7*, 265-272.

106. Albanese, D. C. M., and Gaggero, N. (2015) Albumin as a promiscuous biocatalyst in organic synthesis, *RSC Advances 5*, 10588-10598.

107. Obexer, R., Godina, A., Garrabou, X., Mittl, P. R. E., Baker, D., Griffiths, A. D., and Hilvert, D. (2016) Emergence of a catalytic tetrad during evolution of a highly active artificial aldolase, *Nat Chem advance online publication*.

108. Garrabou, X., Beck, T., and Hilvert, D. (2015) A Promiscuous De Novo Retro-Aldolase Catalyzes Asymmetric Michael Additions via Schiff Base Intermediates, *Angewandte Chemie 54*, 5609-5612.

109. Garrabou, X., Wicky, B. I., and Hilvert, D. (2016) Fast Knoevenagel Condensations Catalyzed by an Artificial Schiff-Base-Forming Enzyme, *J Am Chem Soc 138*, 6972-6974.

110. Chevalley, A., and Salmain, M. (2012) Enantioselective transfer hydrogenation of ketone catalysed by artificial metalloenzymes derived from bovine [small beta]-lactoglobulin, *Chemical Communications 48*, 11984-11986.

111. Chevalley, A., Cherrier, M. V., Fontecilla-Camps, J. C., Ghasemi, M., and Salmain, M. (2014) Artificial metalloenzymes derived from bovine [small beta]-lactoglobulin for the asymmetric transfer hydrogenation of an aryl ketone - synthesis, characterization and catalytic activity, *Dalton Transactions 43*, 5482-5489.

112. Zhou, W., Wan, Y., Guo, R., Deng, M., Deng, K., Wang, Z., Zhang, Y., and Wang, F. (2017) Generation of beta-lactoglobulin knock-out goats using CRISPR/Cas9, *PLOS ONE 12*, e0186056.

113. Jabed, A., Wagner, S., McCracken, J., Wells, D. N., and Laible, G. (2012) Targeted microRNA expression in dairy cattle directs production of beta-lactoglobulin-free,

high-casein milk, *Proceedings of the National Academy of Sciences of the United States of America 109*, 16811-16816.

114. Marcon-Genty, D., Tome, D., Kheroua, O., Dumontier, A. M., Heyman, M., and Desjeux, J. F. (1989) Transport of Beta-Lactoglobulin Across Rabbit Ileum In vitro, *Amer J Physiol 256*, G943-948.

115. Invernizzi, G., Ragona, L., Brocca, S., Pedrazzoli, E., Molinari, H., Morandini, P., Catalano, M., and Lotti, M. (2004) Heterologous expression of bovine and porcine [beta]-lactoglobulins in Pichia pastoris: towards a comparative functional characterisation, *Journal of Biotechnology 109*, 169-178.

116. Chatel, J.-M., Adel-Patient, K., Créminon, C., and Wal, J.-M. (1999) Expression of a Lipocalin in Prokaryote and Eukaryote Cells: Quantification and Structural Characterization of Recombinant Bovine [beta]-Lactoglobulin, *Protein expression and purification 16*, 70-75.

117. Hyttinen, J.-M., Korhonen, V.-P., Hiltunen, M. O., Myöhänen, S., and Jänne, J. (1998) High-level expression of bovine β-lactoglobulin gene in transgenic mice, *Journal of biotechnology 61*, 191-198.

118. Berkmen, M. (2012) Production of disulfide-bonded proteins in Escherichia coli, *Protein expression and purification 82*, 240-251.

119. Ponniah, K., Loo, T. S., Edwards, P. J., Pascal, S. M., Jameson, G. B., and Norris, G. E. (2010) The production of soluble and correctly folded recombinant bovine beta-lactoglobulin variants A and B in Escherichia coli for NMR studies, *Protein expression and purification 70*, 283-289.

120. Sun, P., Tropea, J. E., and Waugh, D. S. (2011) Enhancing the Solubility of Recombinant Proteins in Escherichia coli by Using Hexahistidine-Tagged Maltose-Binding Protein as a Fusion Partner, In *Heterologous Gene Expression in E.coli: Methods and Protocols* (Evans, J. T. C., and Xu, M.-Q., Eds.), pp 259-274, Humana Press, Totowa, NJ.

121. Kapust RB, T. J., Fox JD, Anderson DE, Cherry S, Copeland TD, Waugh DS. . (2001 Dec) Tobacco etch virus protease: mechanism of autolysis and rational design of stable mutants with wild-type catalytic proficiency., *Protein Eng. 14*, 993-1000.

122. Evans, J. R. (2001) Risk Factors for Age-related Macular Degeneration, *Progress in Retinal and Eye Research 20*, 227-253.

123. Bench, B. J., Liu, C., Evett, C. R., and Watanabe, C. M. (2006) Proline Promoted Synthesis of Ring-Fused Homodimers: Self-Condensation of Alpha,Beta-Unsaturated Aldehydes, *J Org Chem 71*, 9458-9463.

124. NarayanAlison, R. H., Jiménez-Osés, G., Liu, P., Negretti, S., Zhao, W., Gilbert, M. M., Ramabhadran, R. O., Yang, Y.-F., Furan, L. R., Li, Z., Podust, L. M., Montgomery, J., Houk, K. N., and Sherman, D. H. (2015) Enzymatic hydroxylation of an unactivated methylene C–H bond guided by molecular dynamics simulations, *Nat Chem 7*, 653-660.

125. Rogers, T. A., and Bommarius, A. S. (2010) Utilizing Simple Biochemical Measurements to Predict Lifetime Output of Biocatalysts in Continuous Isothermal Processes, *Chemical engineering science 65*, 2118-2124.

126. Huang, S., Mahanta, N., Begley, T. P., and Ealick, S. E. (2012) Pseudouridine Monophosphate Glycosidase: A New Glycosidase Mechanism, *Biochemistry 51*, 9245-9255.

127. Koeller, K. M., and Wong, C.-H. (2001) Enzymes for chemical synthesis, *Nature 409*, 232-240.

128. Cheriyan, M., Toone, E. J., and Fierke, C. A. (2012) Improving upon nature: active site remodeling produces highly efficient aldolase activity toward hydrophobic electrophilic substrates, *Biochemistry 51*, 1658-1668.

129. Wörsdörfer, B., Henning, L. M., Obexer, R., and Hilvert, D. (2012) Harnessing Protein Symmetry for Enzyme Design, *ACS Catalysis 2*, 982-985.

130. Windle, C. L., Muller, M., Nelson, A., and Berry, A. (2014) Engineering aldolases as biocatalysts, *Current opinion in chemical biology 19*, 25-33.

131. Barbas, C. F., Heine, A., Zhong, G., Hoffmann, T., Gramatikova, S., Björnestedt, R., List, B., Anderson, J., Stura, E. A., Wilson, I. A., and Lerner, R. A. (1997) Immune Versus Natural Selection: Antibody Aldolases with Enzymic Rates But Broader Scope, *Science 278*, 2085-2092.

132. Wagner, J., Lerner, R. A., and Barbas, C. F. (1995) Efficient Aldolase Catalytic Antibodies That Use the Enamine Mechanism of Natural Enzymes, *Science 270*, 1797-1800.

133. Giger, L., Caner, S., Obexer, R., Kast, P., Baker, D., Ban, N., and Hilvert, D. (2013) Evolution of a designed retro-aldolase leads to complete active site remodeling, *Nat Chem Biol 9*, 494-498.

134. Teng, Z., Xu, R., and Wang, Q. (2015) Beta-lactoglobulin-based encapsulating systems as emerging bioavailability enhancers for nutraceuticals: a review, *RSC Advances 5*, 35138-35154.

135. Li, X.-y., Asato, A. E., and Liu, R. S. H. (1990) β-Lactoglobulin directed photoisomerization of retinal and related compounds, *Tetrahedron Letters 31*, 4841-4844.

136. Jellimann, C., Mathé-Allainmat, M., Andrieux, J., Kloubert, S., Boutin, J. A., Nicolas, J.-P., Bennejean, C., Delagrange, P., and Langlois, M. (2000) Synthesis of Phenalene and Acenaphthene Derivatives as New Conformationally Restricted Ligands for Melatonin Receptors, *Journal of Medicinal Chemistry 43*, 4051-4062.

137. Wang, G., Chen, X., Miao, G., Yao, W., and Ma, C. (2013) Divergent NHC-Catalyzed Oxidative Transformations of 3-Bromoenal: Selective Synthesis of 2H-Pyran-2-ones and Chiral Dihydropyranones, *The Journal of Organic Chemistry 78*, 6223-6232.

138. Zlokovic, B., Skundric, D., Segal, M., Lipovac, M., Mackic, J., and Davson, H. (1990) A saturable mechanism for transport of immunoglobulin G across the blood-brain barrier of the guinea pig, *Experimental neurology 107*, 263-270.

139. Wu, Q., Applegate, B. E., and Yeh, A. T. (2011) Cornea microstructure and mechanical responses measured with nonlinear optical and optical coherence microscopy using sub-10-fs pulses, *Biomed. Opt. Express 2*, 1135-1146.

140. Smith, R. S., John, S. W., Nishina, P. M., and Sundberg, J. P. (2001) *Systematic evaluation of the mouse eye: anatomy, pathology, and biomethods*, CRC press.

141. Geng, Y., Schery, L. A., Sharma, R., Dubra, A., Ahmad, K., Libby, R. T., and Williams, D. R. (2011) Optical properties of the mouse eye, *Biomedical optics express 2*, 717-738.

APPENDIX

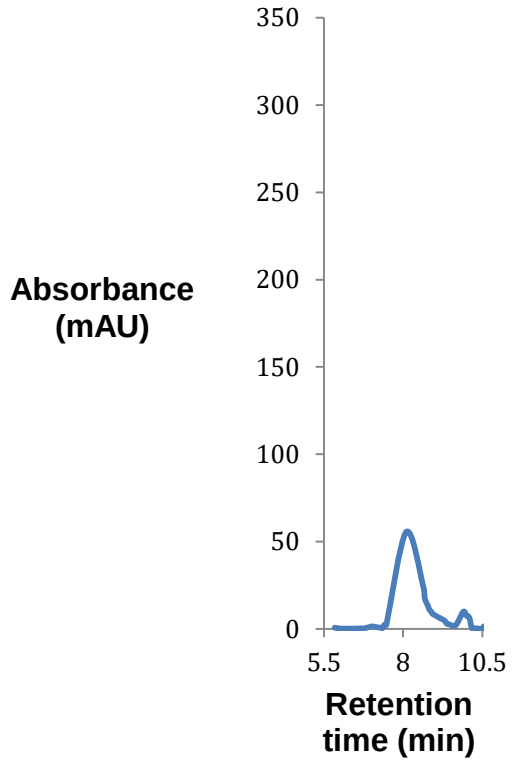

Figure A 1 Representative Co-injection of wt-BLG reaction with synthetic cycloretinal: See S7 for details on reaction conditions

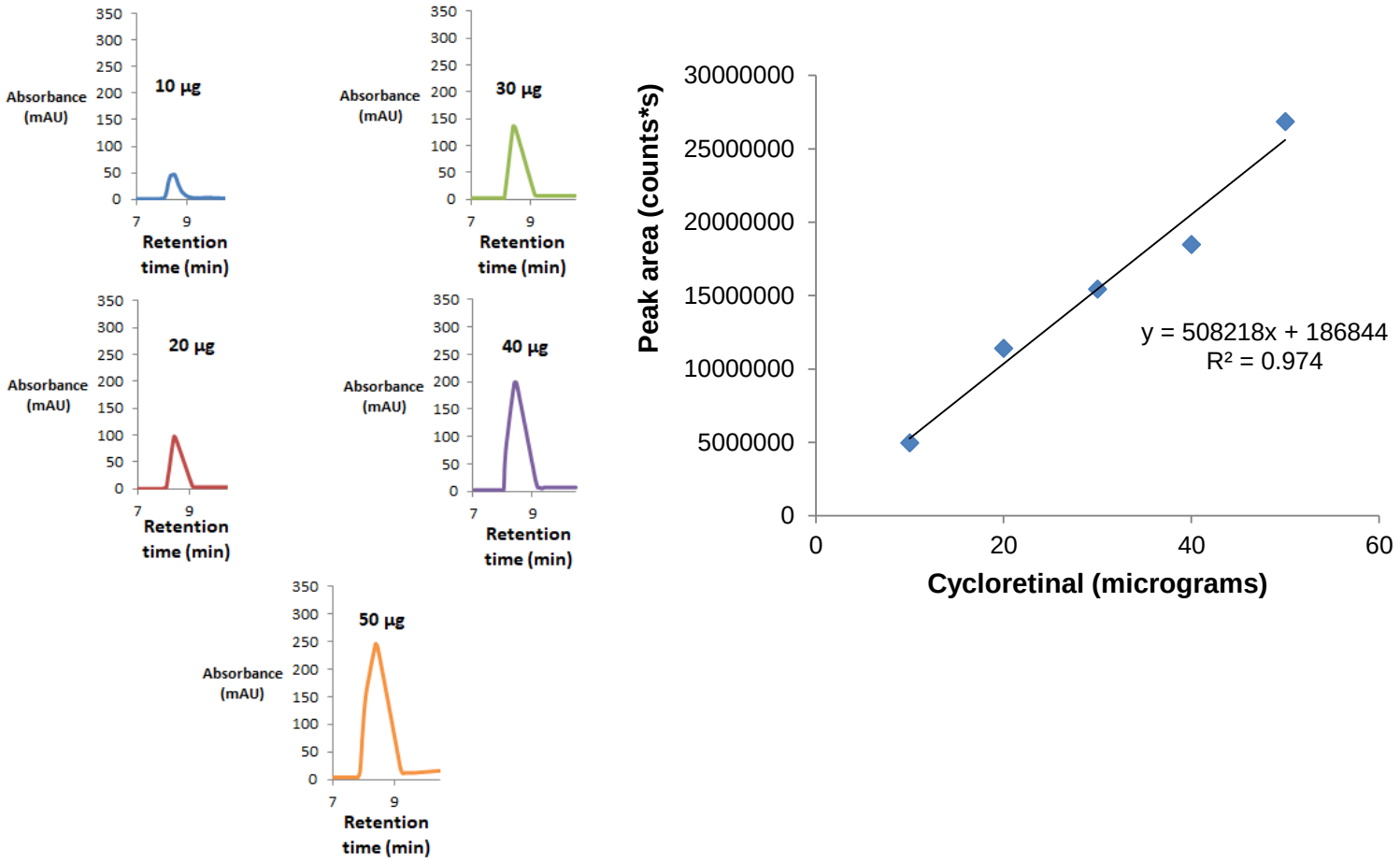

Figure A 2 Standard curve generated by analyzing different amounts of cycloretinal: synthetic cycloretinal was derivatized with 2,4-dinitrophenylhydrazine

LYSINE 77

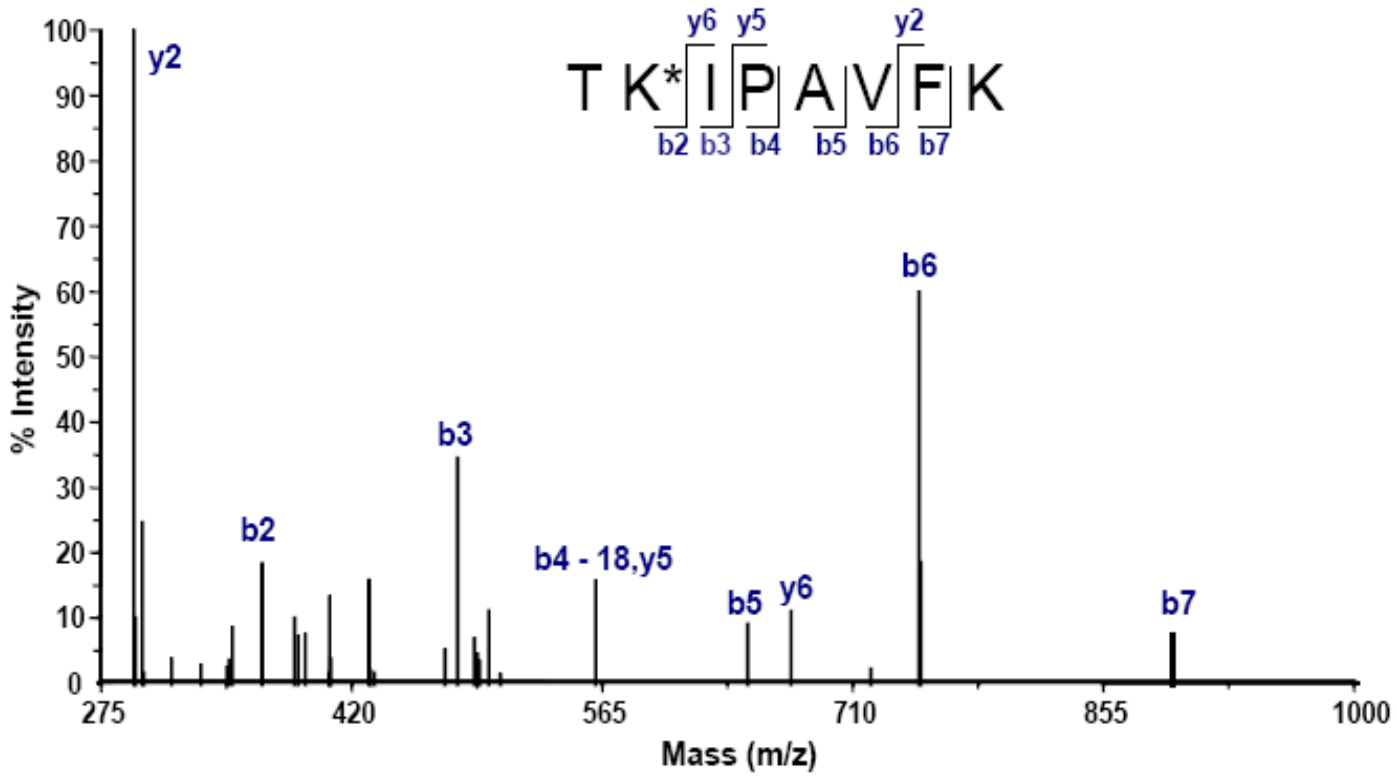

Figure A 3 Mass spectrometric results obtained after trypsin digestion of BLG showing citral bound to K77

LYSINE 91

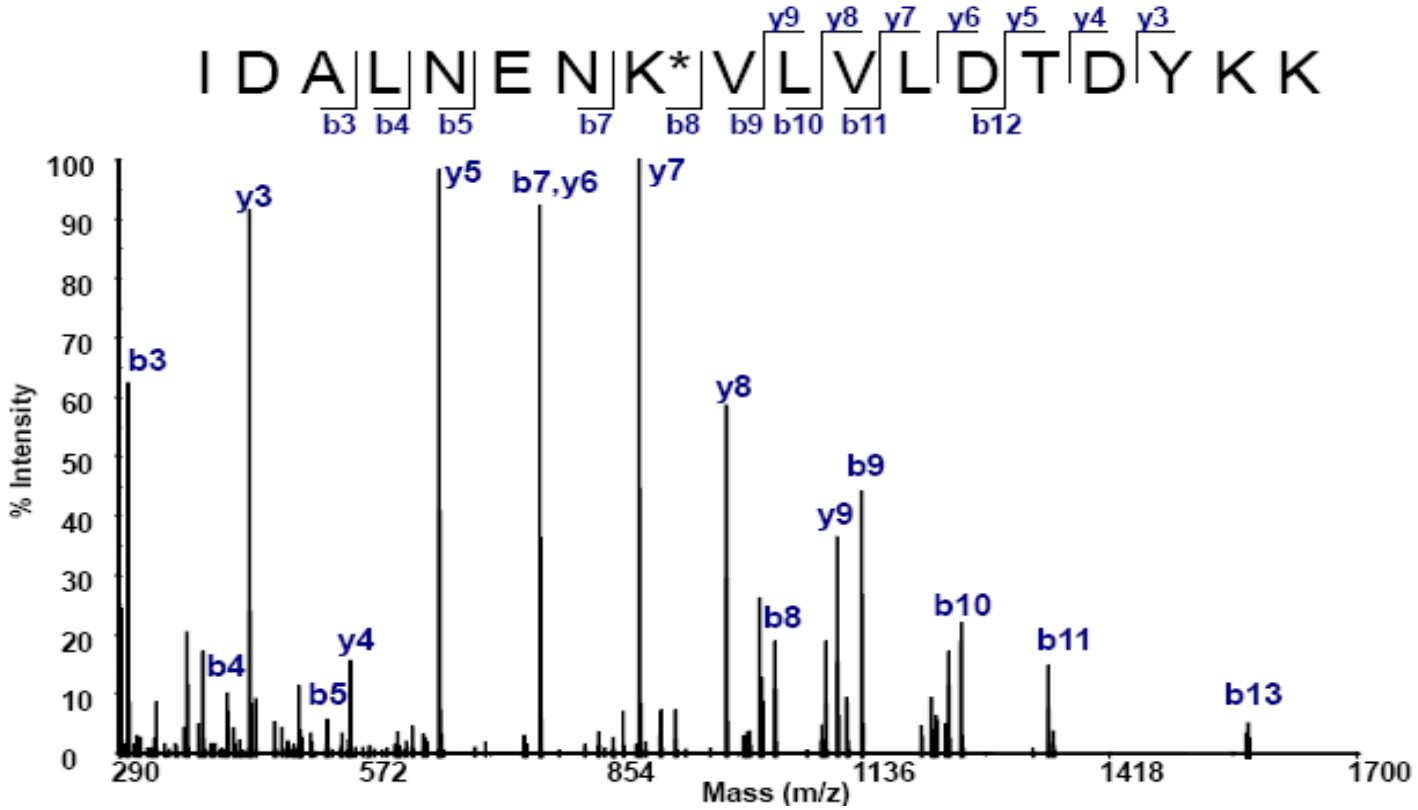

Figure A 4 Mass spectrometric results obtained after trypsin digestion of BLG showing citral bound to K91

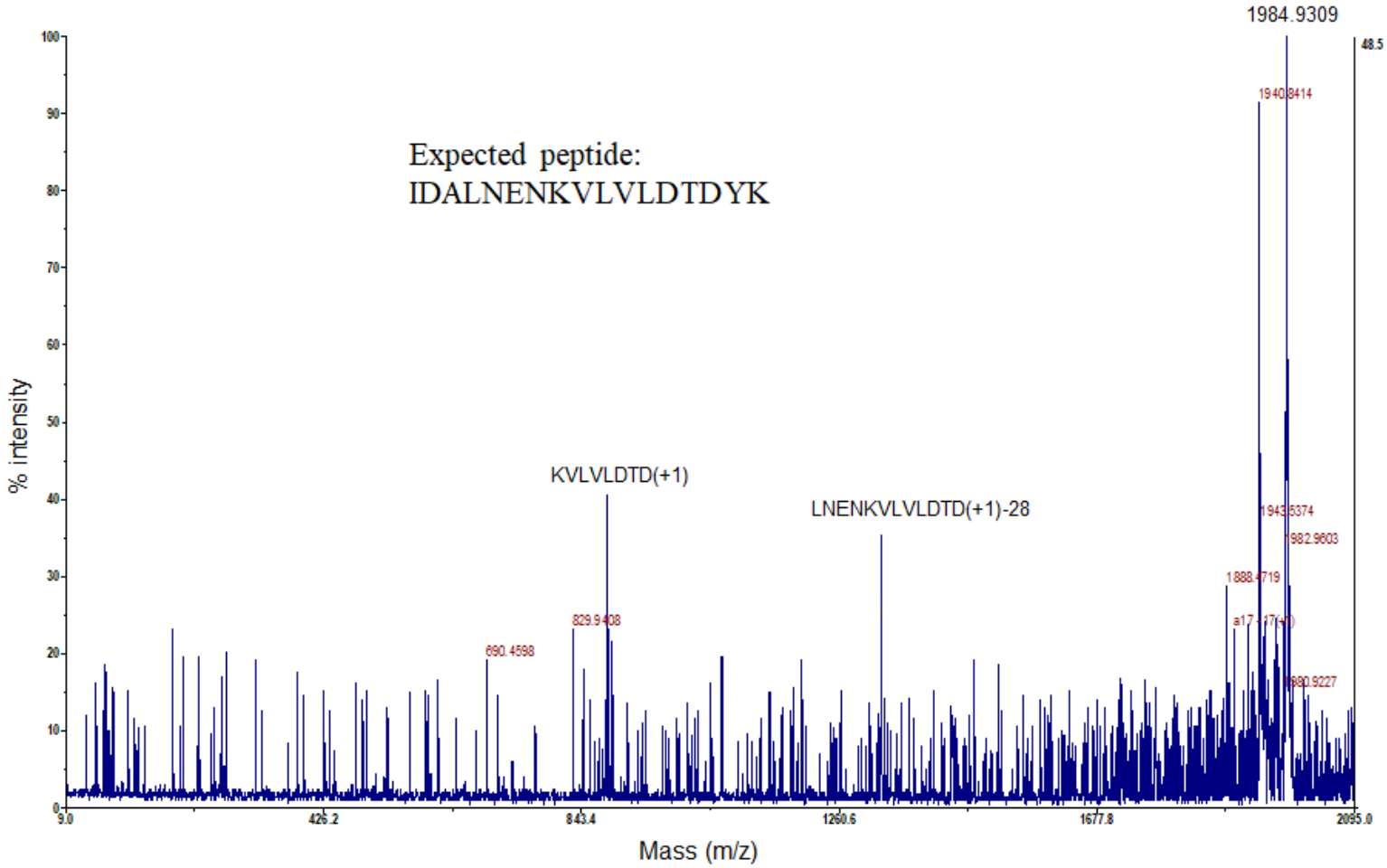

Figure A 5 MS/MS results obtained after trypsin digestion of **3.9**-bound BLG

Table A 1 Comparison of the Peptides Obtained from BLG Incubated with Compound 6 to Control BLG

Labelled lysine	Sequence[a]	Modifications	Charge	MH+ [Da]	ΔM [ppm]	RT [min]	Missed Cleavages
Lysine 91+ 6	IDALNEnkVLVLDTDYK	K8(VGTAMU)	3	2094.07560	1.69	34.41	1
Lysine 91 control	IDALNEnKVLVLDTDYK	No modification	2	1964.01897	-1.72	25.77	1
Lysine 60+ 6	VYVEELkPTPEGDLEILLQK	K7(VGTAMU)	3	2443.30313	-2.24	38.85	1
Lysine 60 control	VYVEELKPTPEGDLEILLqK	No modification	4	2314.25258	4.17	30.95	1
Lysine 135 + 6	TPEVDDEALEKFDkALK	K14(VGTAMU)	3	2078.02585	-7.18	26.03	2
Lysine 135 control	TPEVDDEALEKFDKALK	No modification	2	1947.98454	-3.35	19.56	2
Lysine 8 or 14 (peptide 1-40)	LIVTQTMkGLDIQKVAGTWYSLAMAASDISLLDAQSAPLR	K8(VGTAMU)	4	4406.31557	-1.43	41.83	2
Control peptides 1-14	VAGTWYSLAMAASDISLLDAQSAPLR	No modification	3	2707.36777	-3.08	48.87	0
Control peptide 15-40	LIVTQTMKGLDIQK	No modification	3	1587.90580	-5.12	23.26	1

[a]Peptides obtained by digesting the proteins with trypsin were subjected to mass spectrometric analysis

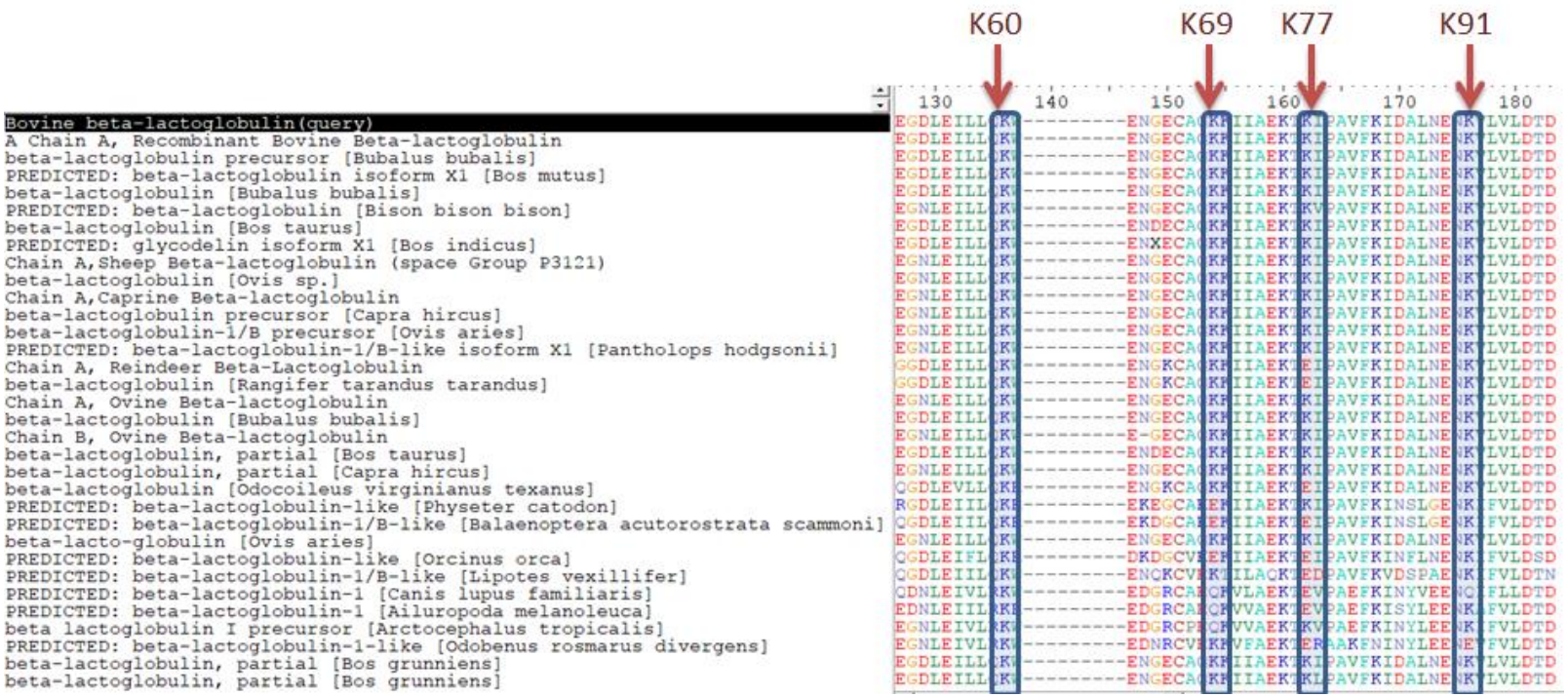

Figure A 6 BLAST analysis showing conservation of lysines 60, 69, 77 and 91 among closely related species

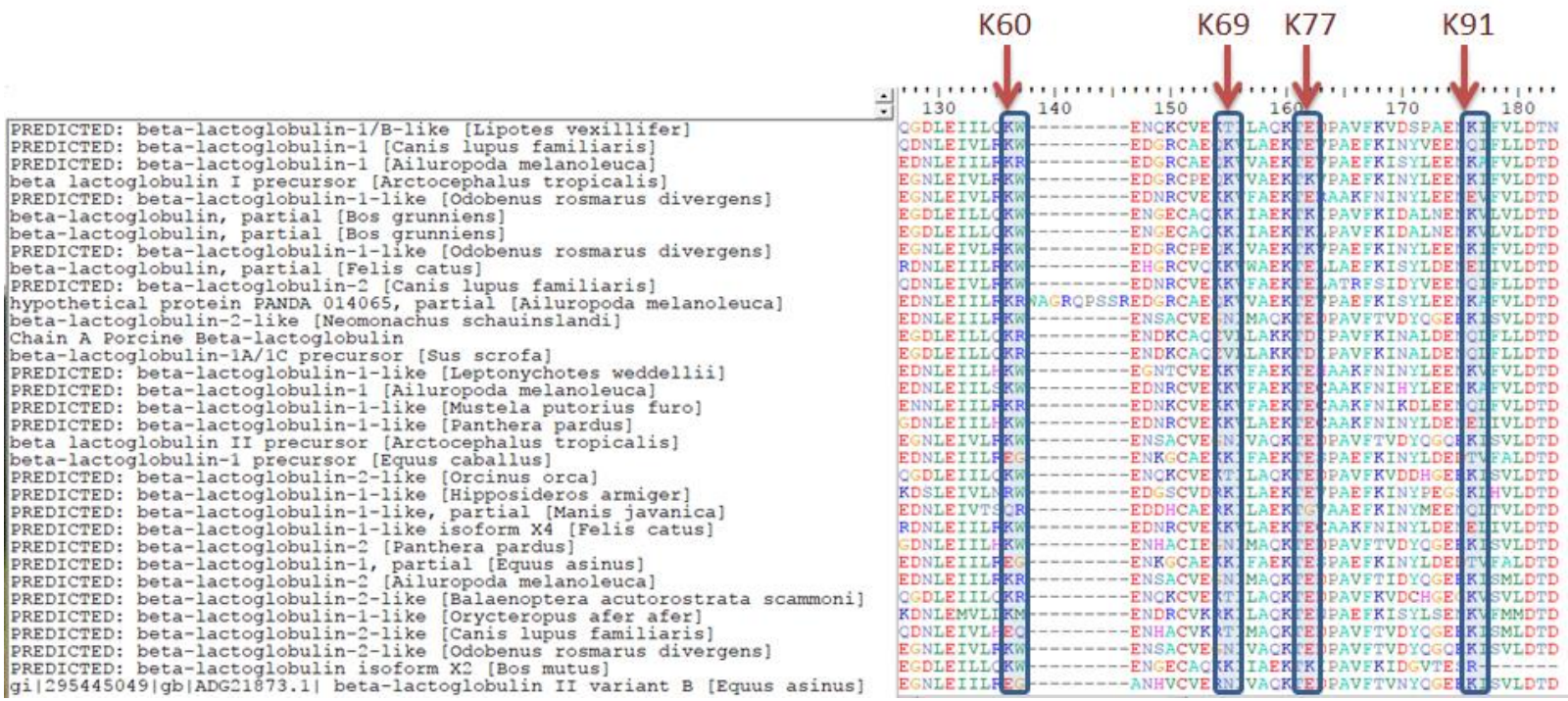

Figure A 7 BLAST analysis showing conservation of lysines 60, 69 and 91 among distantly related species

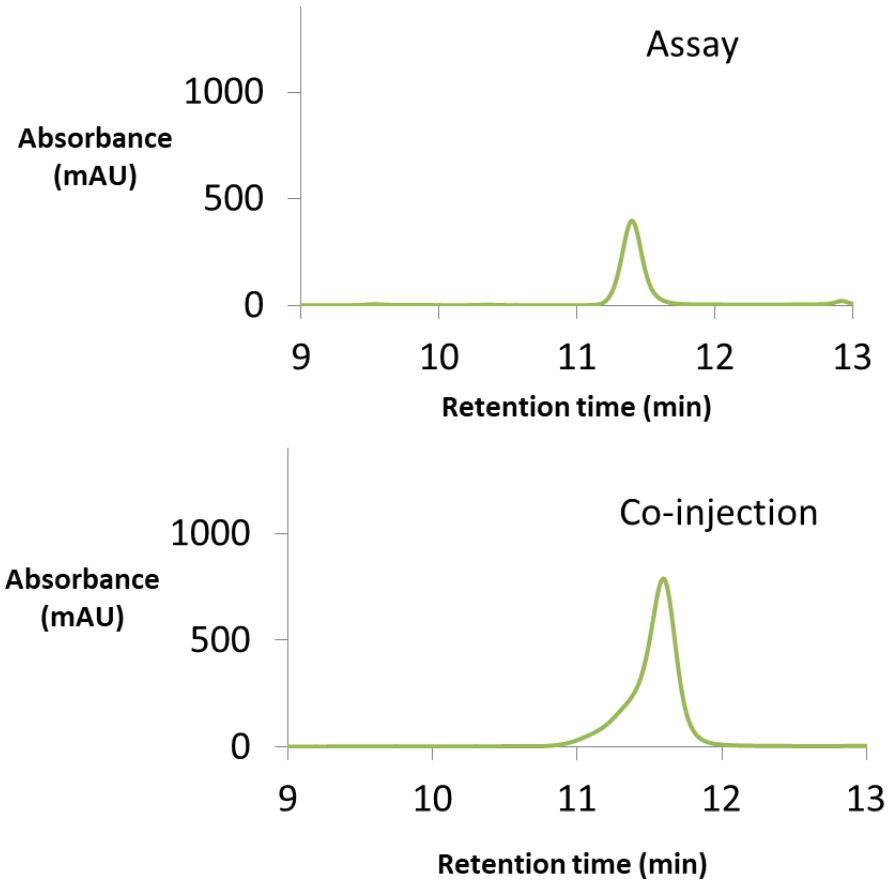

Figure A 8 HPLC analysis of BLG assay with compound **4.9**

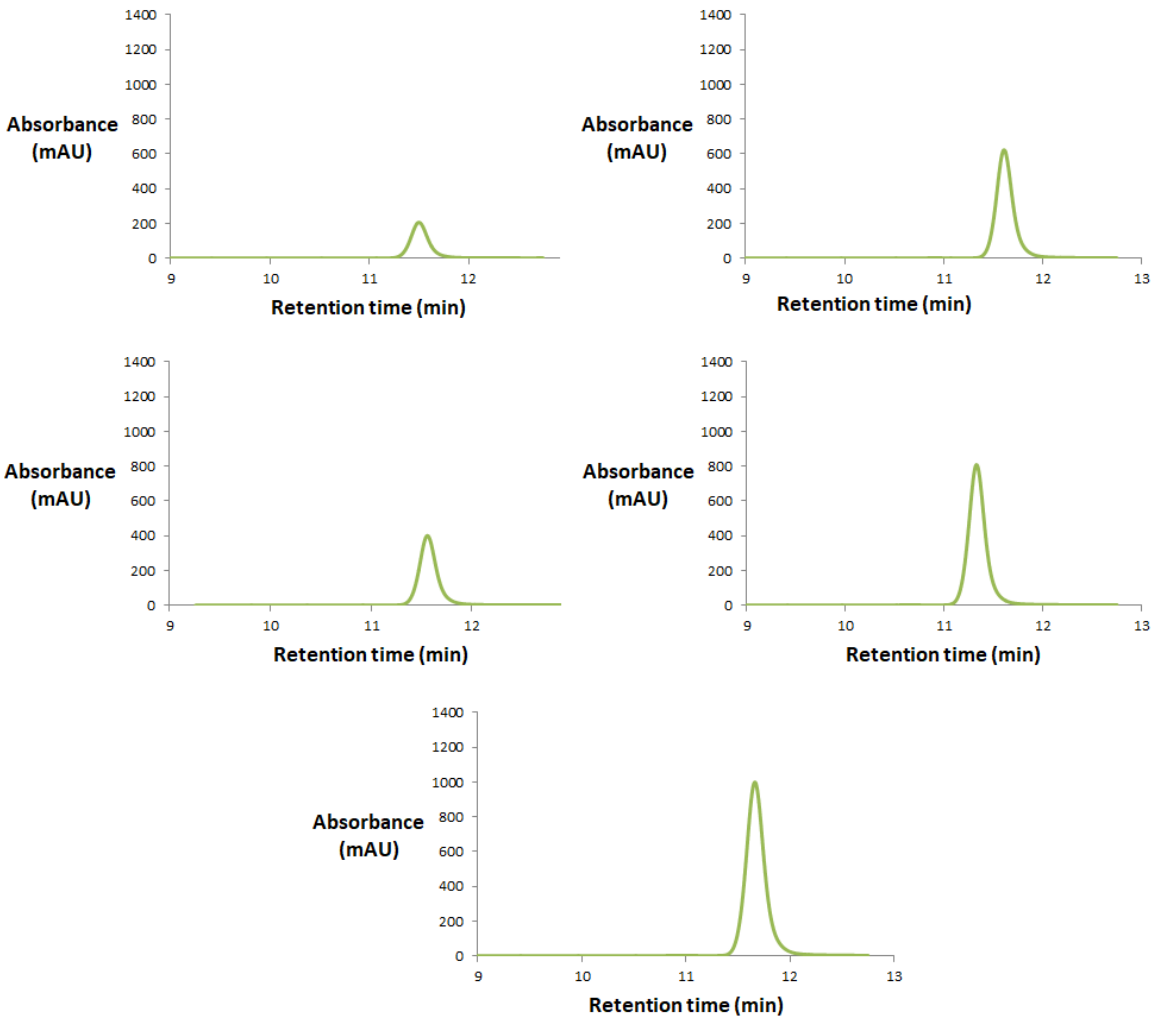

Figure A 9 Analysis of synthetic ketone product of **4.9** to generate standard curve

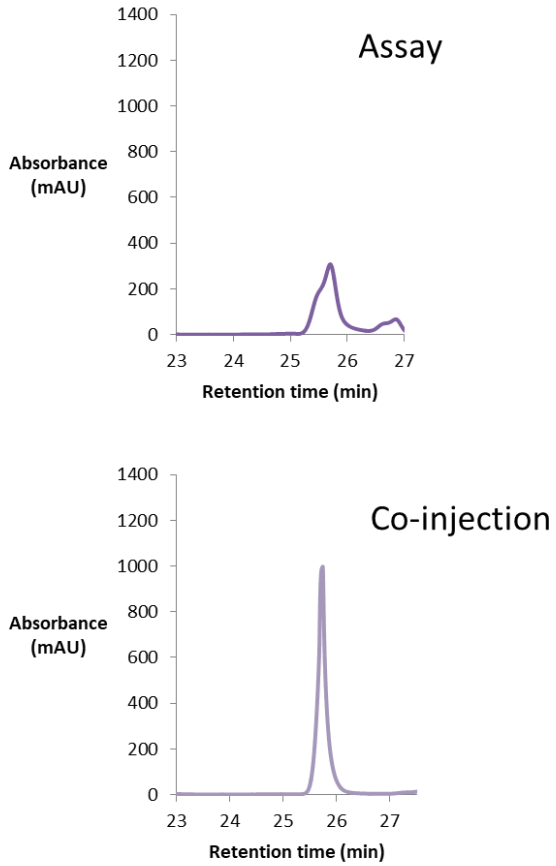

Figure A 10 HPLC analysis of BLG assay with compound **4.10**

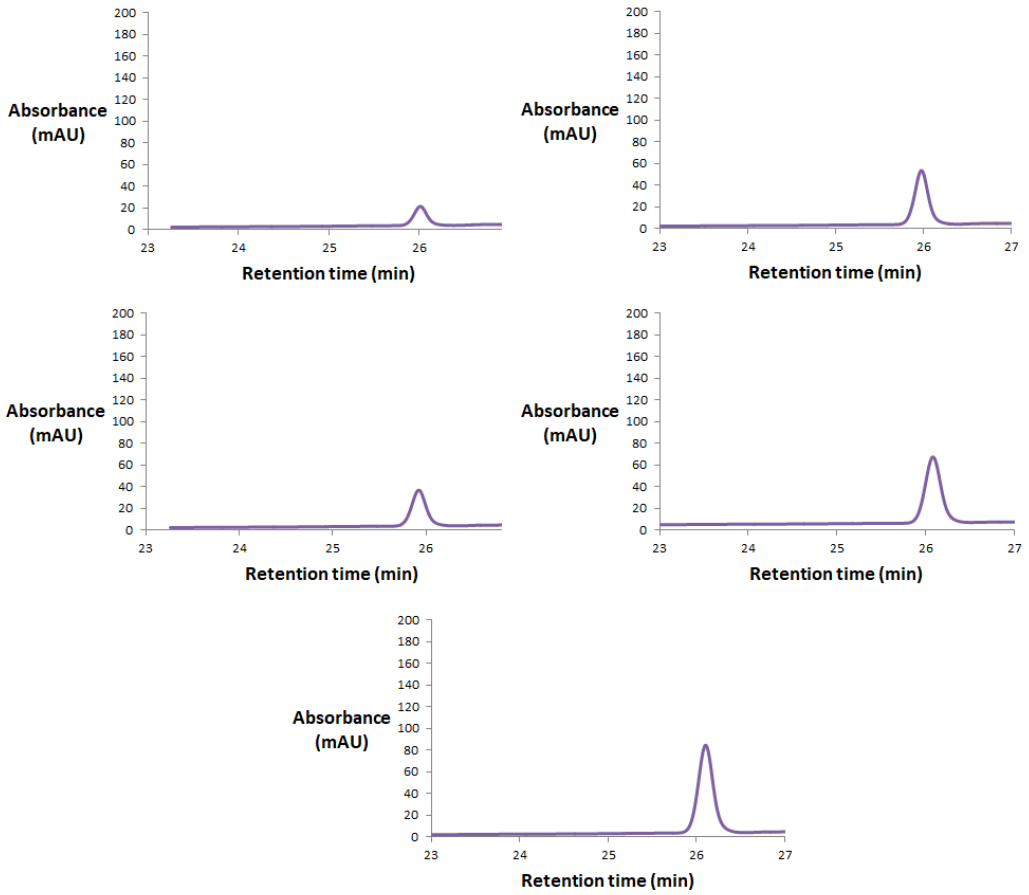

Figure A 11 Analysis of synthetic ketone product of **4.10** to generate standard curve

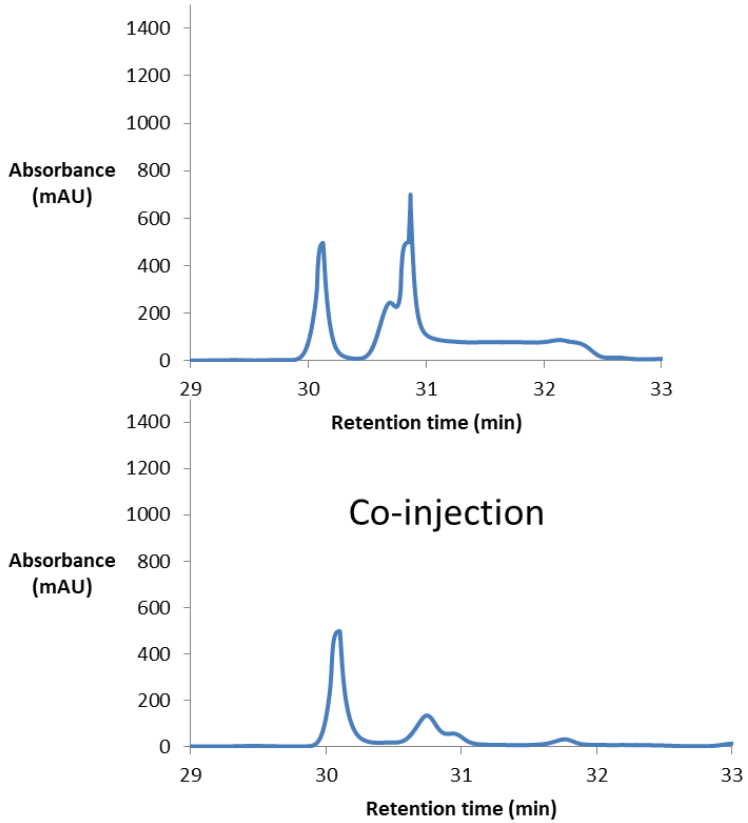

Figure A 12 HPLC analysis of BLG assay with compound **4.11**

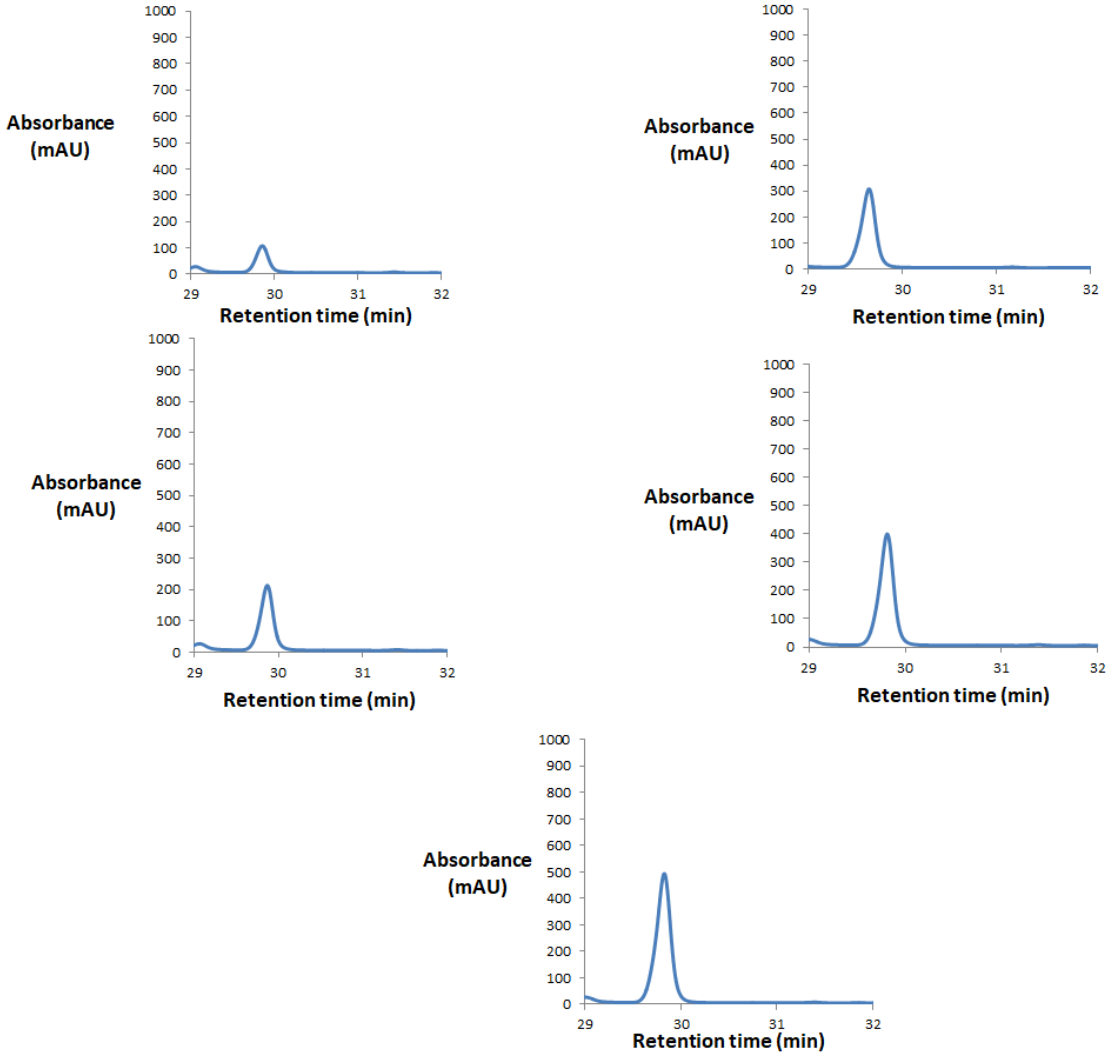

Figure A 13 Analysis of synthetic ketone product of **4.11** to generate standard curve

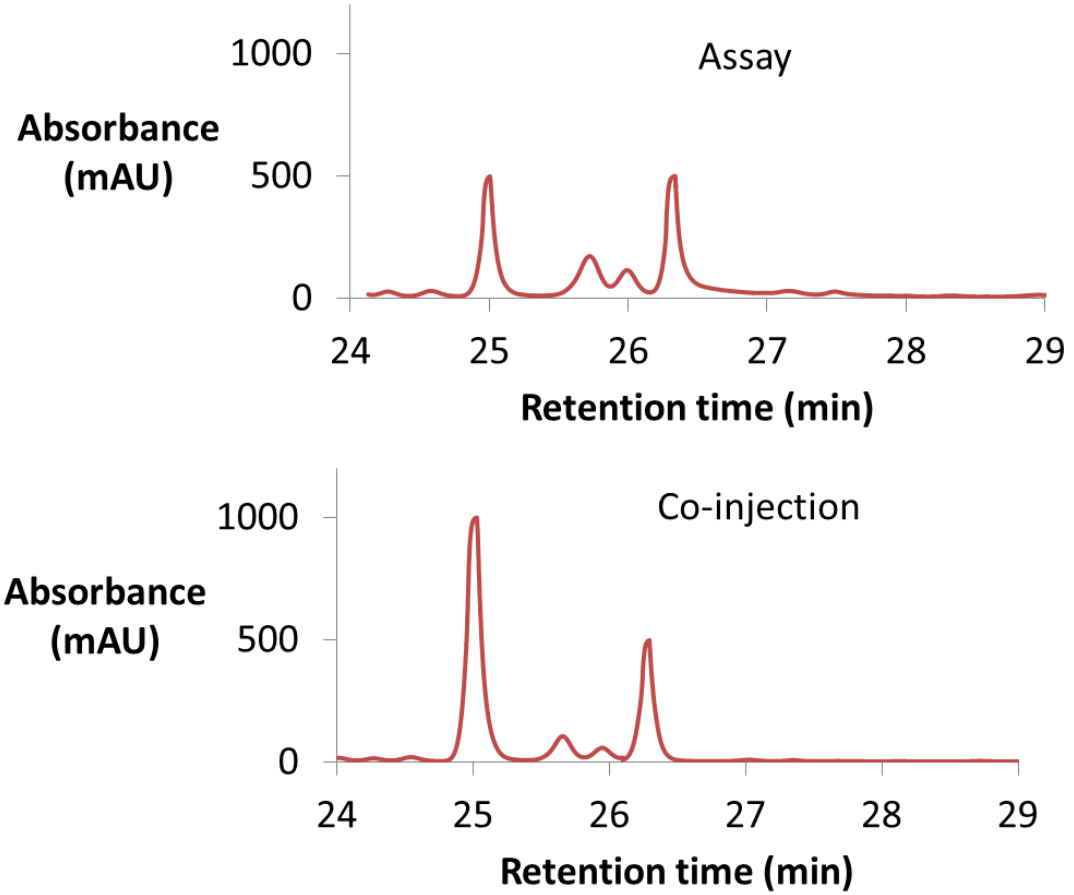

Figure A 14 HPLC analysis of BLG assay with compound **4.12**

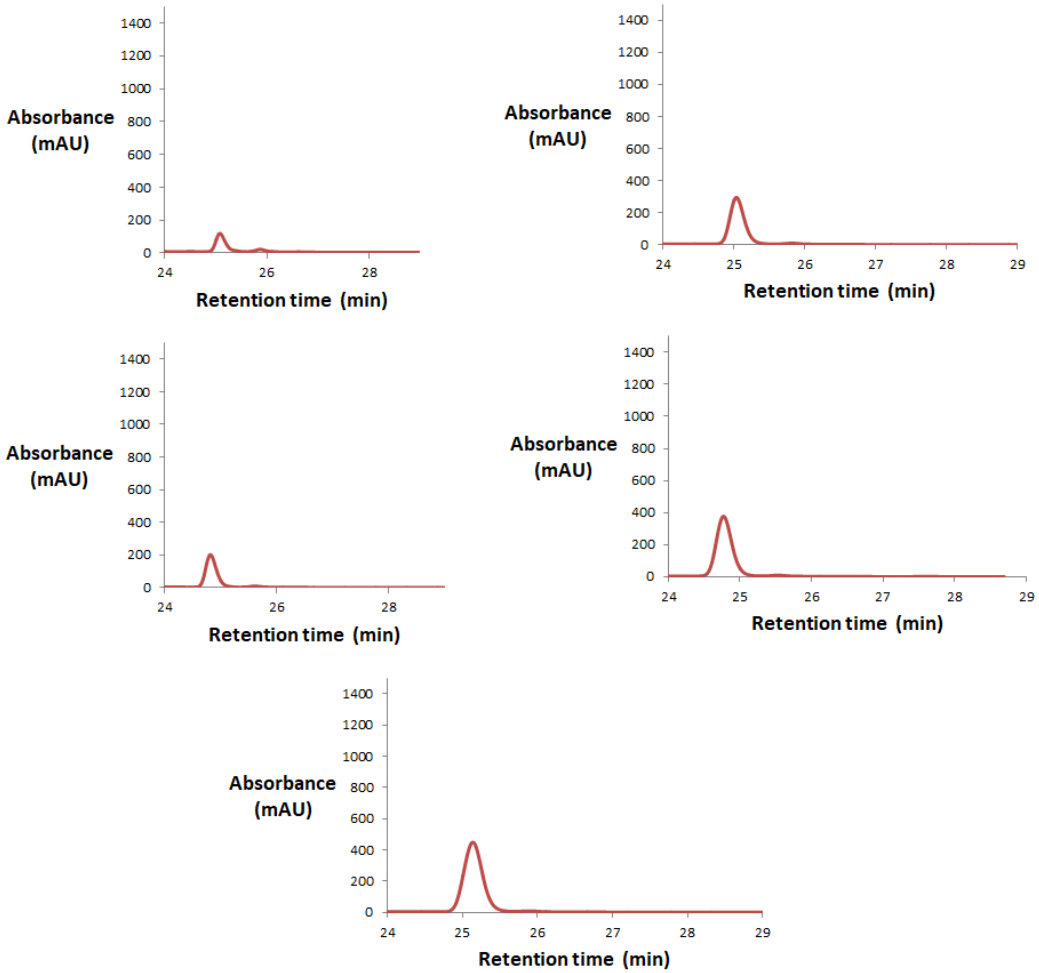

Figure A 15 Analysis of synthetic ketone product of **4.12** to generate standard curve

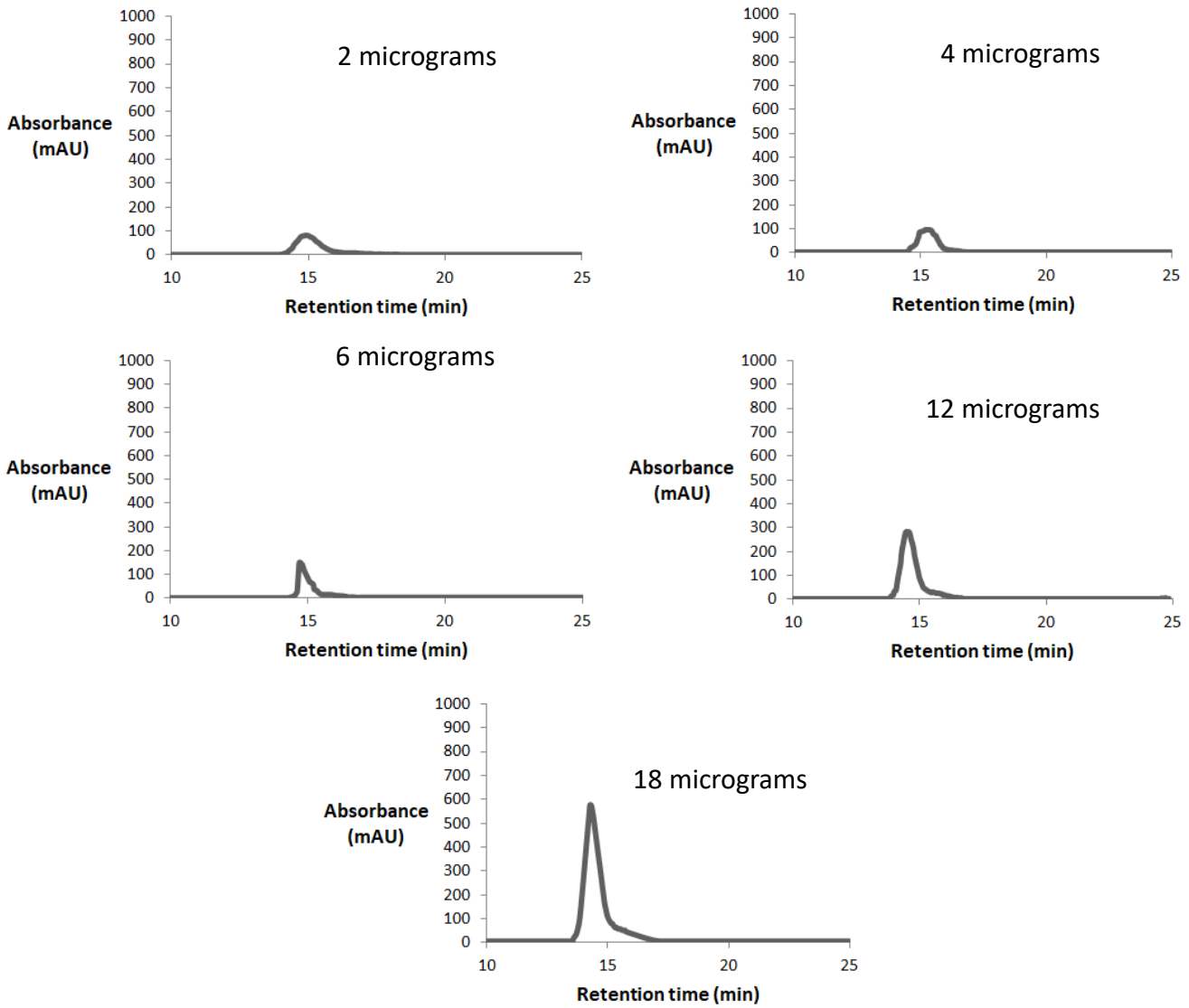

Figure A 16 Analysis of synthetic ketone product of **4.5** to generate standard curve

Observed mass for BLG wild type: 18277 & 18362.5996

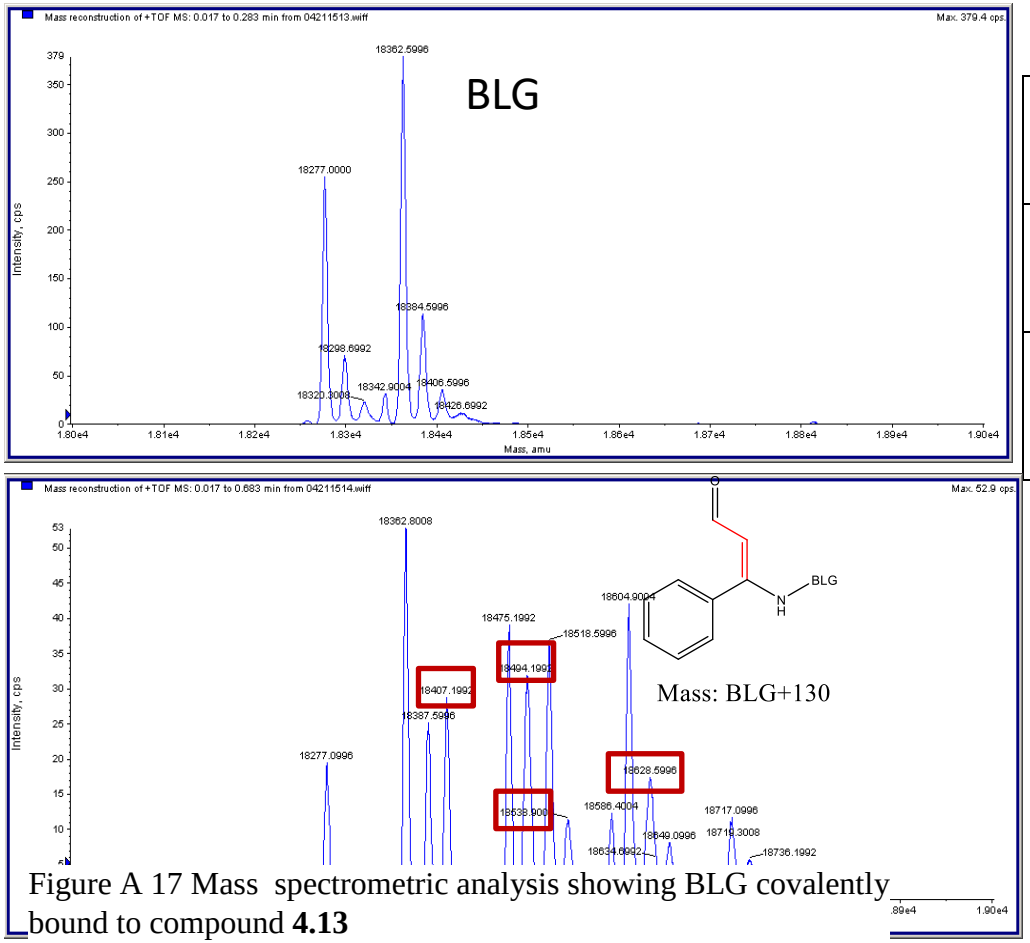

Figure A 17 Mass spectrometric analysis showing BLG covalently bound to compound **4.13**

	Expected mass	Observed mass
BLG + 1 molecule of compound 8	18407.16 &18492.759	18407.1992 &18494.1992
BLG + 2 molecules of compound 8	18538.32 &18623.919	18538.900& 18628.5996

The other major peaks observed are peaks corresponding to the loss of a water molecule from the labelled peaks. This could be due to the formation of an imine bond between

Observed mass for BLG wild-type: 18277 & 18362.5996

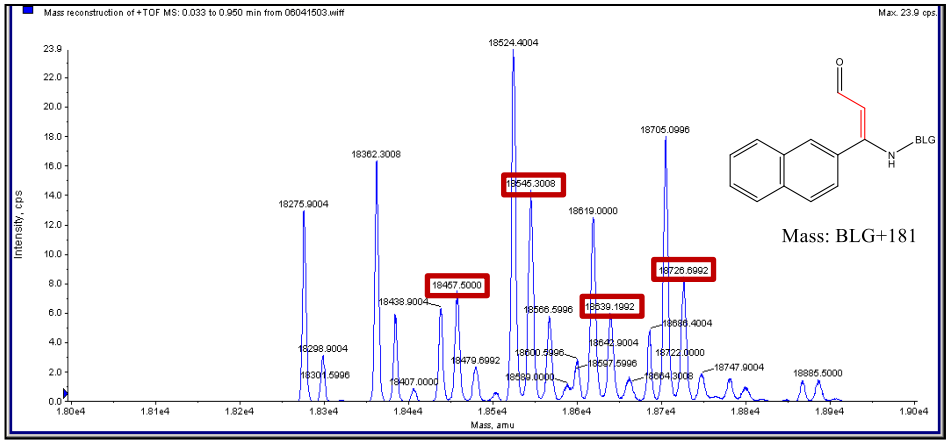

	Expected mass	Observed mass
BLG + 1 molecule of compound 11	18458 &18639	18457.5000 &18639.1992
BLG + 2 molecules of compound 11	18543.5996 &18724.5996	18545.3008& 18726.6992

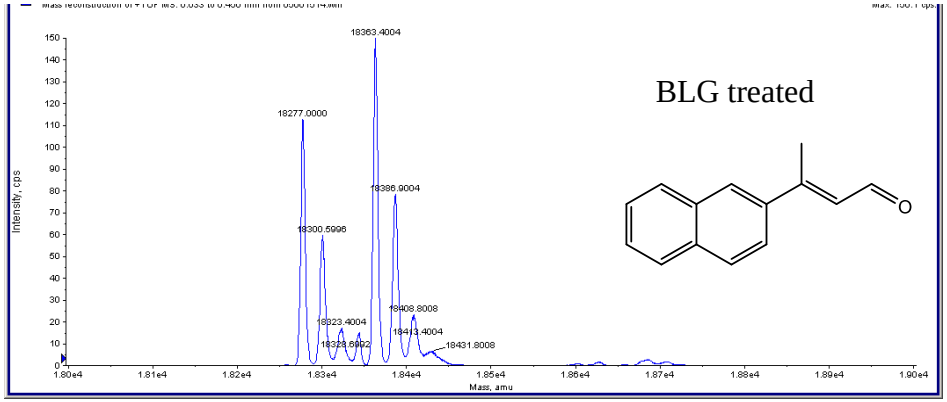

On treatment with compound **11**, BLG shows an increase in mass corresponding to the mass of debrominated compound **11**. However, when BLG was treated with compound **3**, no such increase in mass was observed. This provides

Figure A 18 Mass spectrometric analysis showing BLG covalently bound to compound **4.16**

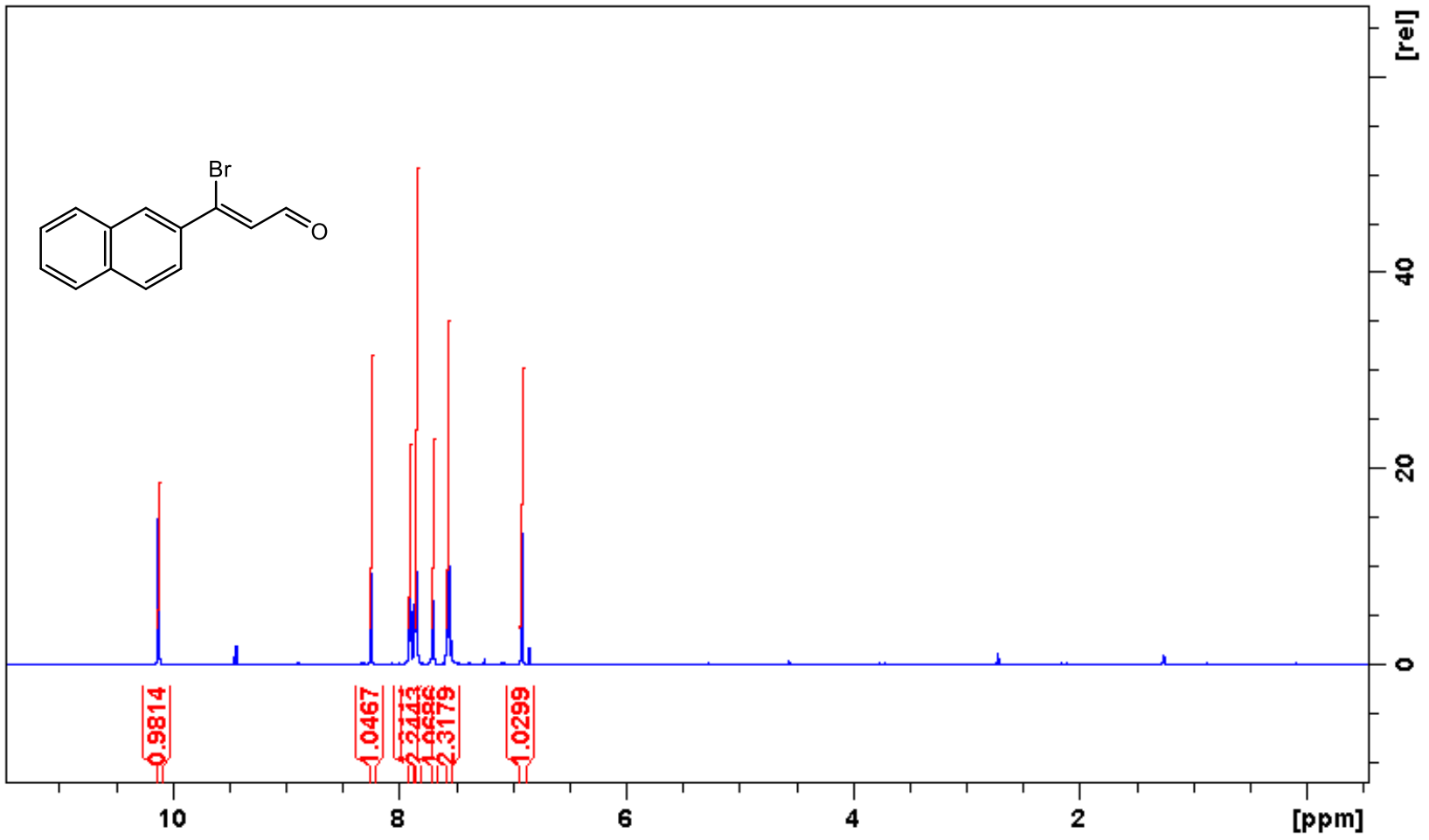

Figure A 19 Characterization of compound **4.16** by 1H-NMR spectroscopy

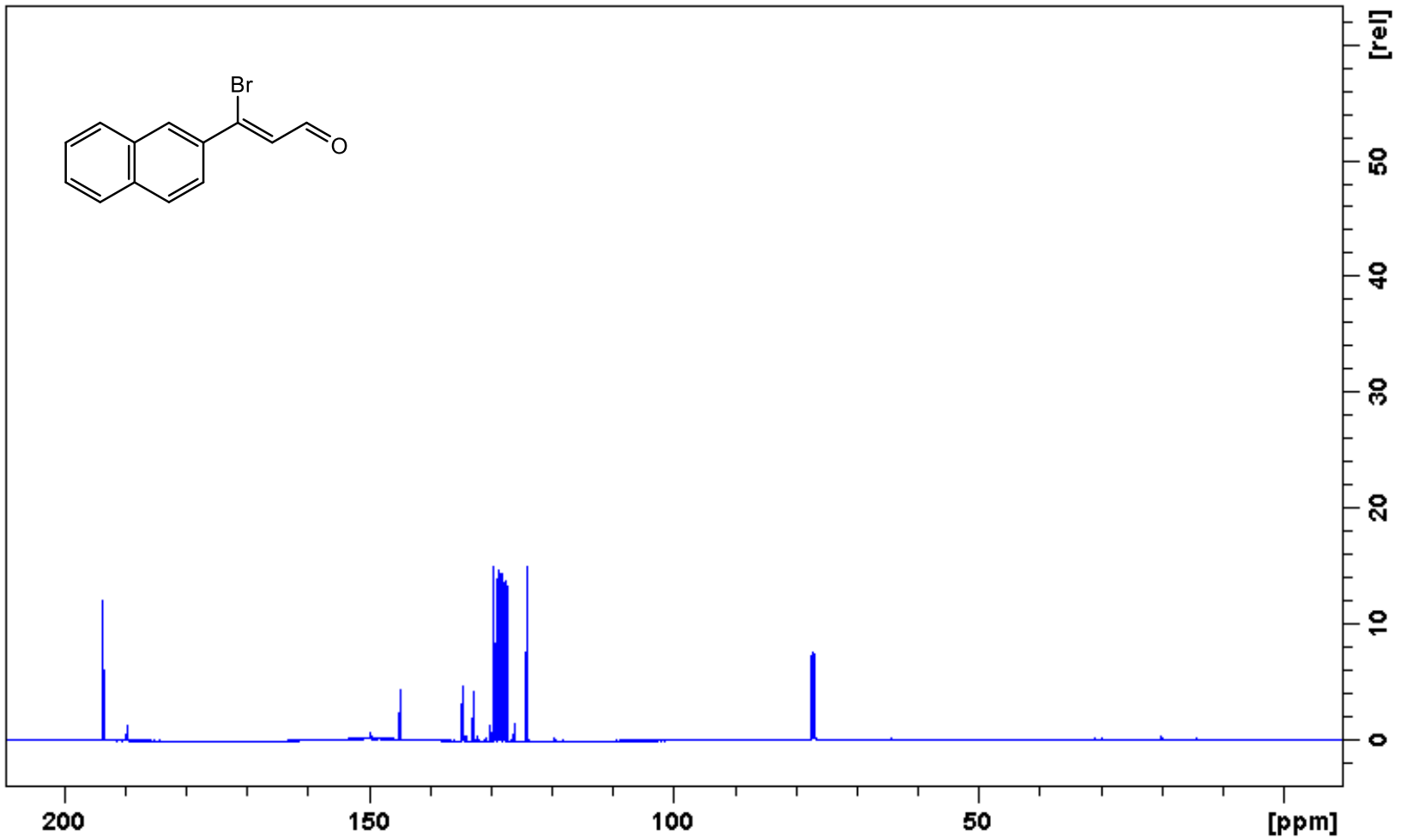

Figure A 20 Characterization of compound **4.16** by 13C-NMR spectroscopy

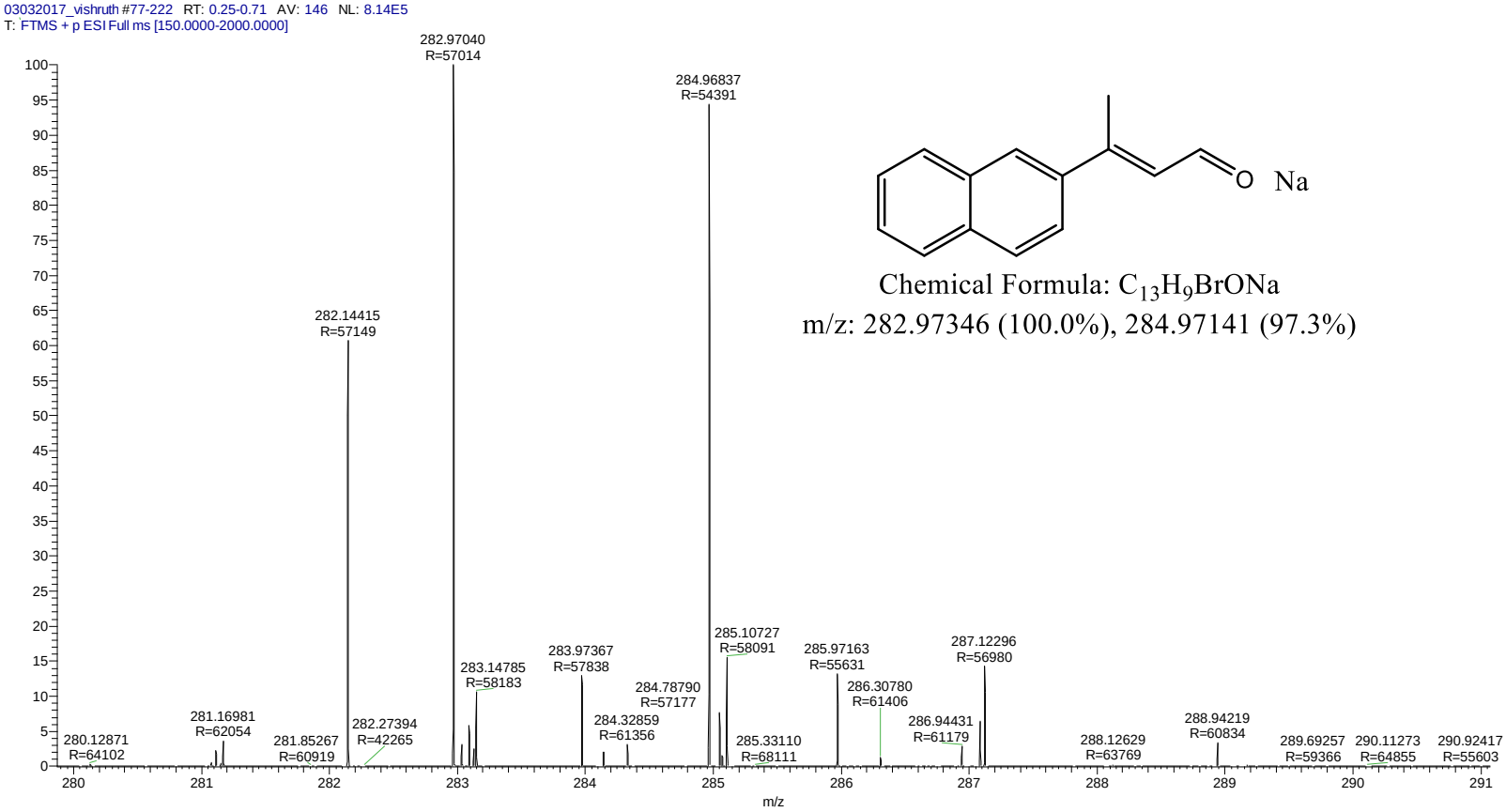

Figure A 21 Characterization of compound **4.16** by mass spectrometry

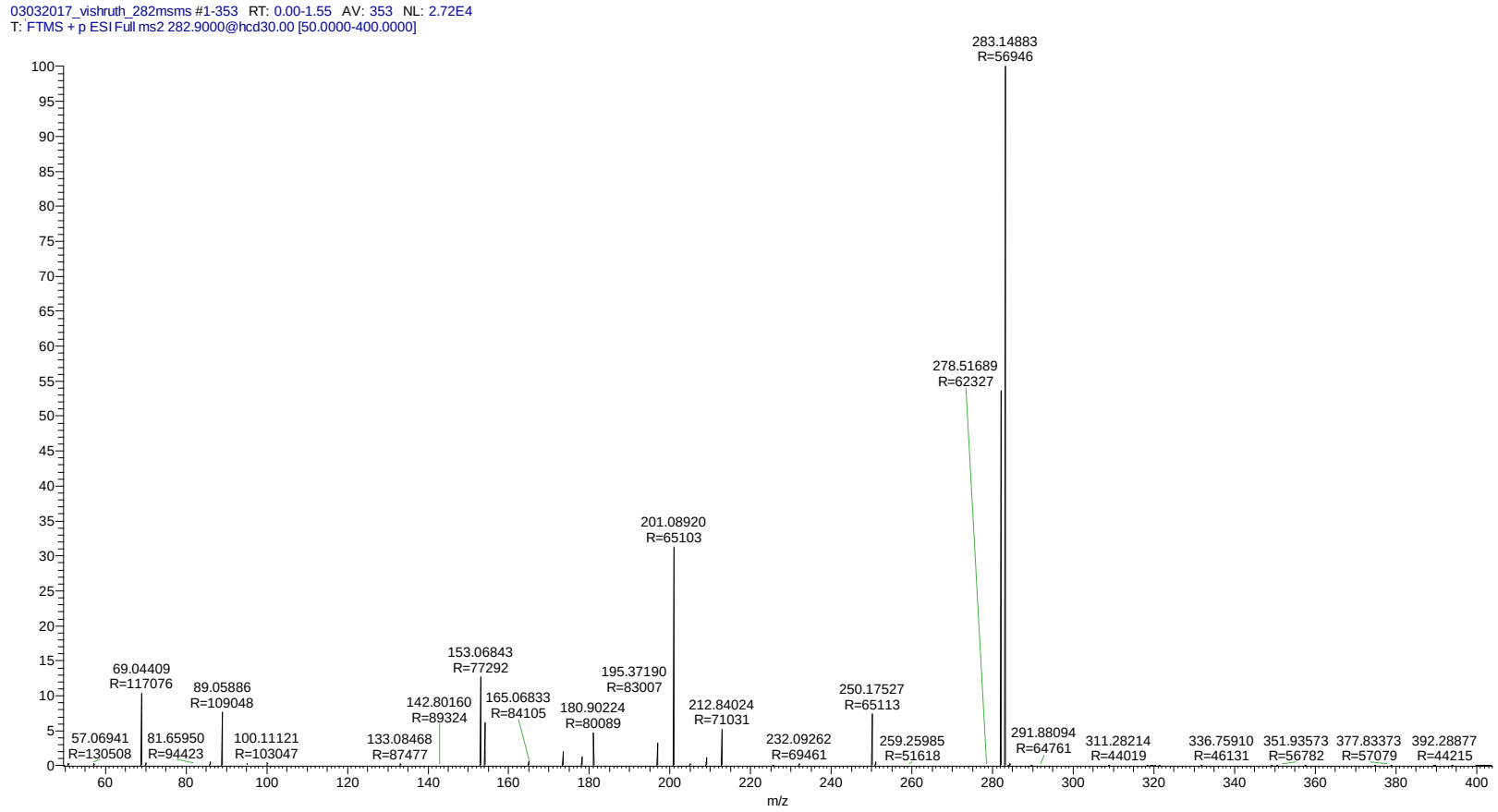

Figure A 22 Characterization of compound **4.16** by MS/MS spectrometry

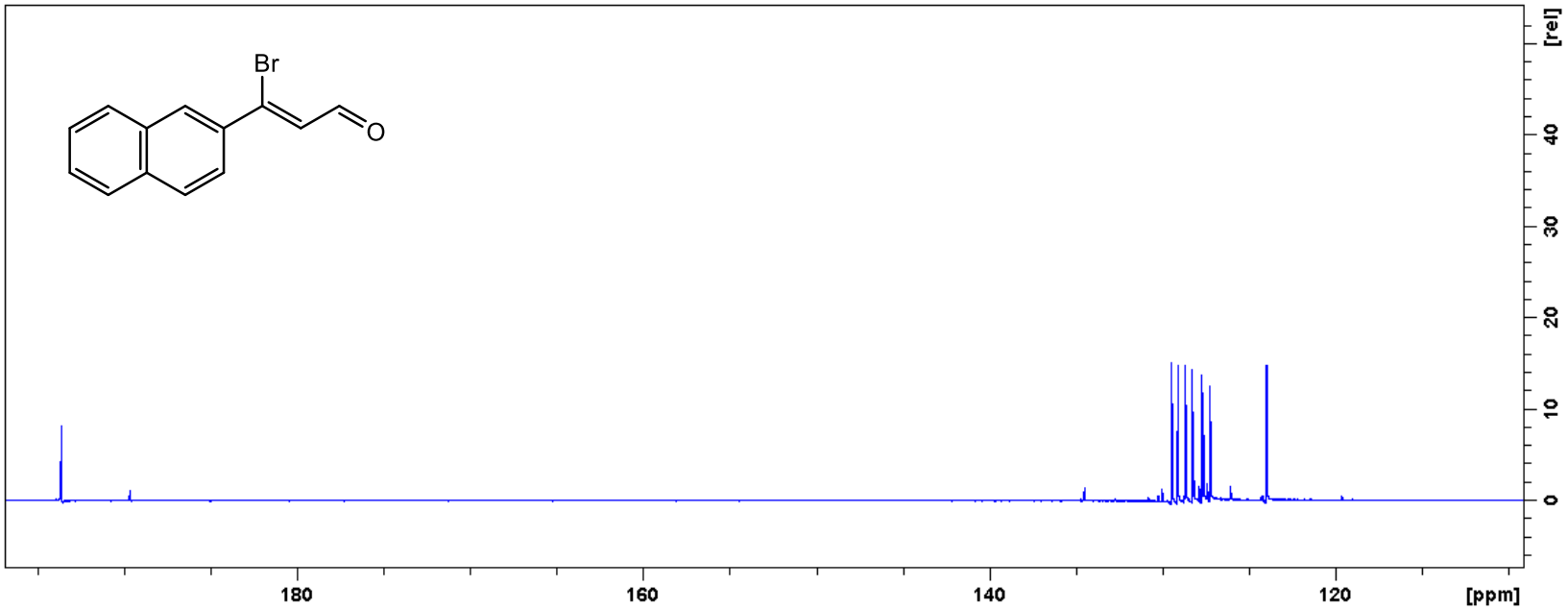

Figure A 23 Characterization of compound **4.16** by DEPT 90

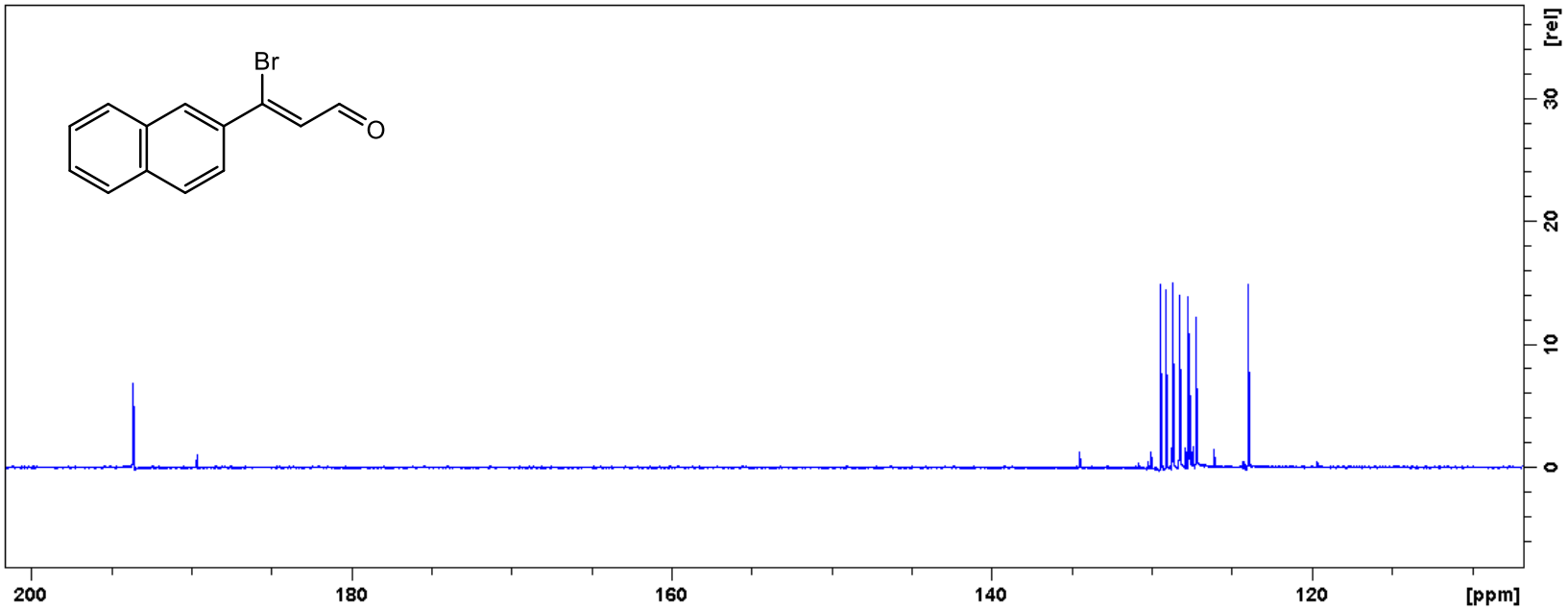

Figure A 24 Characterization of compound **4.16** by DEPT 135

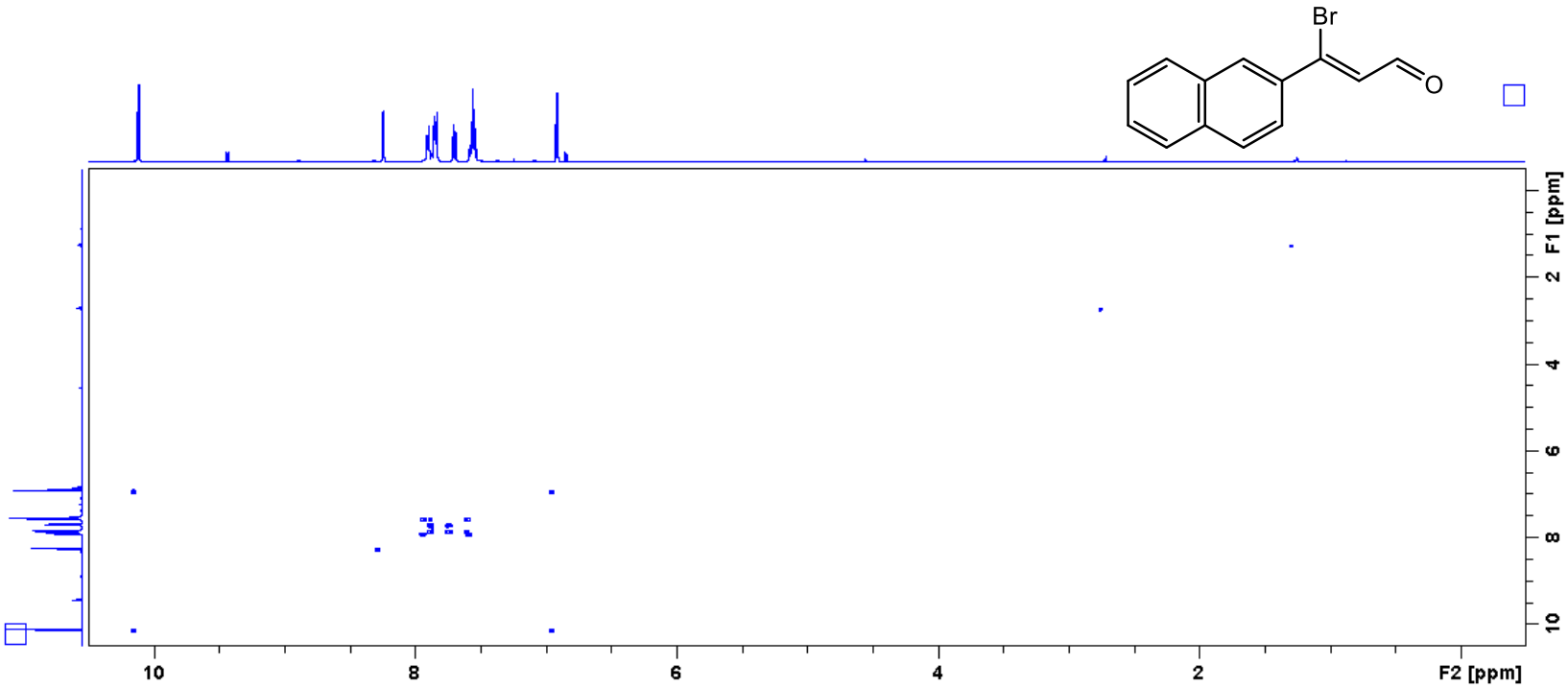

Figure A 25 H, H-COSY of compound **4.16**

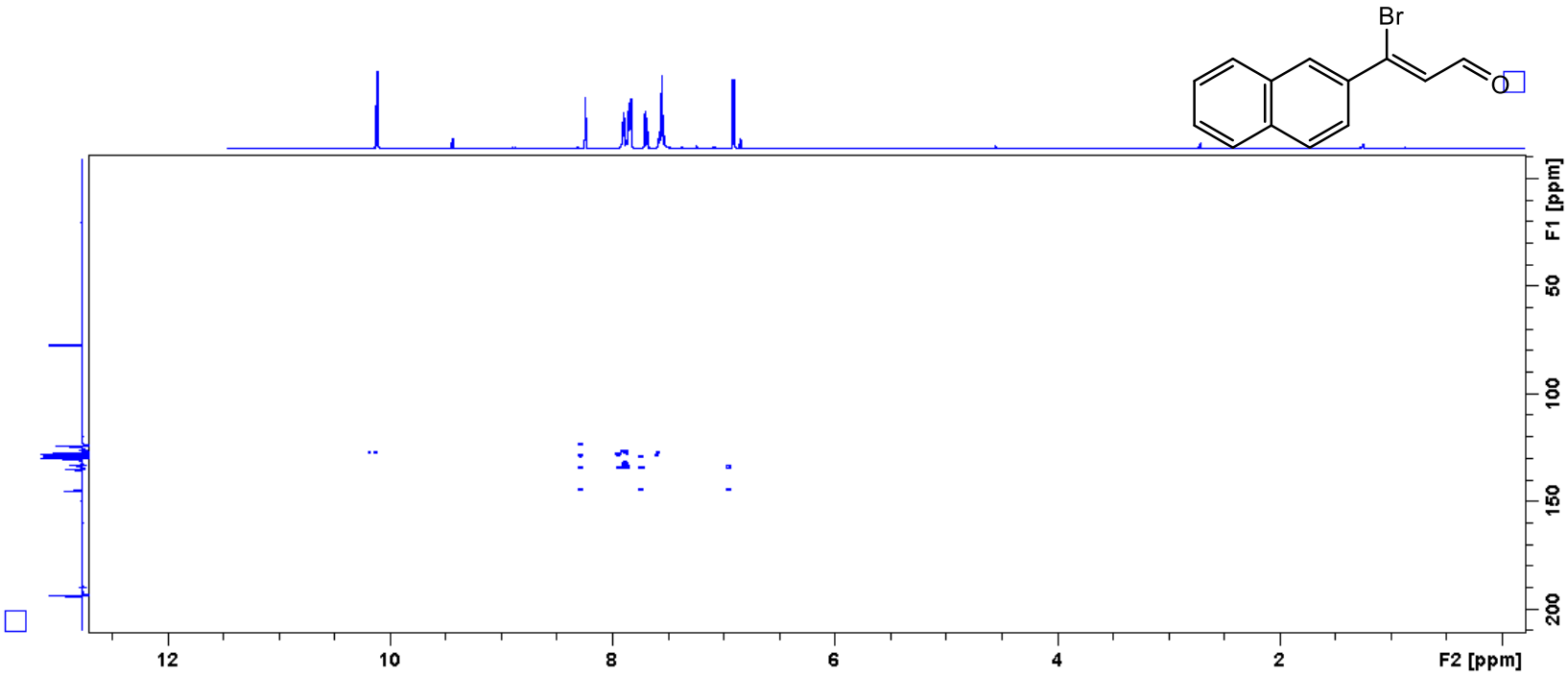

Figure A 26 HMBC of compound **4.16**

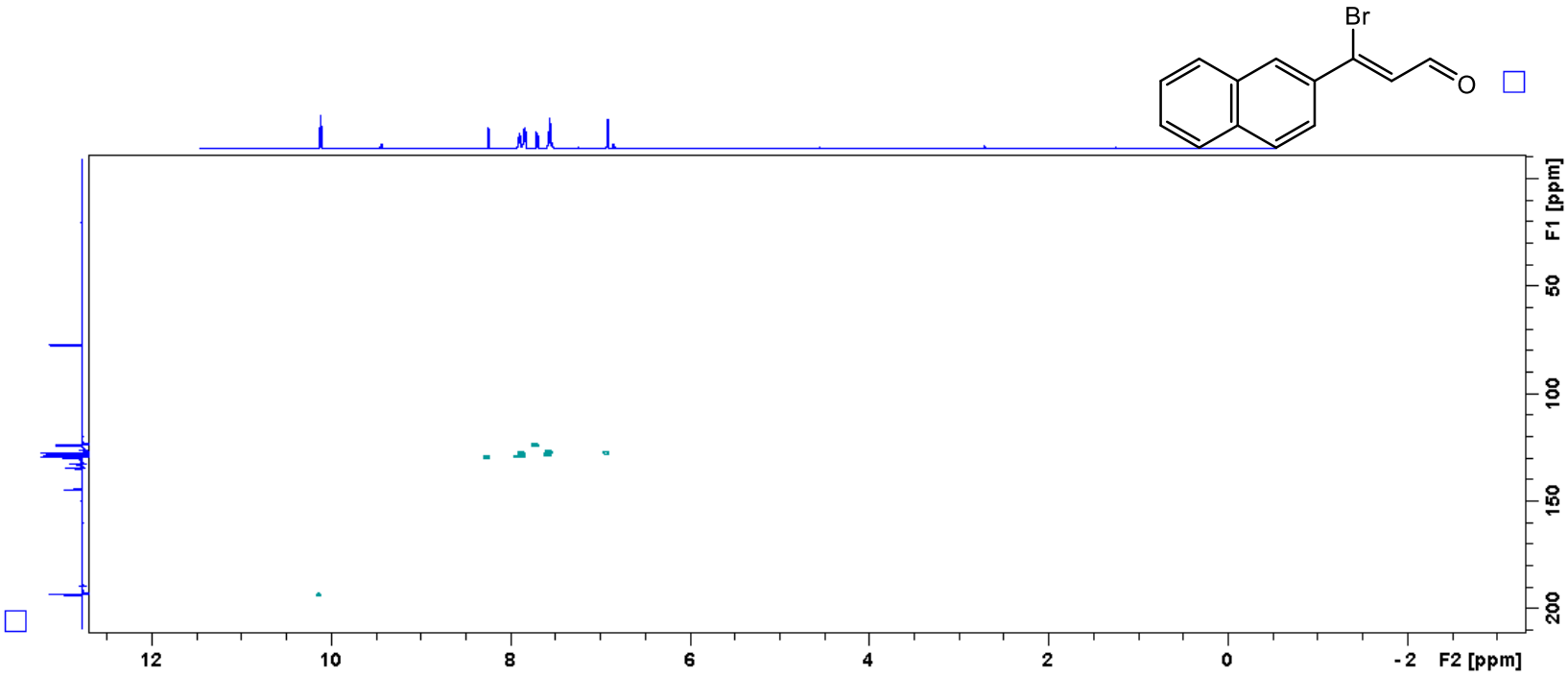

Figure A 27 HSQC of compound **4.16**

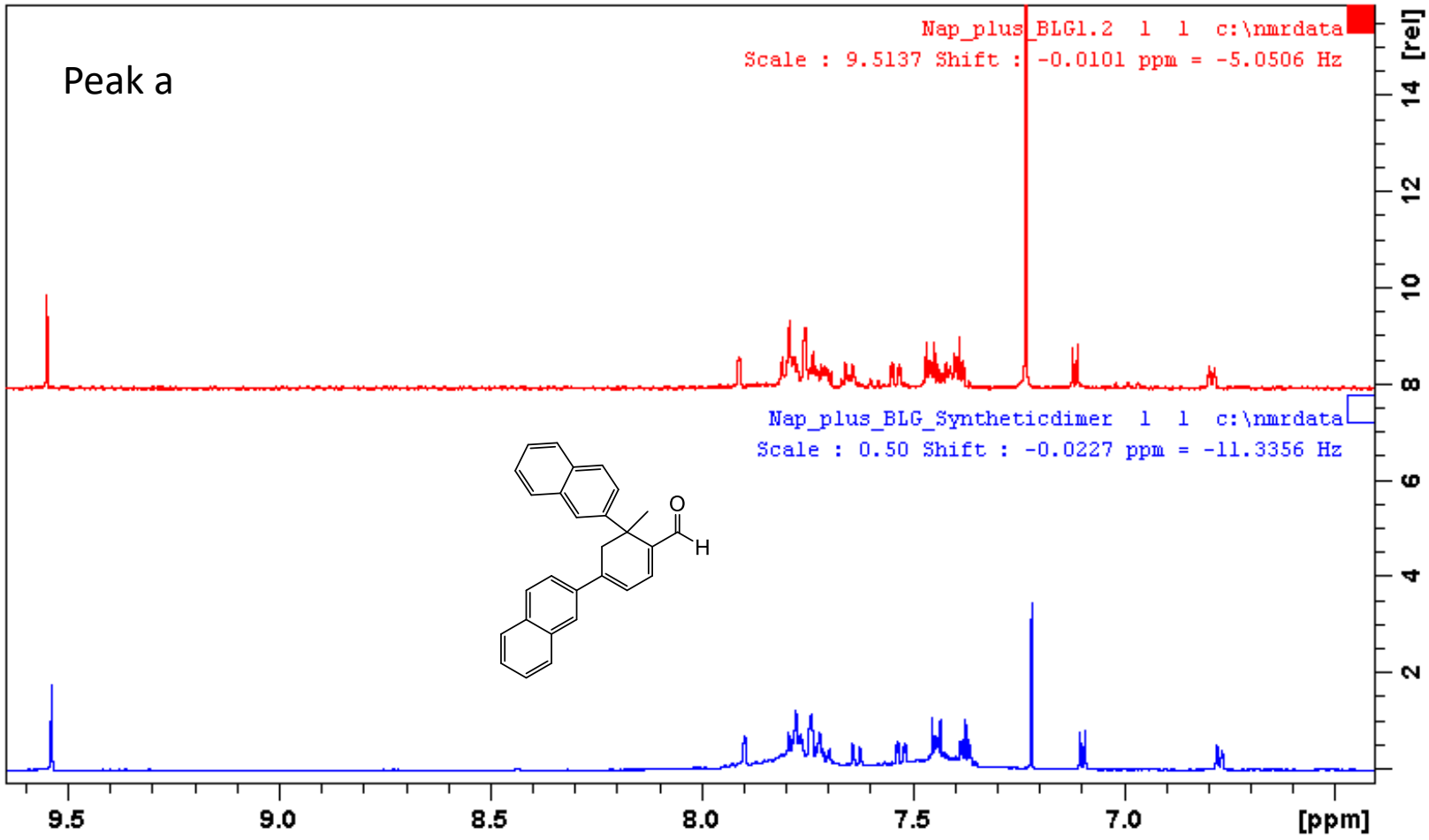

Homodimer standard was synthesized according to procedures previously reported by Bench, et. al [(123)].

Figure A 28 Characterization of peak '**a**' by 1H-NMR spectroscopy

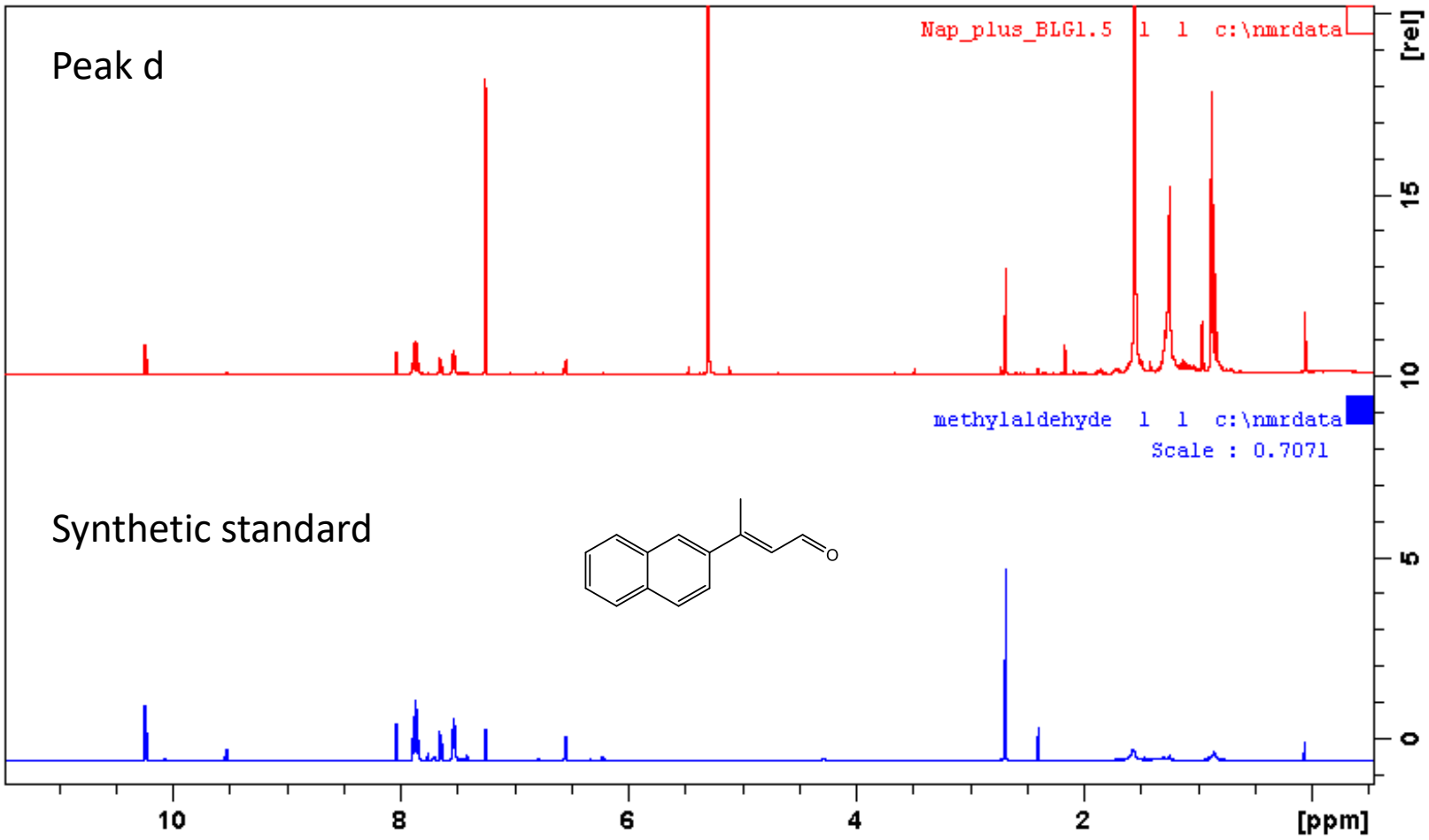

Figure A 29 Characterization of peak‘**d**’ by 1H-NMR spectroscopy

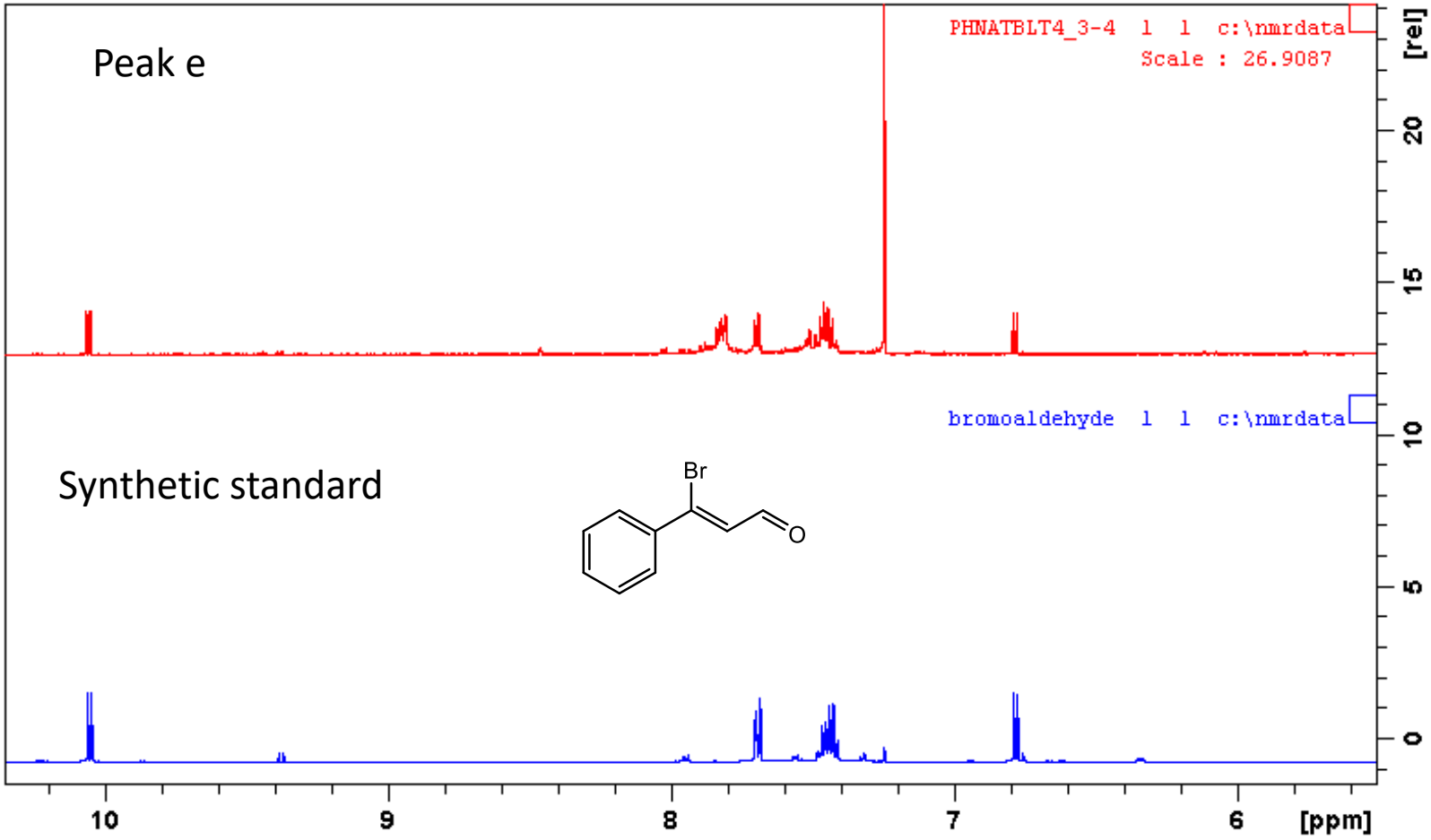

Figure A 30 Characterization of peak '**e**' by 1H-NMR spectroscopy

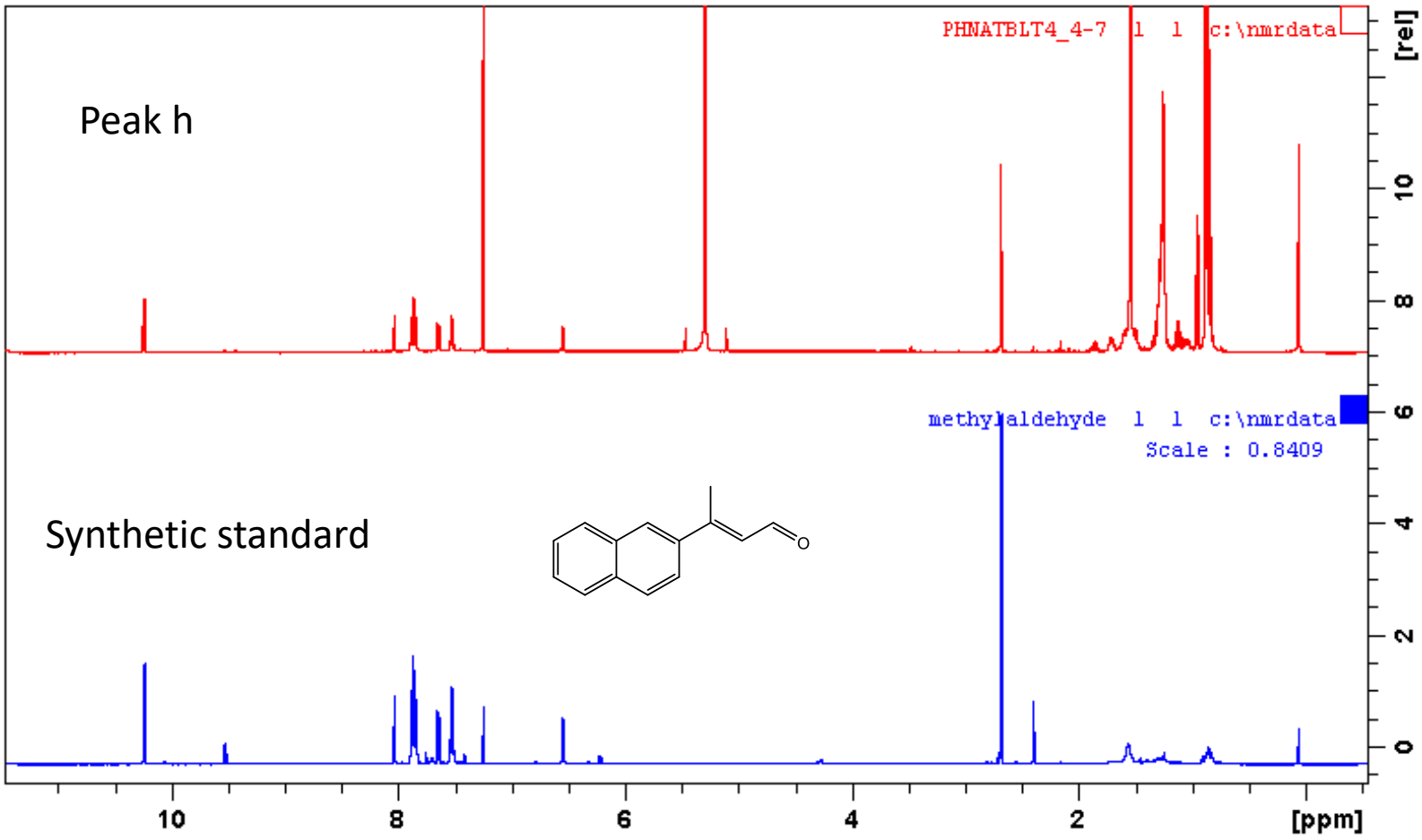

Figure A 31 Characterization of peak **'h'** by 1H-NMR spectroscopy

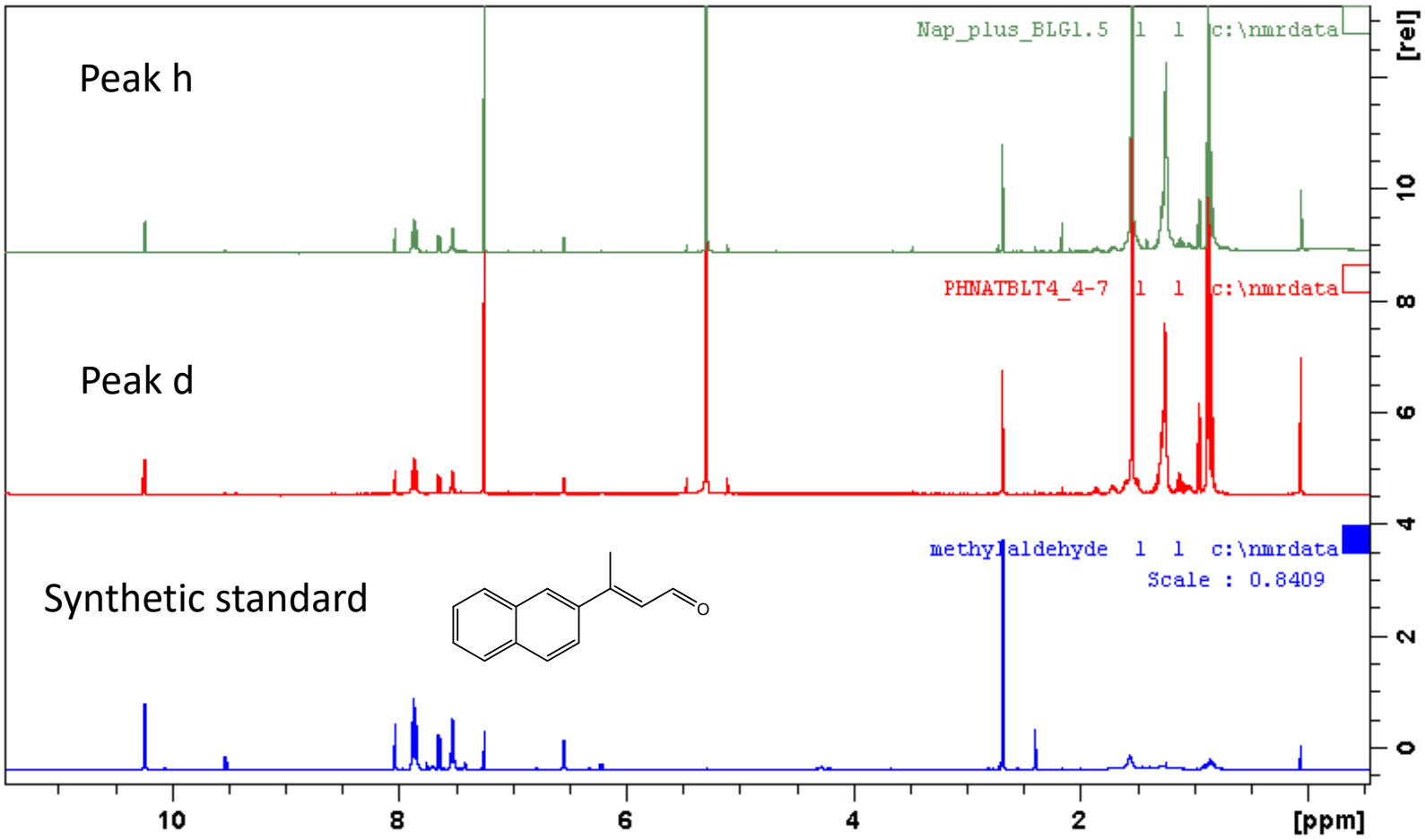

Figure A 32 Comparison of 1H-NMR spectra of peak‘**d**’ and peak ‘**h**’

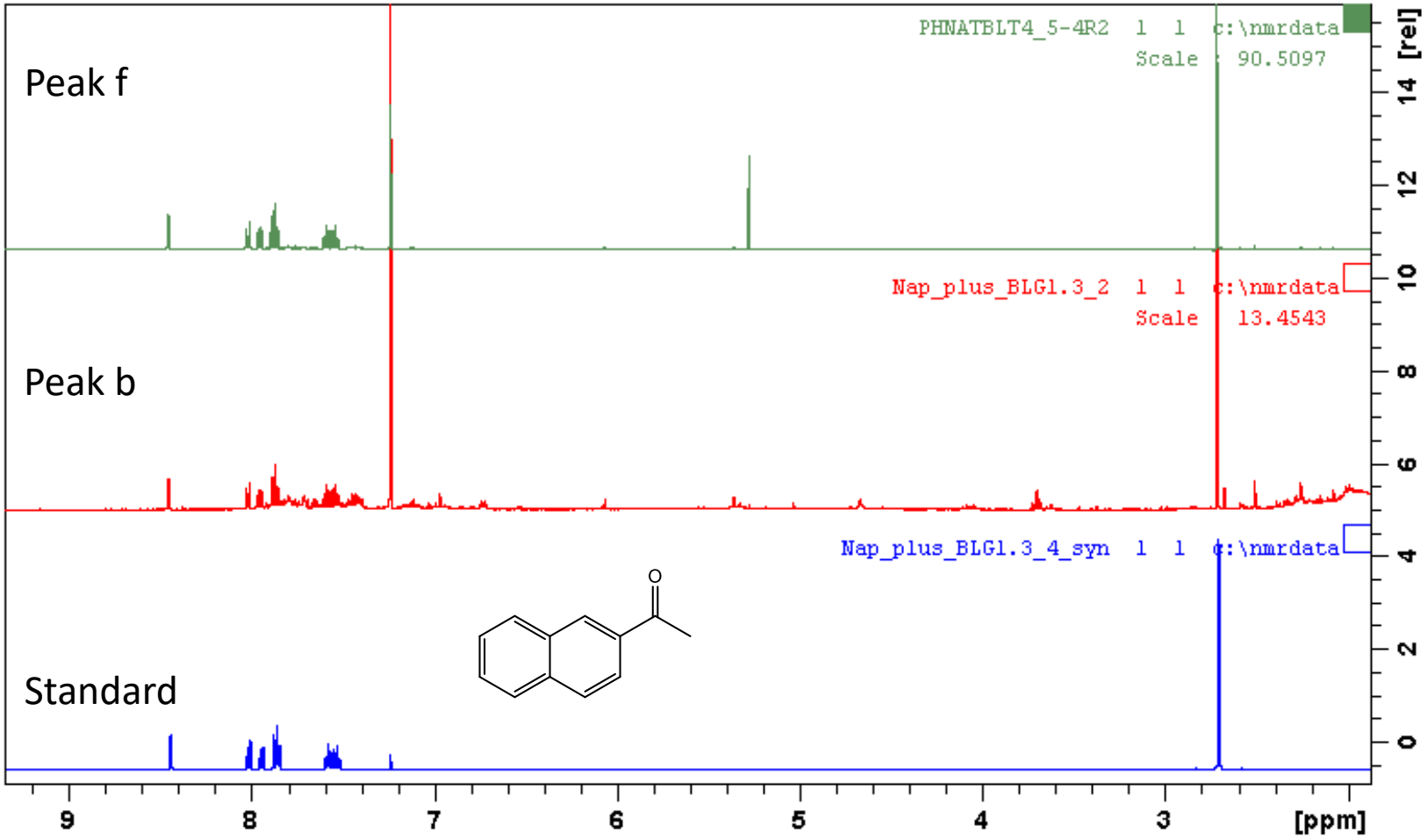

Figure A 33 Characterization of peaks '**b**' and '**f**' by 1H-NMR spectroscopy

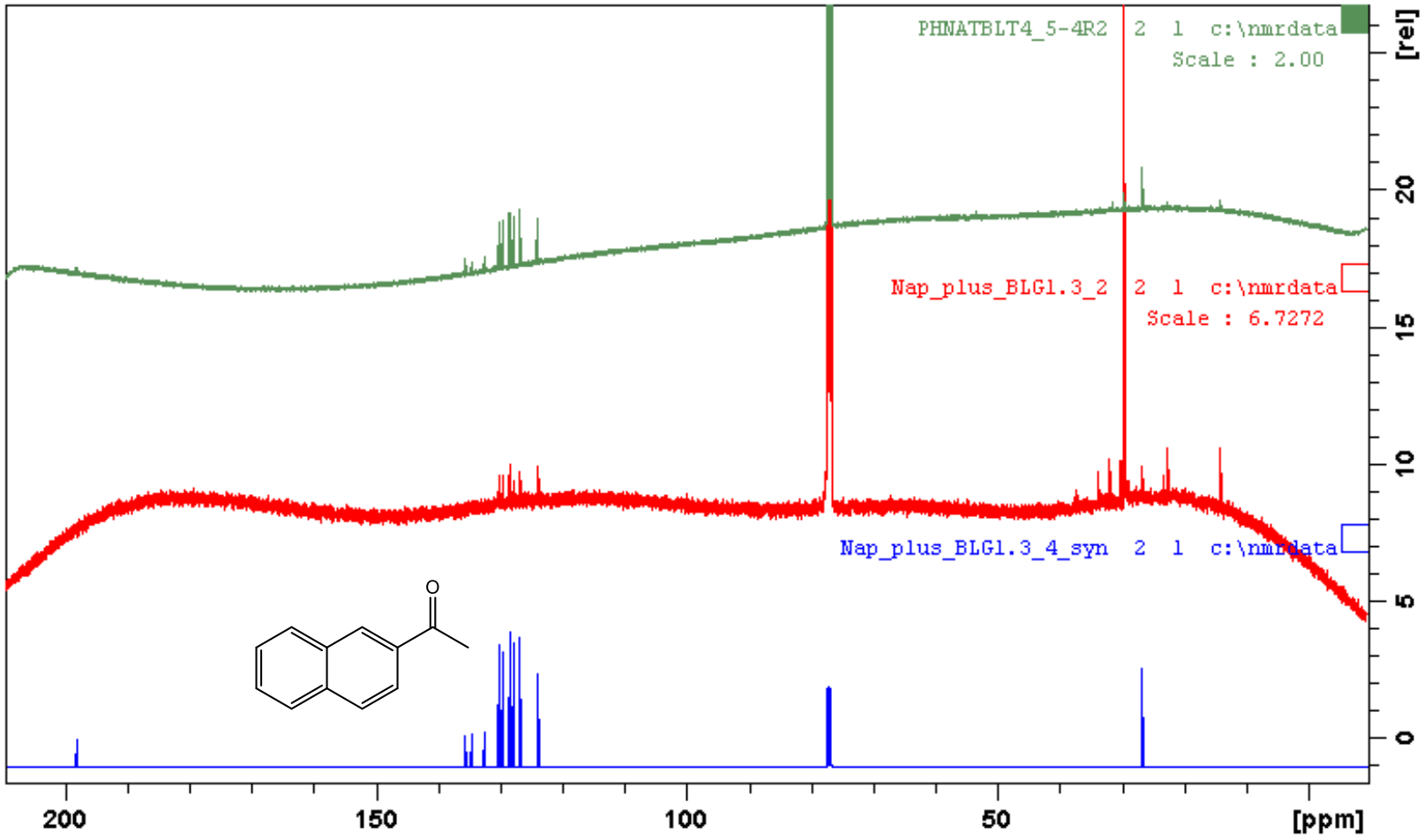

Figure A 34 Characterization of peaks '**b**' and '**f**' by 13C-NMR spectroscopy

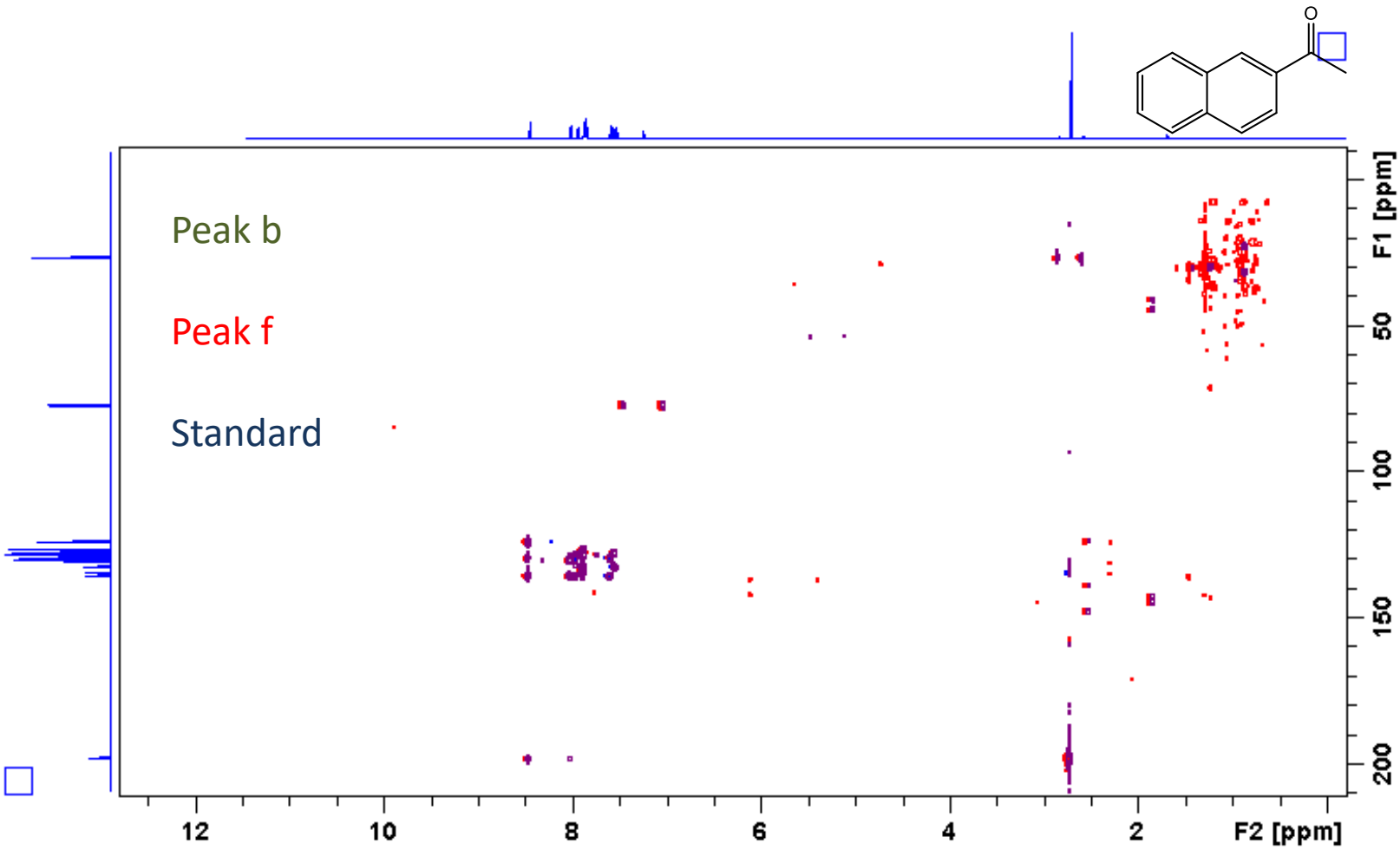

Figure A 35 Characterization of peaks '**b**' and '**f**' by HSQC correlation

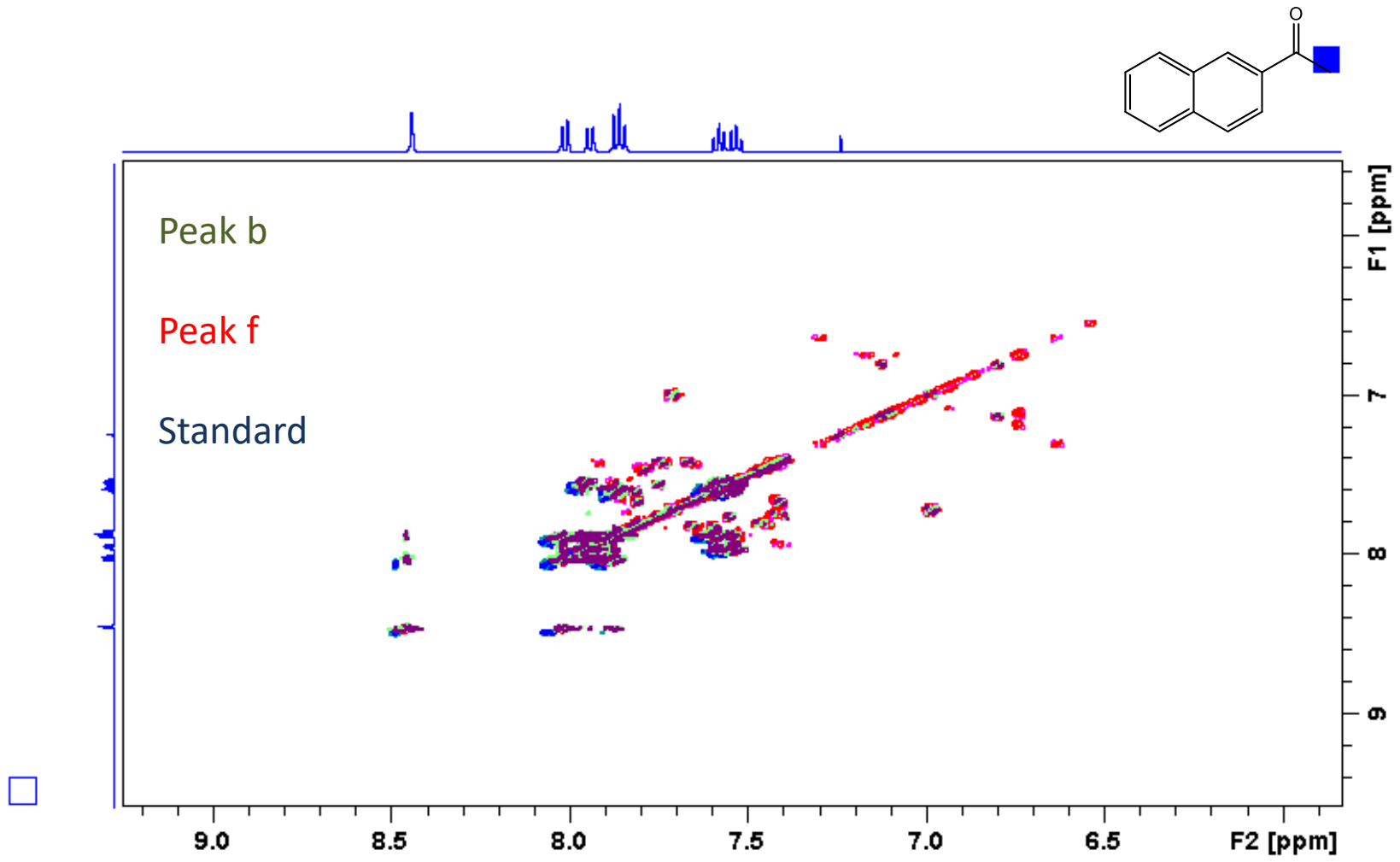

Figure A 36 Characterization of peaks '**b**' and '**f**' by COSY correlation

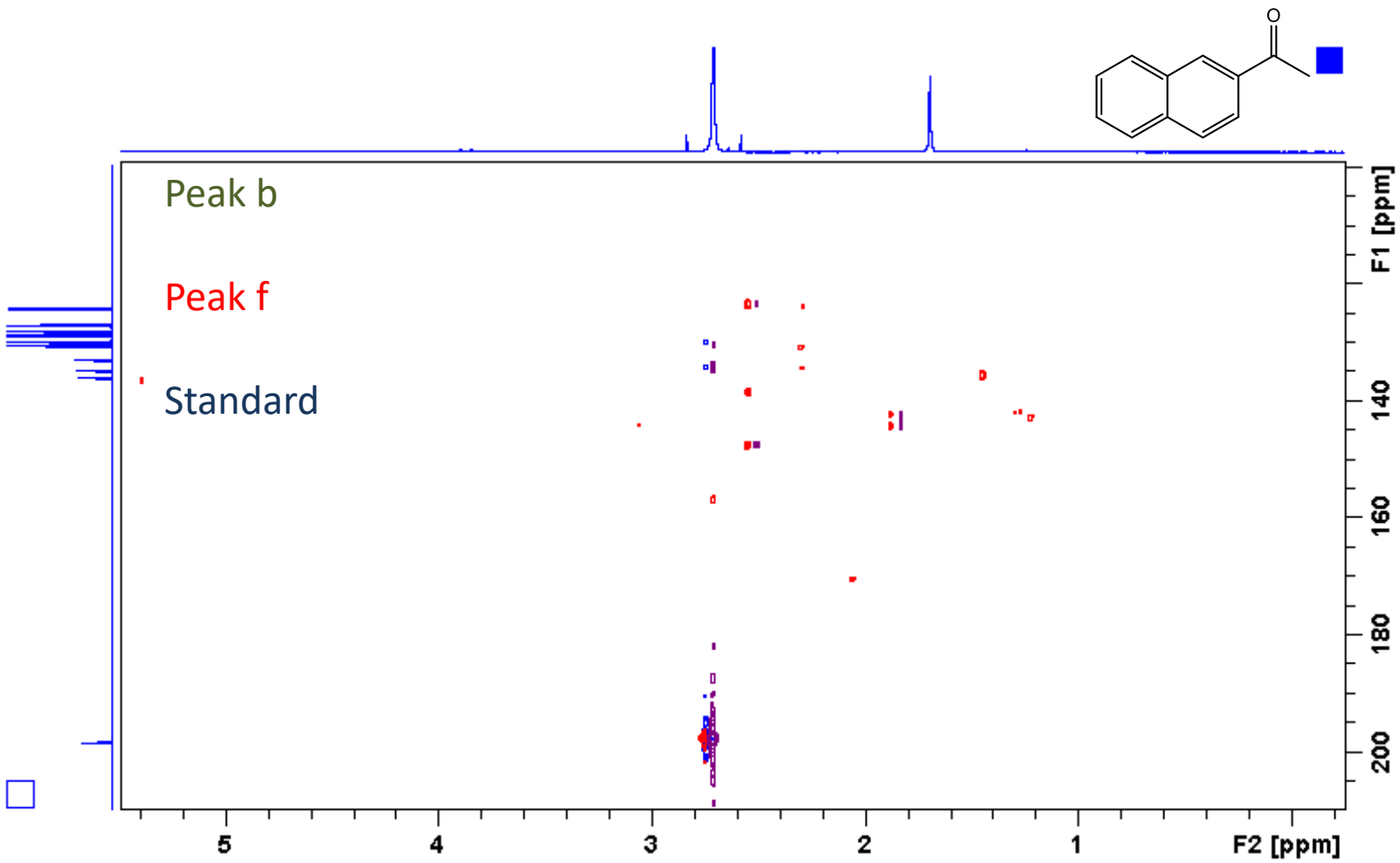

Figure A 37 Characterization of peaks '**b**' and '**f**' by low energy HMBC correlation

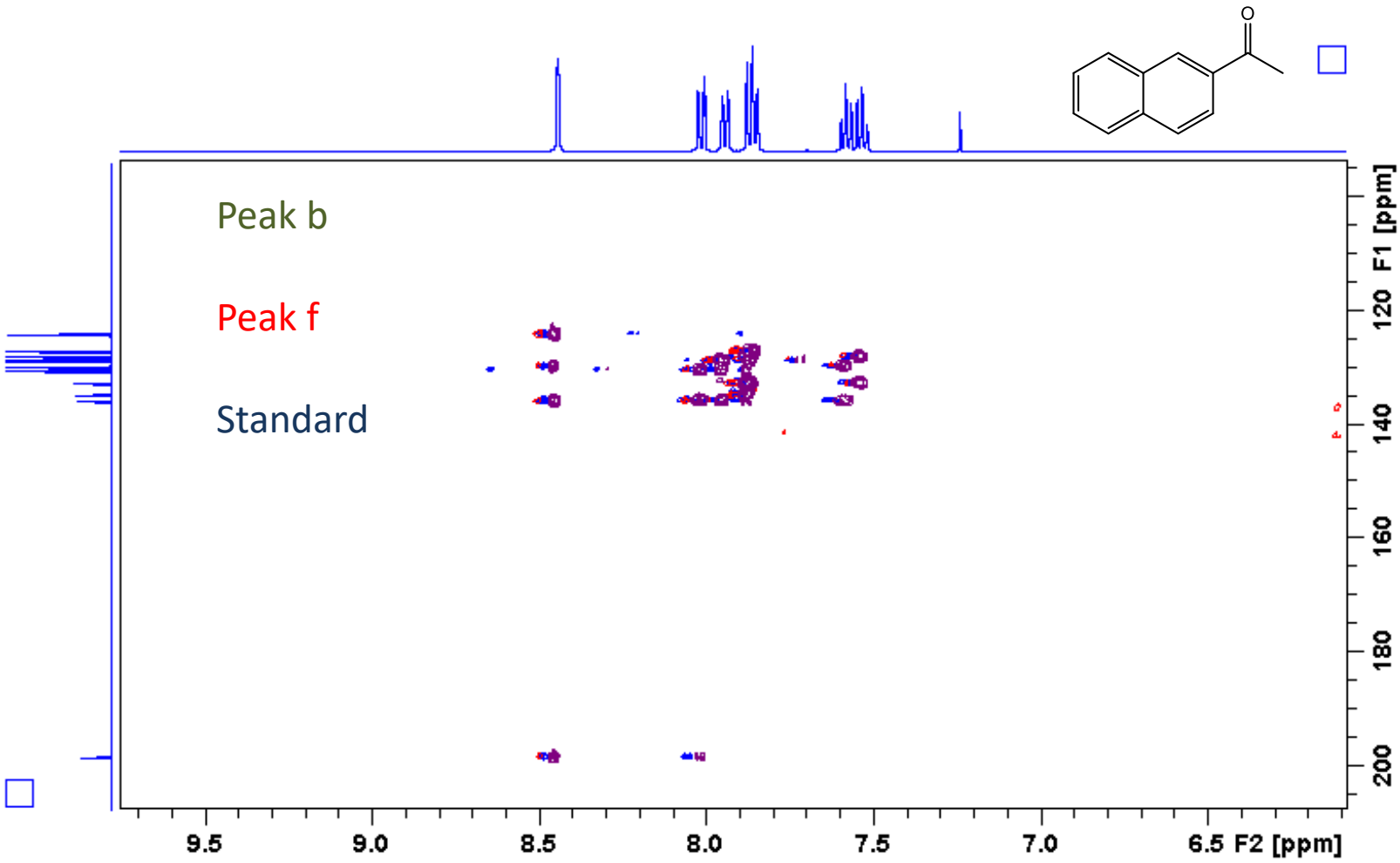

Figure A 38 Characterization of peaks '**b**' and '**f**' by high energy HMBC correlation